

## THE COLUMBIA CO SURVEY OF MOLECULAR CLOUDS IN THE FIRST GALACTIC QUADRANT

R. S. COHEN, T. M. DAME, AND P. THADDEUS

Columbia University and Goddard Institute for Space Studies

Received 1985 May 2; accepted 1985 September 23

### ABSTRACT

Using the Columbia millimeter-wave telescope, a 1.2 m Cassegrain with a beamwidth of 8', we have made a survey of 2.6 mm CO emission from the Galactic disk from  $l=12^\circ$  to  $l=60^\circ$  and  $|b| \leq 1^\circ$ . The survey comprises over 3000 spectra taken every  $0^\circ 125$ , approximately every beamwidth, for  $|b| \leq 0^\circ 5$  and every  $0^\circ 25$  elsewhere. The velocity resolution is  $1.3 \text{ km s}^{-1}$ , and the coverage is from  $-13$  to  $153 \text{ km s}^{-1}$  at  $l < 55^\circ$  and from  $-55$  to  $111 \text{ km s}^{-1}$  for  $l \geq 55^\circ$ . The noise is  $0.45 \text{ K rms}$  per  $1.3 \text{ km s}^{-1}$  resolution element.

The calibration of the instrument has been compared with that of other telescopes. When the different beams are taken into account, it agrees well with measurements of individual molecular clouds ( $\pm 17\%$ ) and the Galactic plane ( $\pm 26\%$ ) done with both the Bell Laboratories 7 m and the NRAO 11 m telescopes. A measurement of the Sun with a standard gain horn differs from our measurement by only 6%.

This paper presents the entire collection of spectra as well as spatial and longitude-velocity maps.

*Subject headings:* interstellar: molecules — galaxies: Milky Way — galaxies: structure

### I. INTRODUCTION

Knowledge of interstellar molecular clouds is derived largely from observations of trace molecules, the most abundant molecule, H<sub>2</sub>, being nearly undetectable in most clouds, owing to low temperature and high UV obscuration. The tracer most widely used is the very stable carbon monoxide molecule, CO. Its fundamental rotational transition at a wavelength of 2.6 mm is readily detected along the Galactic plane, and there is evidence in nearby clouds from star counts that the CO/H<sub>2</sub> ratio is fairly constant. Most surveys of individual molecular clouds and the large-scale Galactic surveys have used this line.

The first systematic CO investigation of a large section of the Galactic plane was undertaken with the NRAO 11 m telescope in 1972 by Schwartz, Wilson, and Epstein (1973), who selected from the 5 GHz continuum survey of Altenhoff *et al.* (1970) an unequally spaced string of 47 positions between longitudes  $10^\circ$  and  $75^\circ$ . Subsequent surveys (Scoville and Solomon 1975; Burton *et al.* 1975; Burton and Gordon 1978) using the same telescope, then the only millimeter-wave facility with enough sensitivity and spectral range to survey the inner Galaxy, were unbiased but still severely undersampled and restricted primarily to  $b = 0^\circ$ . The last major Galactic survey undertaken with the NRAO telescope, and the only one with significant coverage out of the plane (Sanders, Solomon, and Scoville 1984), was still undersampled in solid angle by a factor of about 600. More recently the FCRAO 14 m telescope has been used to make a much more extensive survey, but one undersampled by a factor of between 15 and 60, depending on Galactic longitude (Solomon, Sanders, and Rivolo 1985). The Bell Laboratories 7 m antenna was used to make a limited survey of the first quadrant, almost fully sampled in latitude but spaced from  $1^\circ 4$  to  $13^\circ$  in longitude.

The beams of all three of these telescopes at 2.6 mm are so small in solid angle, varying from  $2 \times 10^{-4}$  square degrees at the FCRAO telescope to  $8 \times 10^{-4}$  square degrees at Bell Laboratories, relative to Galactic features of interest (10–100 square degrees) that well-sampled surveys are impractical with these facilities; a smaller, dedicated survey instrument is needed.

The Columbia-Goddard millimeter-wave telescope was designed with this in mind. Its beamwidth (8'), slightly smaller than that of the largest steerable antennas at 21 cm, is large enough for fully sampled maps of the Galaxy and of large, nearby clouds to be made in a reasonable time, a few months to a few years. Using this instrument, we completed a systematic, unbiased survey of CO emission from much of the first Galactic quadrant. The survey was extended far enough from the plane to include nearly all molecular clouds beyond the Local arm, and its sensitivity was adequate to detect large molecular clouds in distant parts of the Galaxy.

### II. INSTRUMENT

The telescope (Figs. 1 and 2), on the roof of the Pupin Physical Laboratory of Columbia University in New York City, is housed in an astrodome whose slit is covered by a thin membrane which is almost totally transparent at 2.6 mm. The antenna is a standard radio Cassegrain manufactured by Philco-Ford to Columbia specifications. Its parabolic primary is a lightweight monolithic casting of A256 aluminum alloy, which, after annealing and strain relief, was numerically milled to an rms surface accuracy of  $40 \mu\text{m}$  ( $\lambda/65$  at 2.6 mm) as determined by measurements with a mechanical gauge at 256 points on the surface, an error about half of what is generally acceptable for diffraction-limited telescopes. The primary f/D

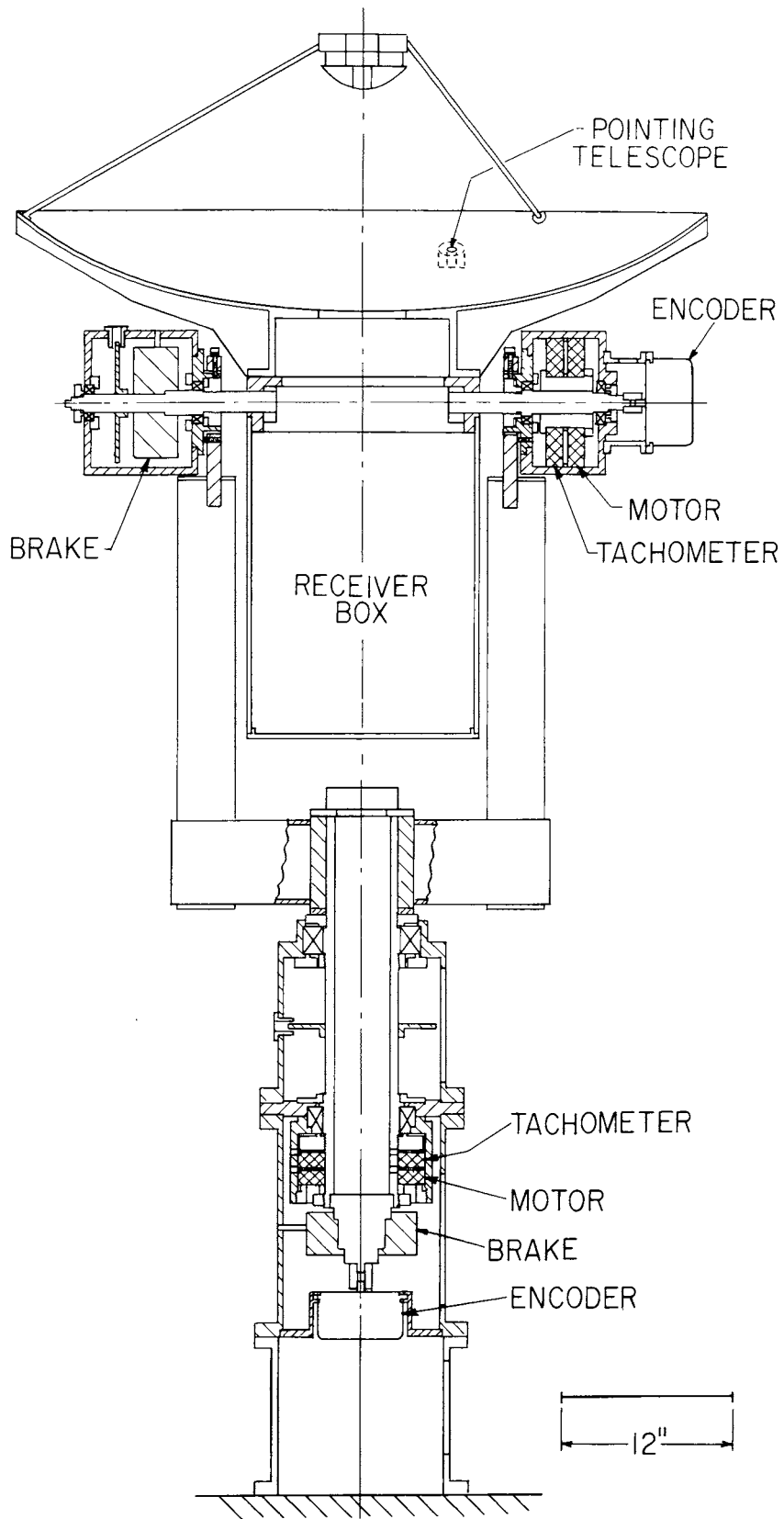


FIG. 1.—The Columbia 1.2 m telescope, an altitude-azimuth Cassegrain driven without a gear train by 15 m newton torque motors mounted directly on the altitude and azimuth axes, as shown, together with the encoders, tachometers, and brakes.

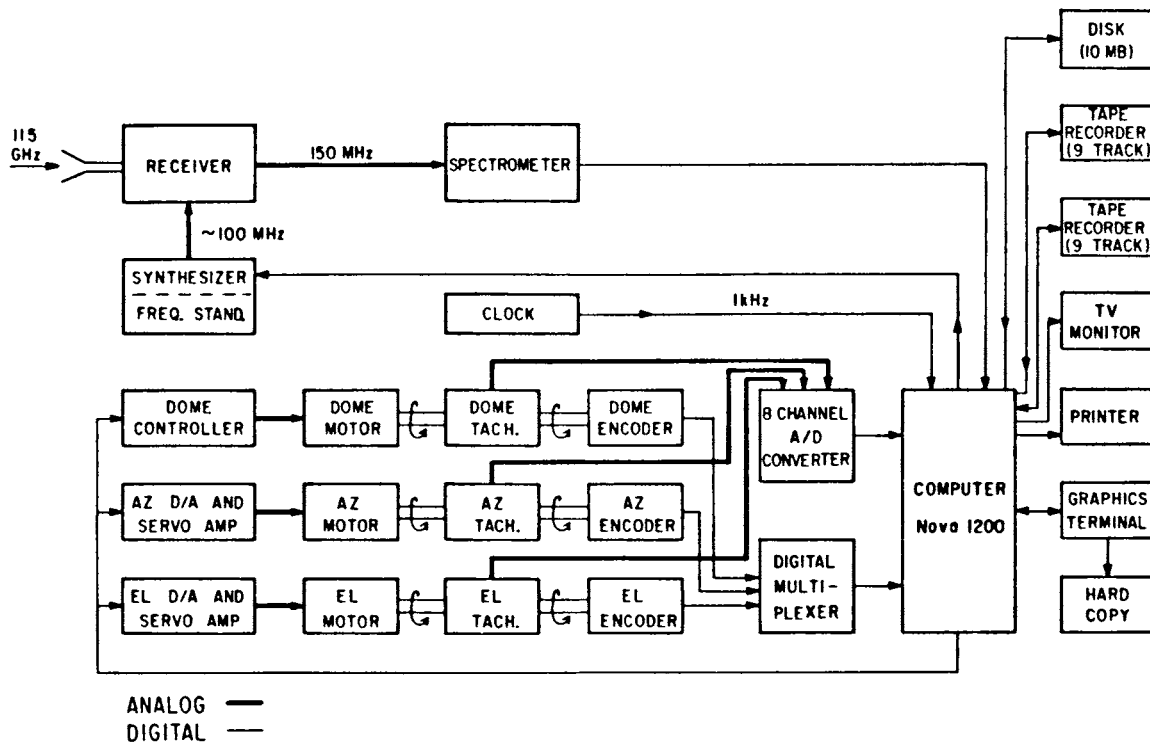


FIG. 2.—Block diagram of the telescope electronics. The system is controlled by a single computer which (1) closes the drive servo loop 100 times per second, (2) calculates the Doppler corrections to the local standard of rest and sets the local oscillator frequency, (3) reads the data from the spectrometer and stores it on disk and tape, (4) displays the spectra under operator command, and (5) executes preliminary data reduction.

ratio is 0.375, and the effective  $f/D$  at the Cassegrain focus (at the vertex of the primary) is only 2.8, permitting a small feed horn readily chopped by a blackbody sector wheel for radiometric calibration. Gravitational deformation of the primary according to numerical calculations using the NASTRAN structural code is less than  $5 \mu\text{m}$ , or  $\lambda/500$  at 115 GHz.

Pattern measurements made by observing a 115 GHz transmitter on a distant ( $0.8 D^2/\lambda$ ) building demonstrated that the intensity and shape of the main beam and inner four sidelobes were very close to those predicted by scalar diffraction theory when aperture blockage by the secondary and its supports was taken into account (Cohen 1978). The depth of the nulls between the sidelobes, more than 28 dB, is evidence that surface errors correlated over more than a quarter of the antenna diameter are less than  $\lambda/60$ .

Initially, the feed was a pyramidal horn that produced a tapered illumination 13 dB down at the edge of the primary mirror. Near the end of the observations the spillover efficiency was significantly improved by replacing this horn with a scalar feed, also with 13 dB edge illumination. For both, the focusing was done with a mechanical alignment jig that held the feed in the correct position.

The receiver (Cong, Kerr, and Mattauch 1979) consisted of a resonant ring local oscillator diplexer, a double-sideband Schottky barrier mixer at room temperature, a low-noise parametric amplifier operating at the first intermediate frequency (IF) of 1390 MHz, and standard commercial components that further amplified the IF signal and converted it to the second IF of 150 MHz, which was sent to the spectrometer. The local

oscillator was initially a klystron operating at 113.9 GHz, later a klystron at 56.9 GHz followed by a frequency doubler. The klystron was stabilized using an NRAO-designed phase-locking circuit. The measured single-sideband receiver noise was 840 K.

The telescope, pointed by an altitude-azimuth mount with direct-drive torque motors, could move to and begin tracking at a new position  $10^\circ$  away within 1 s. By allowing frequent switching (about every 15 s) between the observed position and a reference position several degrees out of the Galactic plane with little lost time, this rapid motion significantly improved the electronic stability of the telescope.

Pointing, which relied on optical shaft encoders with a resolution of  $20''$ , was always better than  $1.0'$  (0.12 beamwidths). Because few point sources can be detected with a small telescope at millimeter wavelengths and none in short integration times, roughly 50 stars, sighted through a 3 cm optical telescope collimated with the radio beam, established the coordinate system. Several times each year the pointing was checked against these stars and every few days checked in the radio directly against the Sun, the center of which can be located to within  $10''$  in 115 GHz continuum emission. During three years of observing, only a few corrections, none more than  $1'$ , were needed.

The spectrometer, a 256 channel filter bank based on the NRAO design for the 11 m telescope (Mauzy 1974; Pace and Payne 1973), had a resolution of 250 KHz, corresponding to a velocity resolution of  $0.65 \text{ km s}^{-1}$ , and a total bandwidth of  $166 \text{ km s}^{-1}$  at the CO frequency. Successive 48 ms samples of

the spectrum were summed in a Data General Nova mini-computer that calibrated the data and stored it on disk. The final calibrated spectra were periodically copied from disk to magnetic tape for further processing with a larger computer.

### III. OBSERVING TECHNIQUE

All observations were made by position switching between the observed (ON) position and reference positions (OFFS). Care was taken to establish that the reference positions were free of CO emission at the sensitivity level of the survey; each was checked by both frequency switching and position switching against at least two other reference positions, yielding the final list of reference positions given in Table 1. When these positions were recently checked to low flux level ( $\sim 0.1$  K rms) with the very sensitive superconductor-insulator-superconductor receiver now on the telescope, several narrow CO lines, listed in Table 1, were found. None of these lines, all below the  $3\sigma$  level of the survey and at low velocities from local clouds, significantly modify the maps or our conclusions with respect to the Galactic distribution of molecular clouds.

In a preliminary study we found some curvature in the baselines, possibly an effect of the Earth's magnetic field on the parametric amplifier, which was proportional to the angle between the source and the reference position. This was eliminated by using three OFF positions, surrounding the ON position, for each observation. The computer automatically adjusted the fraction of the total observation time for each of the three OFFS, so that the time-weighted average of the vectors to the three fell exactly at the ON position. Using this procedure, baselines flat to within the noise were obtained. A straight line, determined by a least-squares fit to emission-free regions of each spectrum, was then subtracted from each spectrum, and, finally, spectra were smoothed to a resolution of 2 channels ( $1.3 \text{ km s}^{-1}$ ) by convolution with the Hanning function  $1/4, 1/2, 1/4$ .

### IV. CALIBRATION

Spectra were calibrated against a blackbody reference by a standard "chopper wheel" method to an absolute accuracy of about 15%. A detailed discussion of the method and the sources of error is given in the Appendix. All line intensities in this paper are antenna temperatures corrected for atmospheric loss and main-beam efficiency and are equal to the radiation

TABLE 1  
REFERENCE OFF POSITIONS AND RESIDUAL LINES

$l, b$ (degrees)	$T_R^*$ (K)	$v$ (km s $^{-1}$ )
12, -5	0.5	10
12, 5	...	...
15, -5	...	...
15, 5	...	...
20, 5	0.8, 0.7	6, 17
22, -5	0.4	12
25, -5	...	...
25, 10	0.5	8
30, -5	...	...
30, 8	0.8	2
35, -5	...	...
35, 5	0.7	7
40, -5	0.7	9
40, 5	...	...
43, -2	1.3	8
45, 2	...	...
45, 3	...	...
50, -3	...	...
50, 2	0.5	19
55, -5	...	...
55, 5	...	...
60, -5	0.8	11
60, 5	...	...

NOTE.— $T_R^*$  and  $v$  are the intensity and velocity of the weak, local lines found at the OFF positions by subsequent observation with a very sensitive SIS receiver on the 1.2 m telescope.

temperature of a source that just fills the main beam. They differ only slightly from  $T_R^*$  as defined by Kutner and Ulich (1981), since they are corrected for radiation lost in the near sidelobes, being approximately equal to  $1.02 T_R^*$ .

We compared the temperature scale of the Columbia 1.2 m telescope with those of three other telescopes: the Bell Laboratories 7 m, the NRAO 11 m, and a standard gain horn. For the Bell Laboratories 7 m comparison, we convolved the beam of the 1.2 m with a Bell Laboratories map of B335 (Frerking 1980) which covers, with close to beamwidth spacing, an area approximately the size of the main beam of the 1.2 m out to the first null in the antenna pattern. For the 11 m, over 200 spectra are required to map the same area, so instead, following the recommendation of Ulich and Haas (1976) for comparing different telescopes, we approximated the Orion A

TABLE 2  
CALIBRATION OF 1.2 METER TELESCOPE COMPARED WITH OTHERS

Source	Emission	Antenna	Source Shape	Predicted Intensity	Measured Intensity	Difference (%)
B335 <sup>a</sup> .....	2.6 mm CO	Bell Laboratories 7 m	Complex; 10' diameter	$3.5 \text{ K km s}^{-1}$	$2.9 \text{ K km s}^{-1}$	-17
Orion A ....	2.6 mm CO	NRAO 11 m	Gaussian; $4' \times 9'$ FWHM	24 K	26 K	+8
Sun .....	2.6 mm continuum	Horn	Disk; 32' diameter	$6090 \text{ K}^b$	$5735 \text{ K}$	-6

NOTE.—The intensities are either in units of corrected antenna temperature,  $T_A^*$ , or  $\int T_A^* dv$ .

<sup>a</sup>R.A.(1950) =  $19^{\text{h}}34^{\text{m}}38^{\text{s}}$ , decl.(1950) =  $+70^{\circ}29'$ .

<sup>b</sup>Intensity of 7250 K, measured by Linsky 1973, is multiplied by a predicted forward coupling efficiency of 84% for the Sun.

TABLE 3  
CALIBRATION: COMPARISON WITH OTHER GALACTIC SURVEYS

Survey	$\langle T_R^* \rangle$ $\langle T_R^* \rangle_{\text{Columbia}}$	Telescope
Burton <i>et al.</i> 1975 .....	1.08	NRAO 11 m prime focus
Scoville and Solomon 1975 .....	0.76	NRAO 11 m prime focus
Cohen and Thaddeus 1977 .....	0.74	Columbia 1.2 m
Corrected (see text) .....	1.11	
Burton and Gordon 1978 .....	1.66	NRAO 11 m Cassegrain
Corrected (Liszt <i>et al.</i> 1984) .....	1.16	
Sanders, Solomon, and Scoville 1984 .....	1.27	NRAO 11 m Cassegrain
Stark 1983 .....	1.08	Bell Laboratories 7 m

source as a  $4' \times 9'$  Gaussian ridge and convolved this with the 1.2 m beam. For the horn we used a measurement of the Sun, which, since the Sun is an almost uniform disk at millimeter wavelengths, was easily convolved with the 1.2 m beam. As Table 2 shows, the calibration of these telescopes and that of the Columbia telescope are in satisfactory agreement.

We also compared the temperature scales of our survey and several Galactic CO surveys done on the 7 m and 11 m telescopes. Because of the different beam sizes, beam shapes, and sampling intervals, a point-by-point comparison of the surveys makes little sense. Two surveys at different resolutions can be better compared by summing the emission over all velocities and all points at  $b = 0^\circ$  where data are available from both surveys. As long as both surveys resolve the Galactic plane, these sums on average will be unaffected by convolution with the beam, and their ratio should on average be equal to unity. Since the smallest telescope involved, the Columbia 1.2 m, has even at 20 kpc a beamwidth of only 50 pc, less than half the thickness of the CO layer, such a comparison can be made without correcting for resolution. We have obtained velocity integrals for seven large-scale Galactic surveys of 2.6 mm CO emission: four on the NRAO 11 m telescope (Burton *et al.* 1975; Scoville and Solomon 1975; Burton and Gordon 1978; Sanders, Solomon, and Scoville 1984), one on the Bell Laboratories 7 m (Stark 1983), and two on the Columbia telescope (Cohen and Thaddeus 1977; this paper). As Table 3 shows, all surveys agree reasonably well, ours agreeing best with the Bell Laboratories survey and with the older NRAO survey of Burton *et al.* (1975) done with the 11 m telescope working at prime focus. The Bell Laboratories antenna, with a 90% main-beam efficiency and a well-mapped beam, is one of the best calibrated millimeter-wave telescopes. The two Columbia surveys differ by a factor of 0.74; calculations show that the beam efficiency in the earlier survey was underestimated by 1.45 and that a numerical error of 1.04 was made in the calibration equation. When these corrections are applied, the two differ by only 11%. The worst agreement is with Burton and Gordon (1978). They now recognize, however, that their intensities were too high, and they have subsequently scaled them down to agree with other surveys (Liszt, Burton, and Xiang 1984).

In conclusion, the Columbia calibration agrees well with that of other high-efficiency telescopes, in particular the Bell Laboratories 7 m antenna and a standard horn used for solar measurements. Because of the extensive calibration checks that have been made and the high quality of the antenna, we

believe that no better calibrated large-scale CO survey has yet been undertaken.

##### V. SURVEY PLAN AND RESULTS

Because earlier surveys (e.g., Cohen and Thaddeus 1977) had shown that virtually all Galactic CO emission falls in a strip  $2^\circ$  wide in latitude with a full width at half-maximum of  $0.5^\circ$ , we sampled the inner  $0.5^\circ$  strip every beamwidth and a  $2^\circ$  wide strip every second beamwidth, for a total of 3083 spectra (Fig. 3) between  $l = 12^\circ$  and  $l = 60^\circ$ . A few additional spectra were taken at  $b = \pm 1^\circ 25$ . Since previous surveys (Burton *et al.* 1975; Scoville and Solomon 1975) had not detected CO emission either at negative velocities or beyond the H I rotation curve at positive velocities, the  $166 \text{ km s}^{-1}$  bandwidth of the receiver was set to cover all positive H I allowed velocities; specifically, from  $12^\circ \leq l < 55^\circ$ , the receiver covered  $-13$  to  $153 \text{ km s}^{-1}$  and for  $55^\circ \leq l \leq 60^\circ$ ,  $-55$  to  $111 \text{ km s}^{-1}$ .

The full set of survey spectra is given in Figure 11. Each position was observed for 10–20 minutes, until the calibrated rms noise level was less than  $0.45 \text{ K}$  in the smoothed spectrum, to give an adequate signal-to-noise ratio for typical Galactic features between 2 and 6 K. As already described,

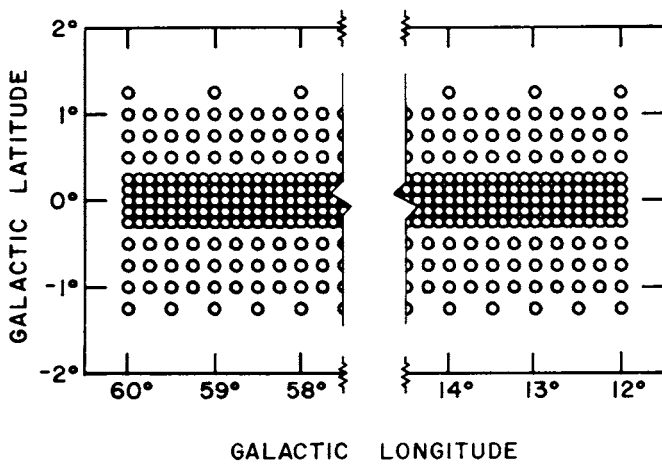
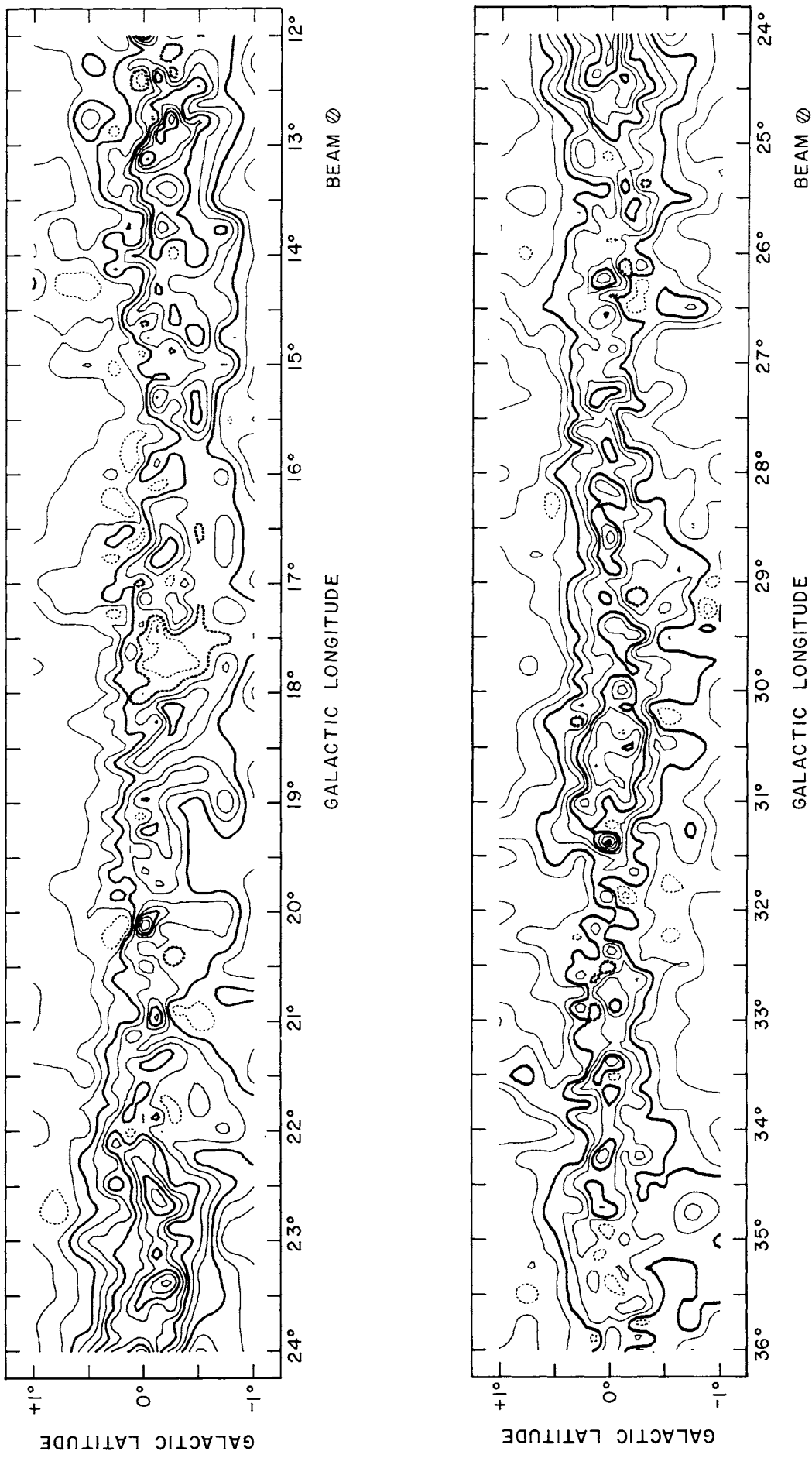


FIG. 3.—Sky coverage of the survey. Each observation is represented by a circle whose diameter ( $0^\circ 125$ ) is approximately equal to the beamwidth of the telescope.



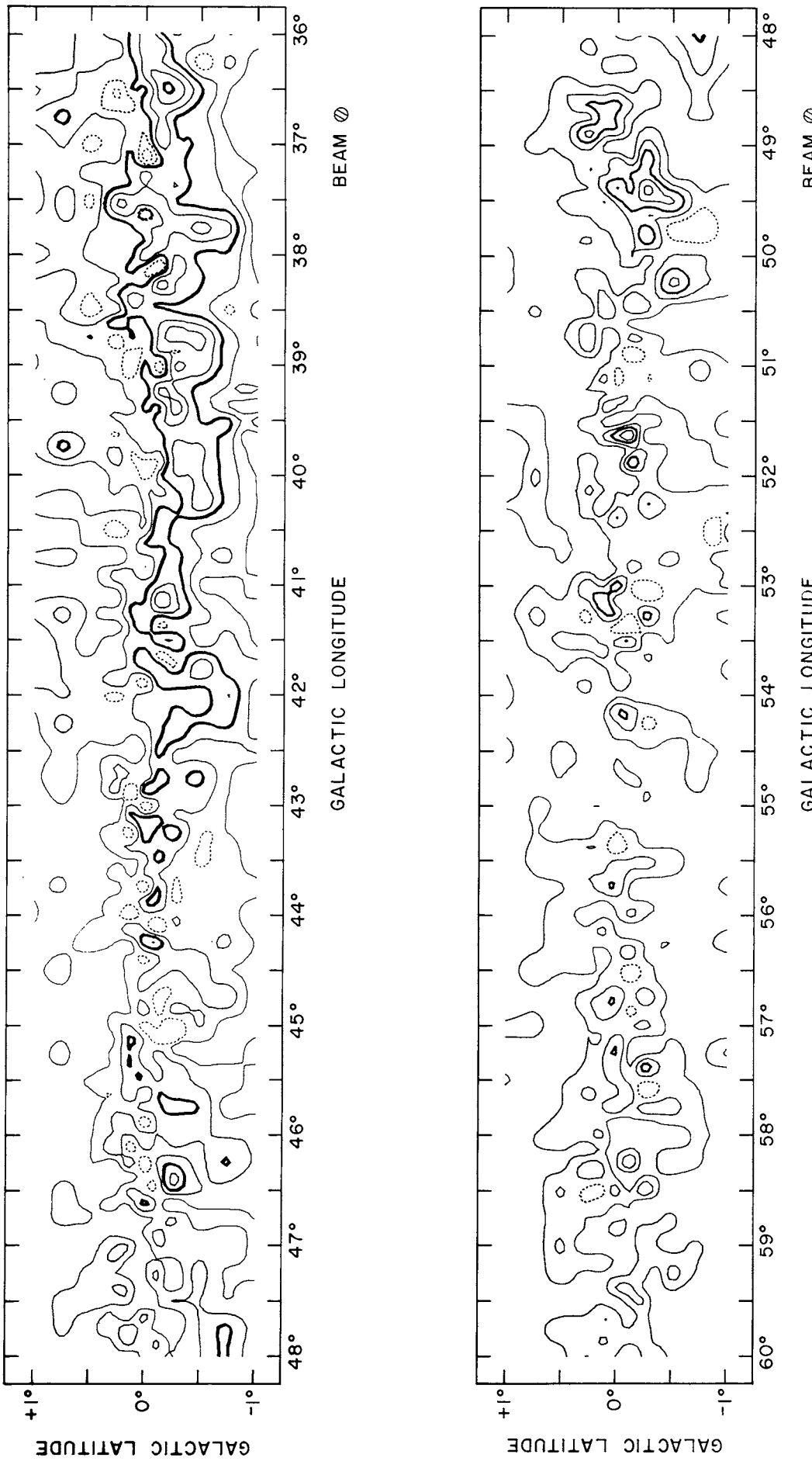


FIG. 4.—Spatial map of CO emission integrated over the entire velocity range observed. For  $|l| < 55^\circ$  the integration is from  $-13$  to  $153 \text{ km s}^{-1}$ ; for  $|l| \geq 55^\circ$ , from  $-55$  to  $111 \text{ km s}^{-1}$ . The contours are uniformly spaced at  $25, 50, \dots, K \text{ km s}^{-1}$ ; every third contour ( $75, 150, \dots, K \text{ km s}^{-1}$ ) is emphasized. Contours enclosing depressions (downgoing contours) are dotted.

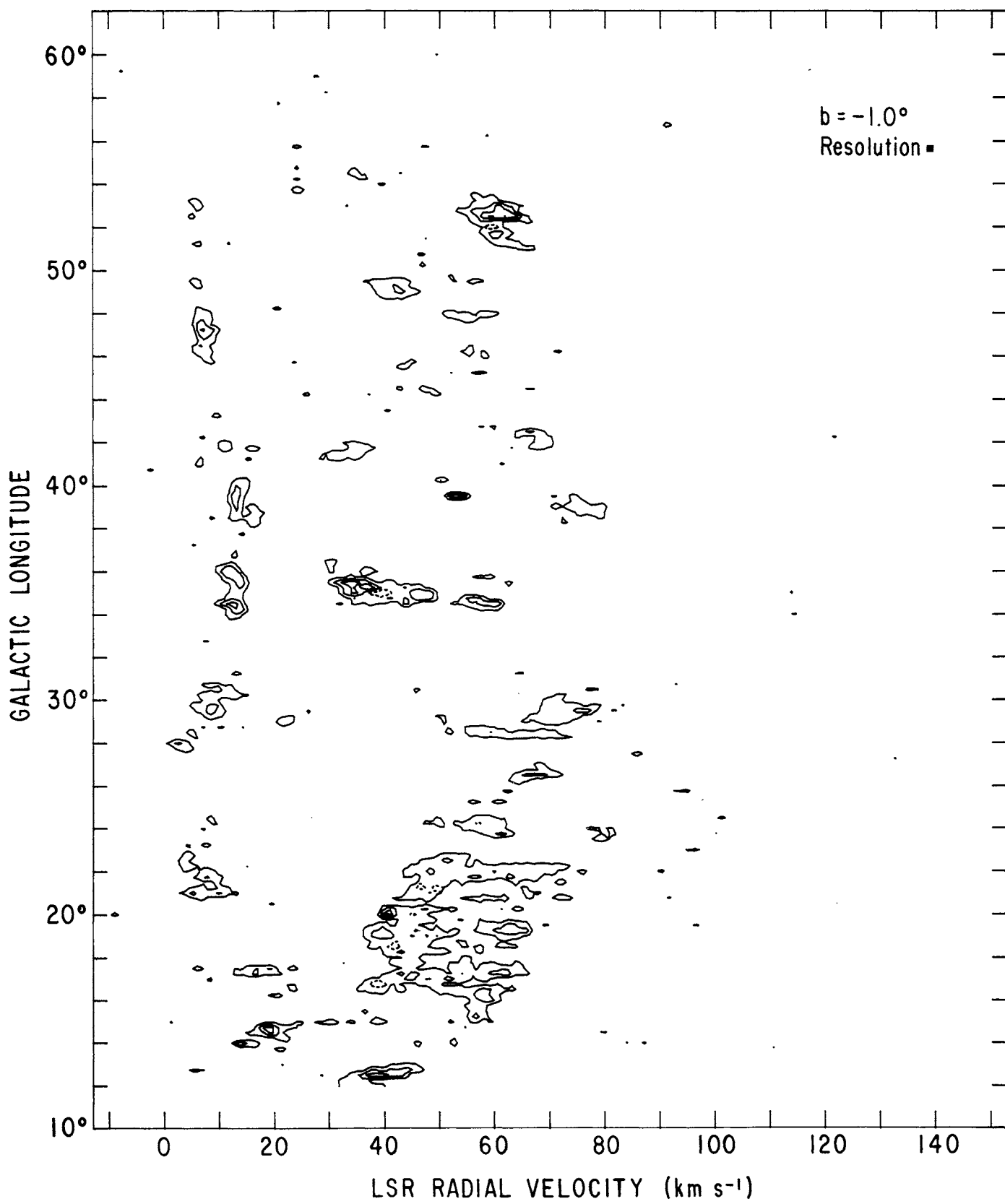


FIG. 5.—A series of longitude-velocity contour diagrams summarizing the data at each observed latitude between  $-1^\circ$  and  $+1^\circ$ . Contours are uniformly spaced at  $1.4, 2.8, \dots$  K. All plots have a velocity resolution of  $1.3 \text{ km s}^{-1}$ . The spatial resolution is  $0.25^\circ$  for  $|b| \leq 0.125$ , and  $0.25^\circ$  for  $0.25^\circ < |b| \leq 1^\circ$ . Contours enclosing depressions (downgoing contours) are dotted.

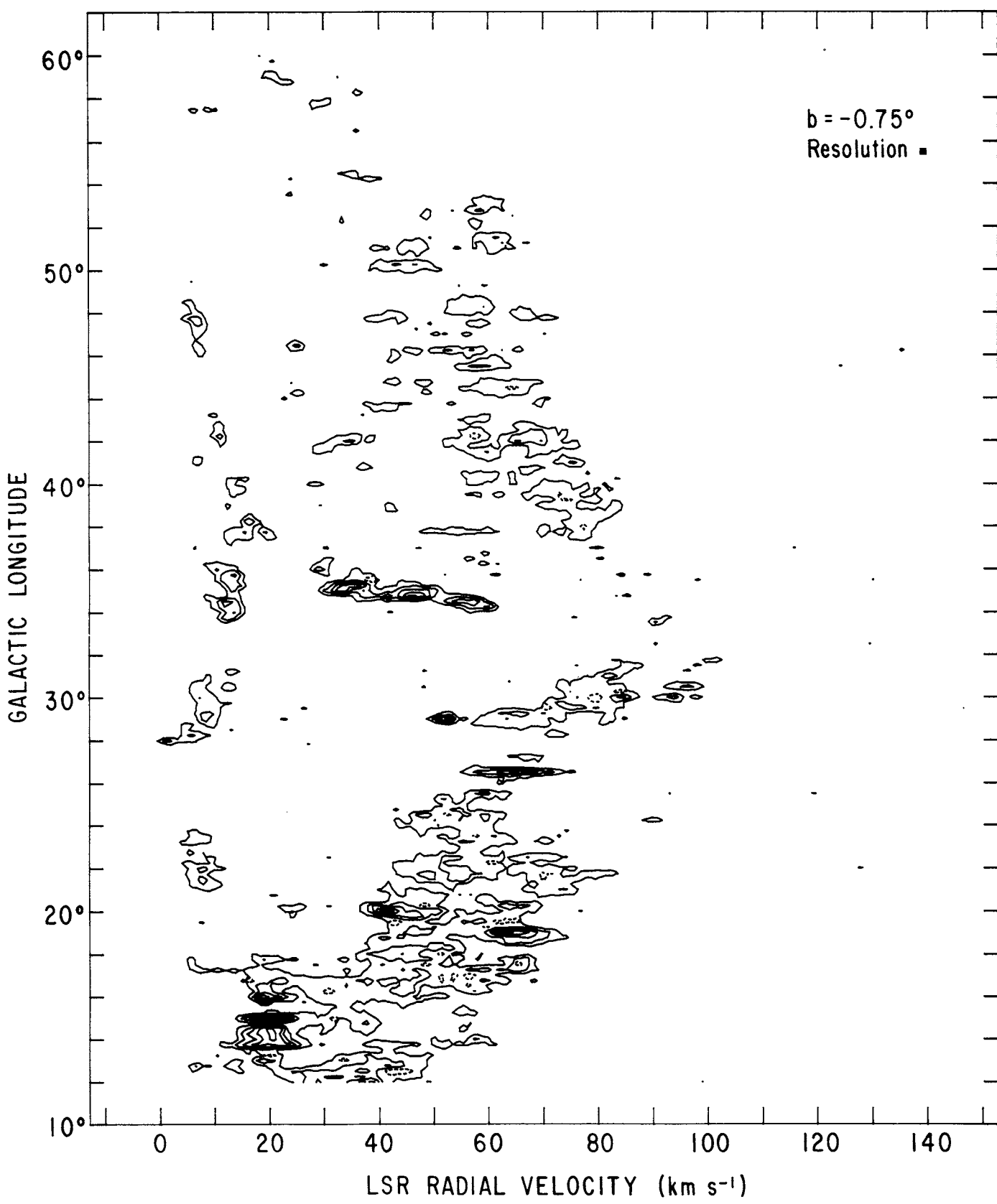


FIG. 5—Continued

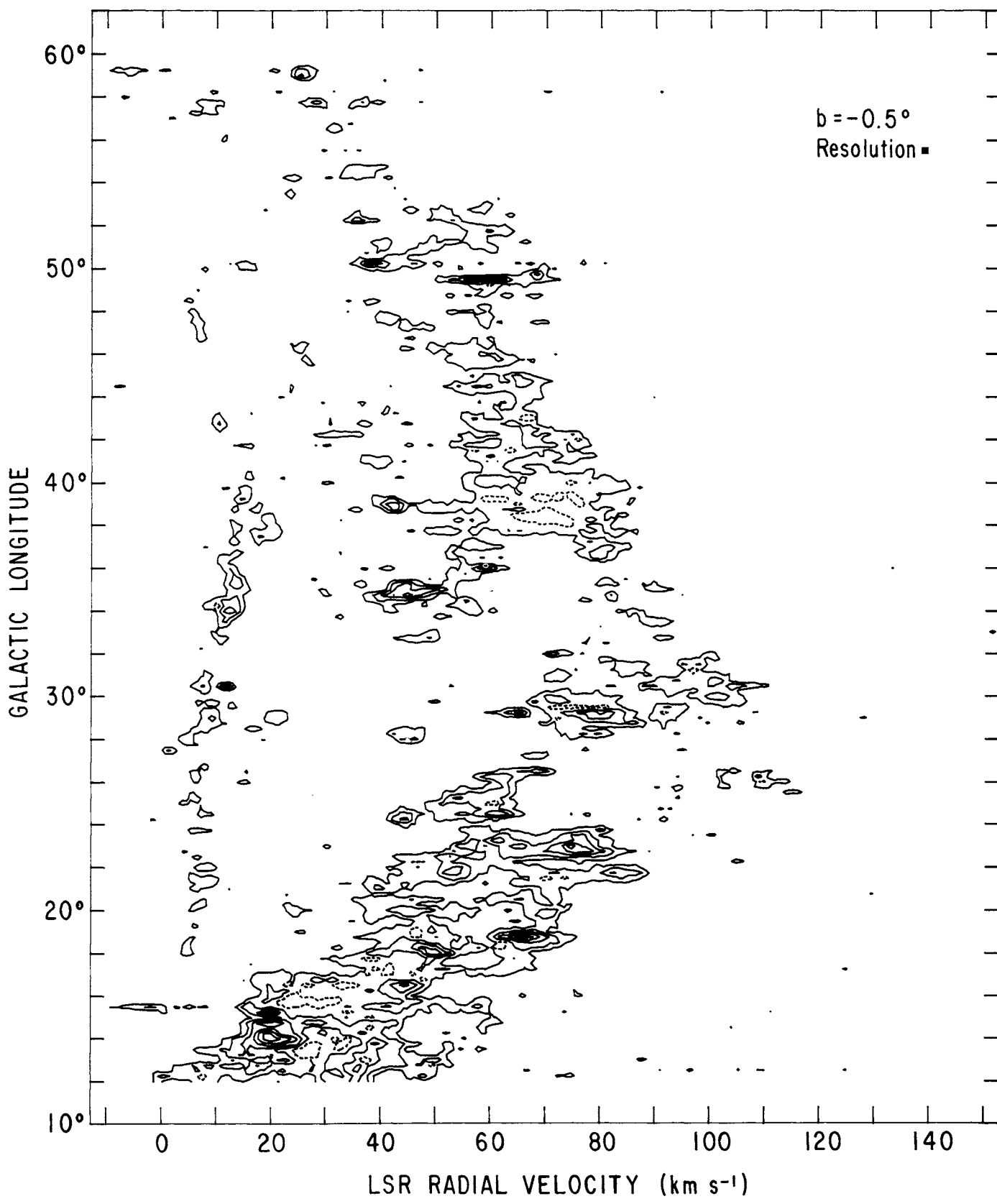


FIG. 5—Continued

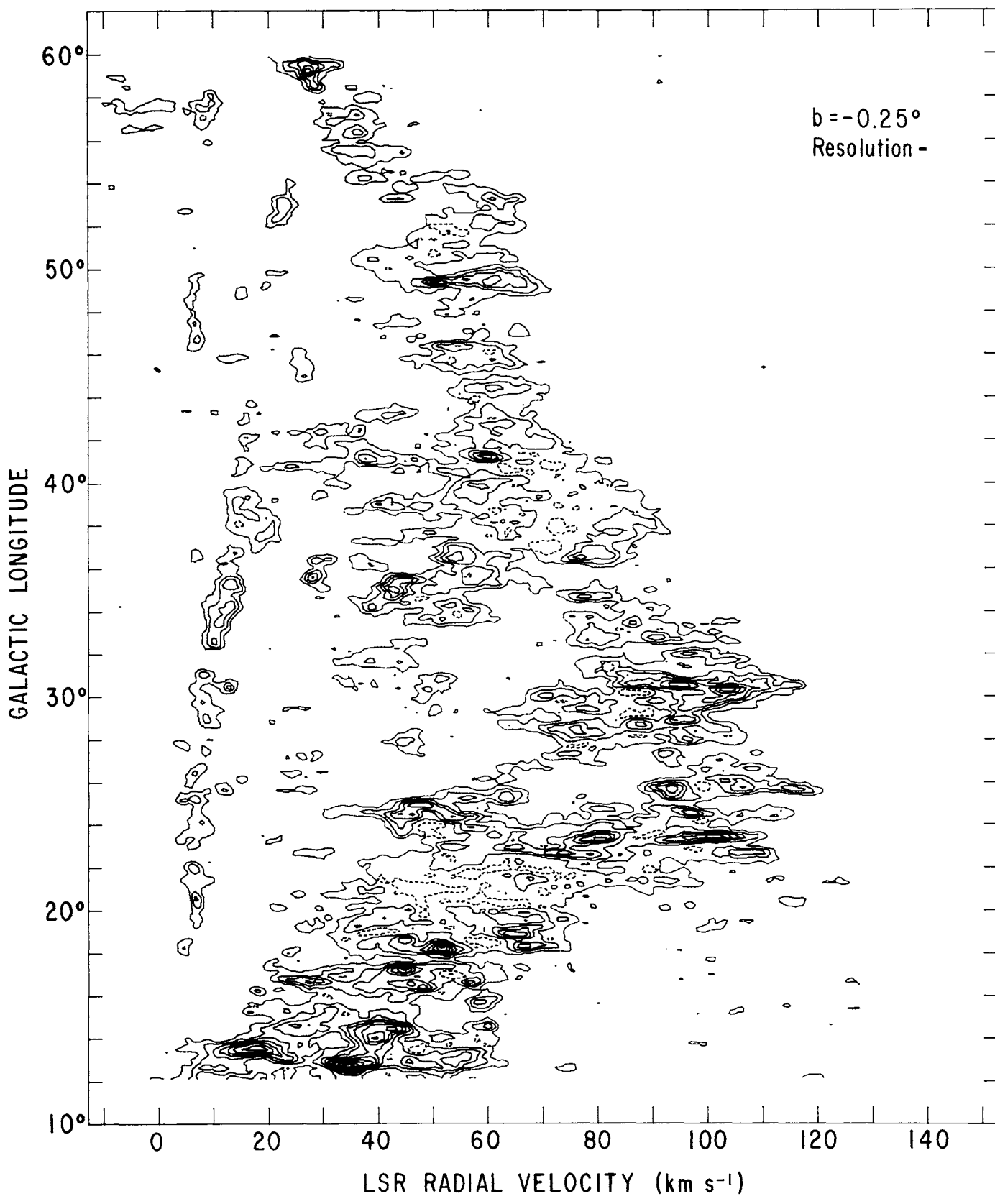


FIG. 5—Continued

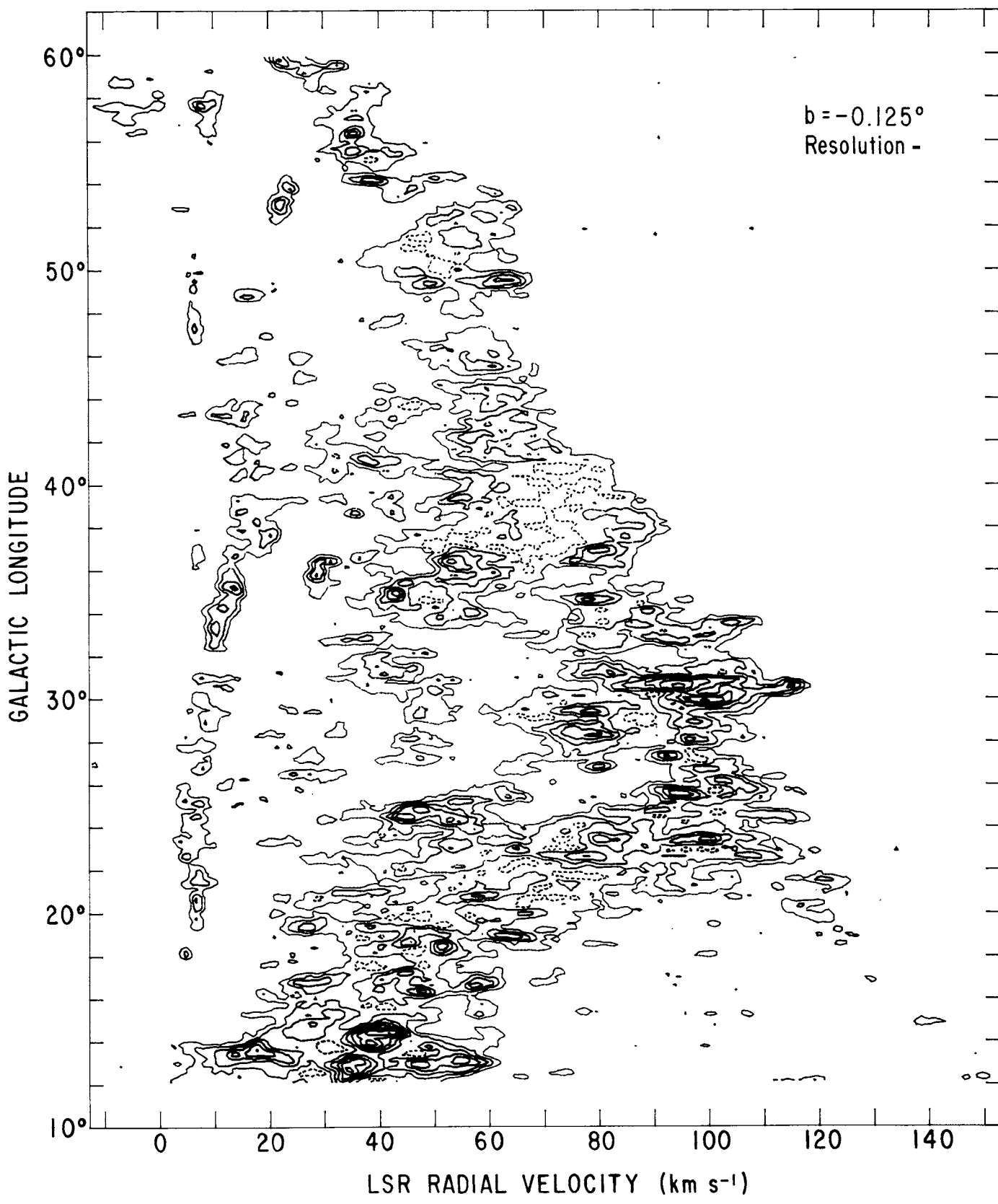


FIG. 5—Continued

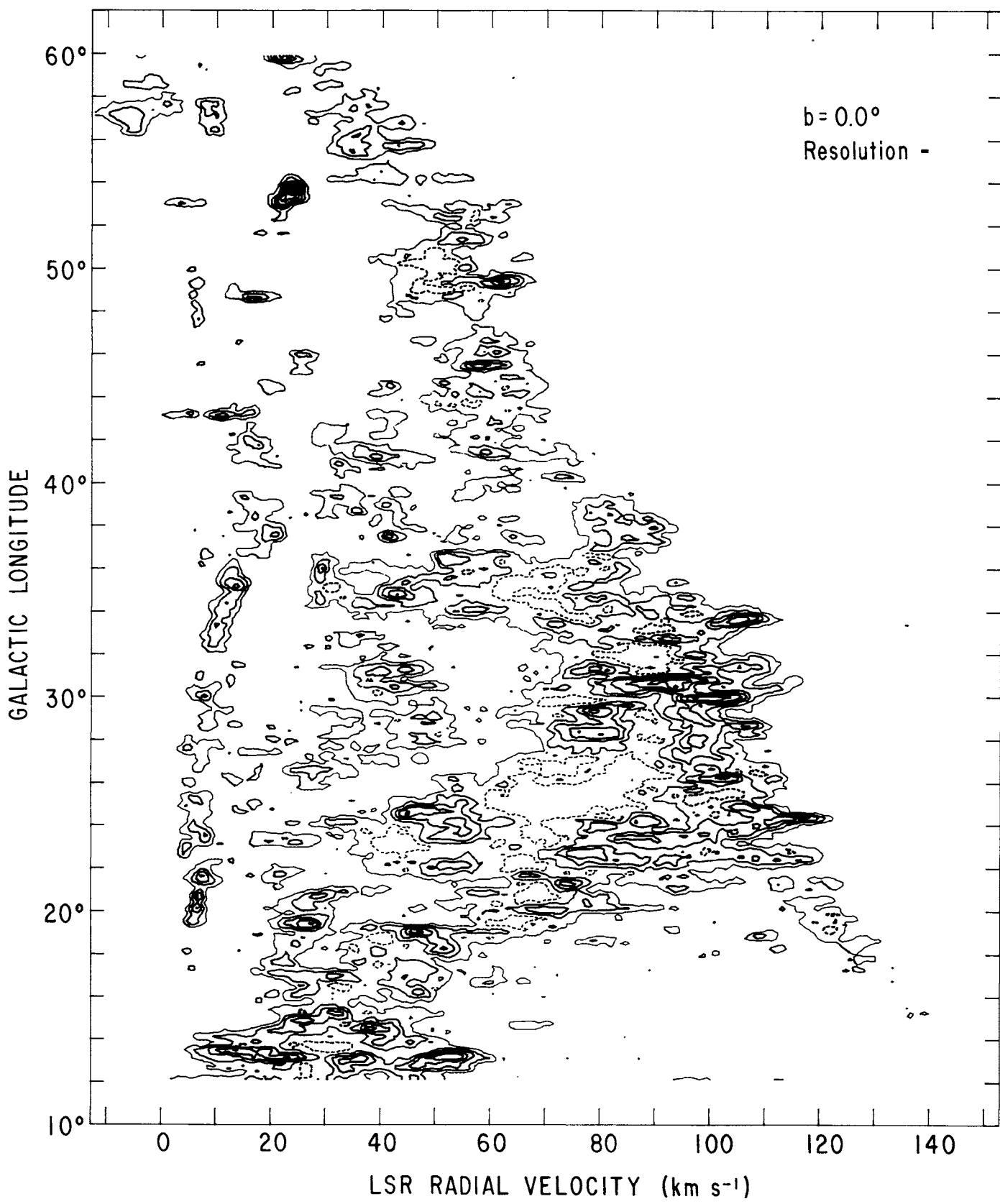


FIG. 5—Continued

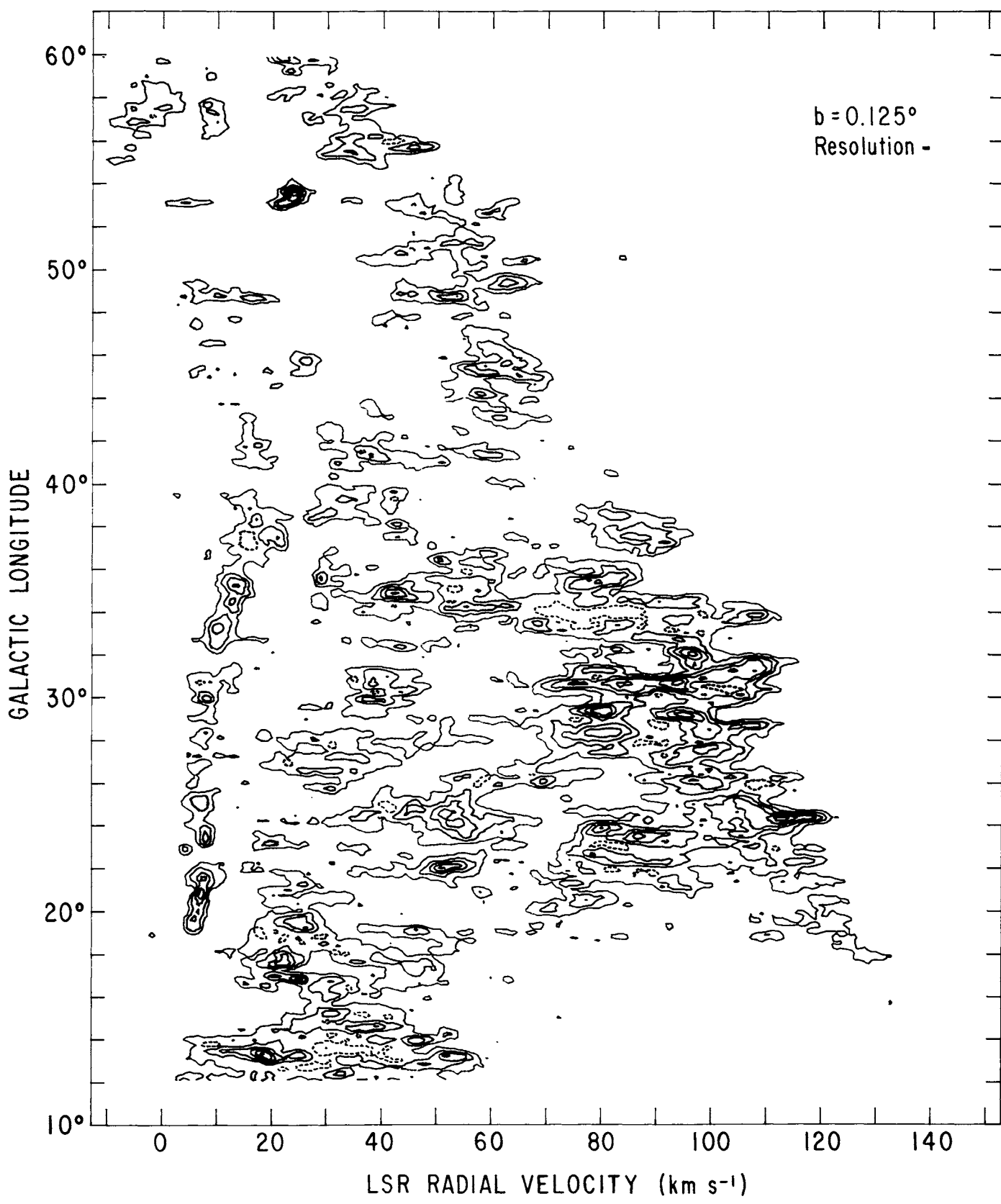


FIG. 5—Continued

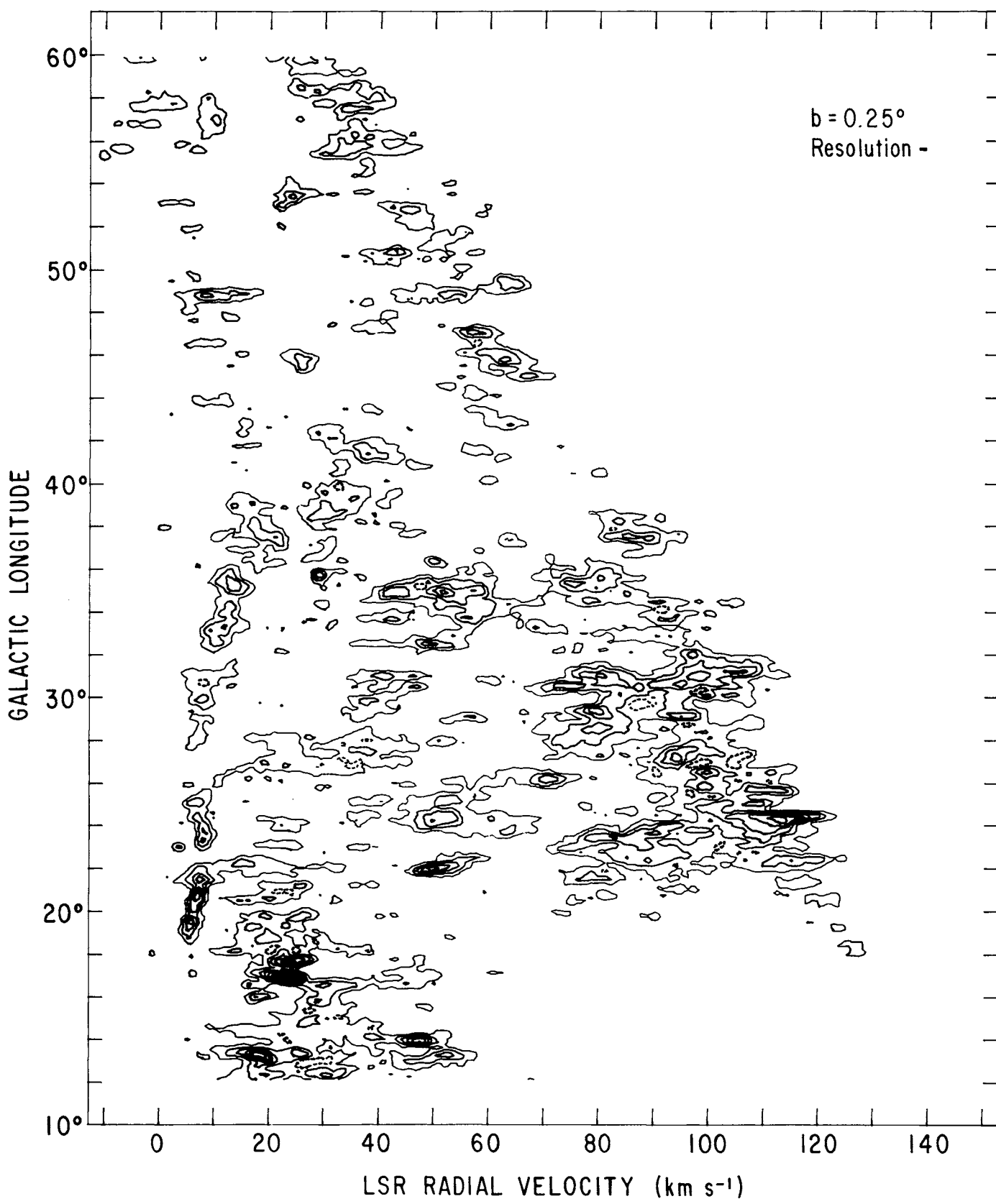


FIG. 5—Continued

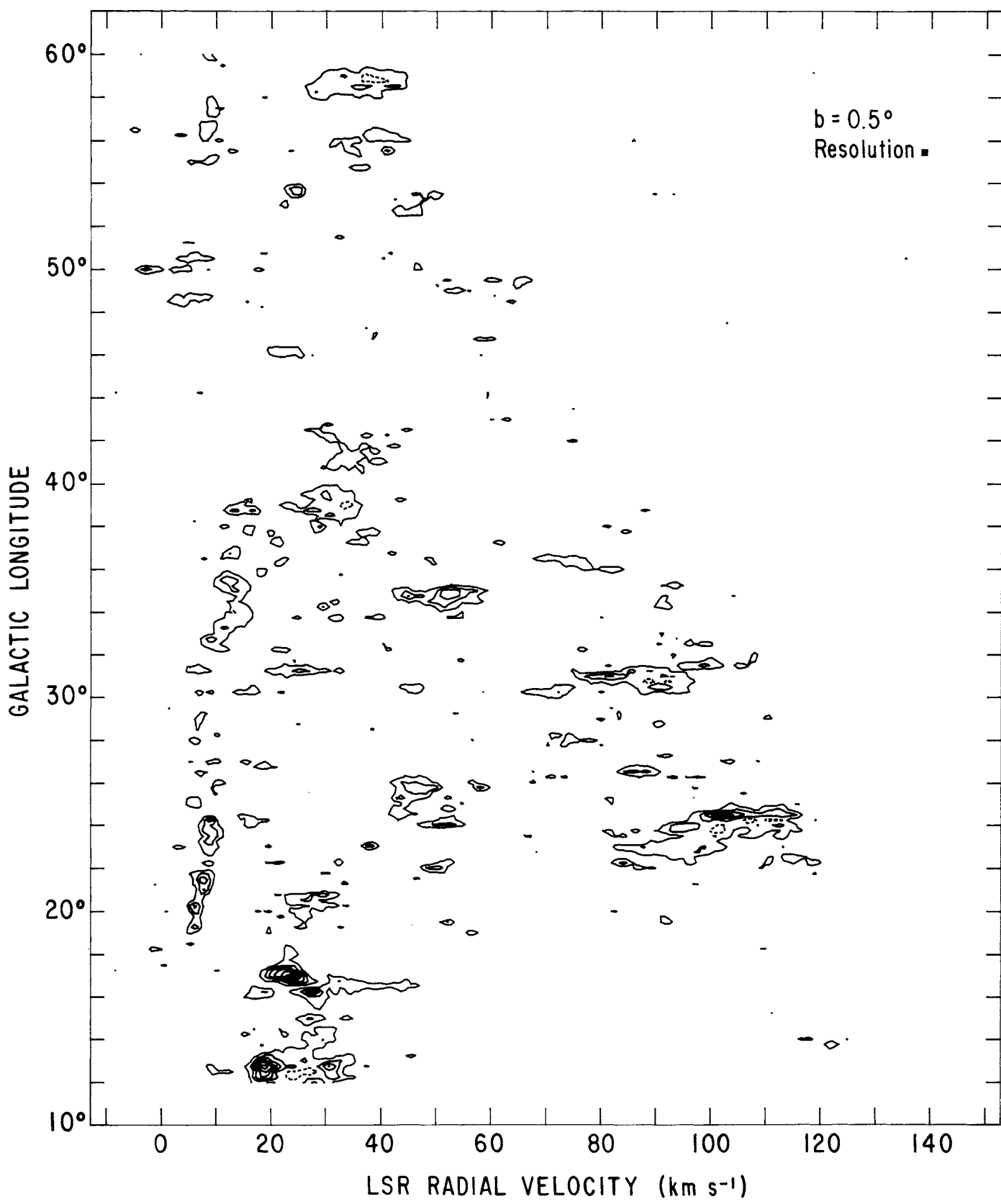


FIG. 5—Continued

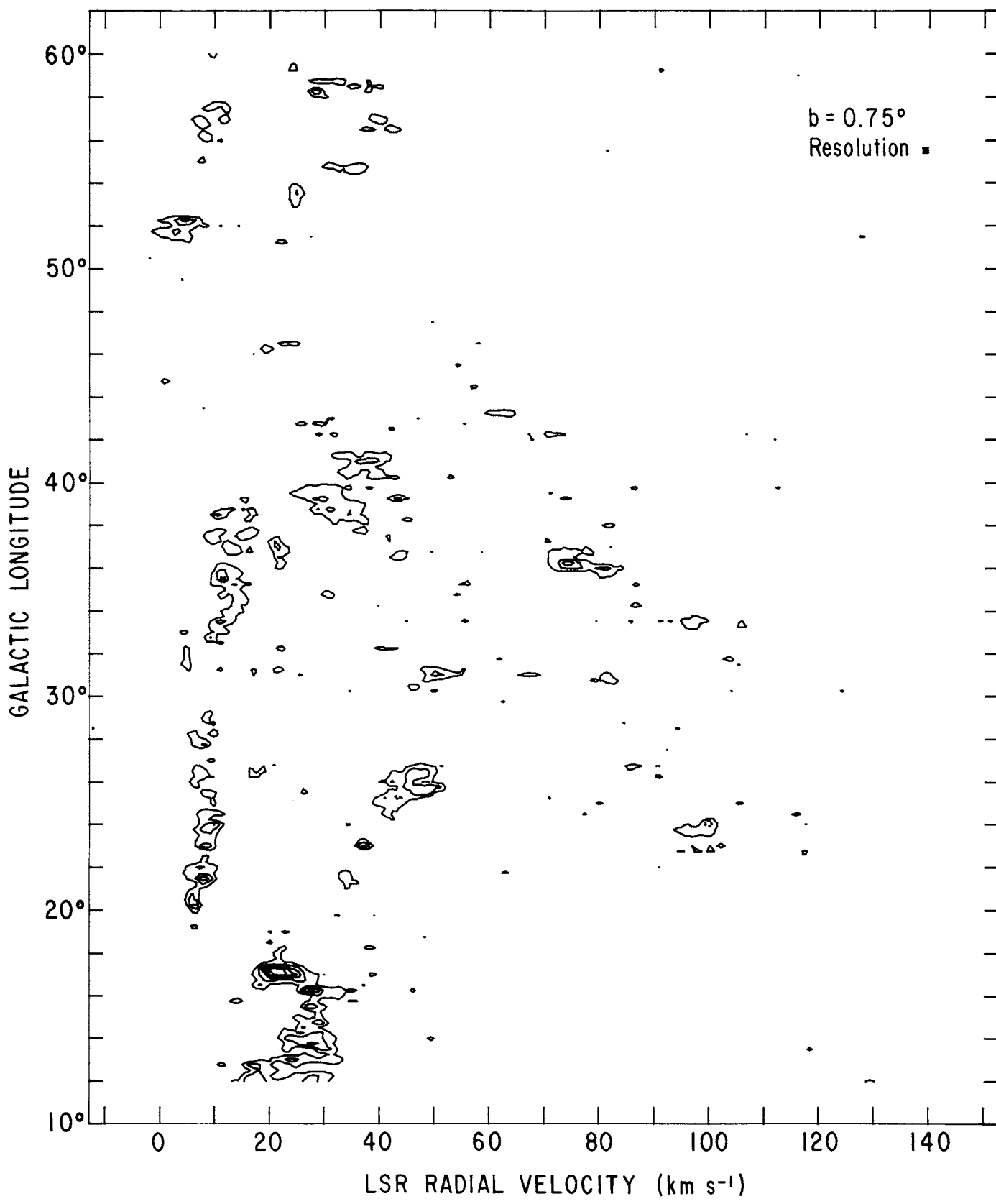


FIG. 5—Continued

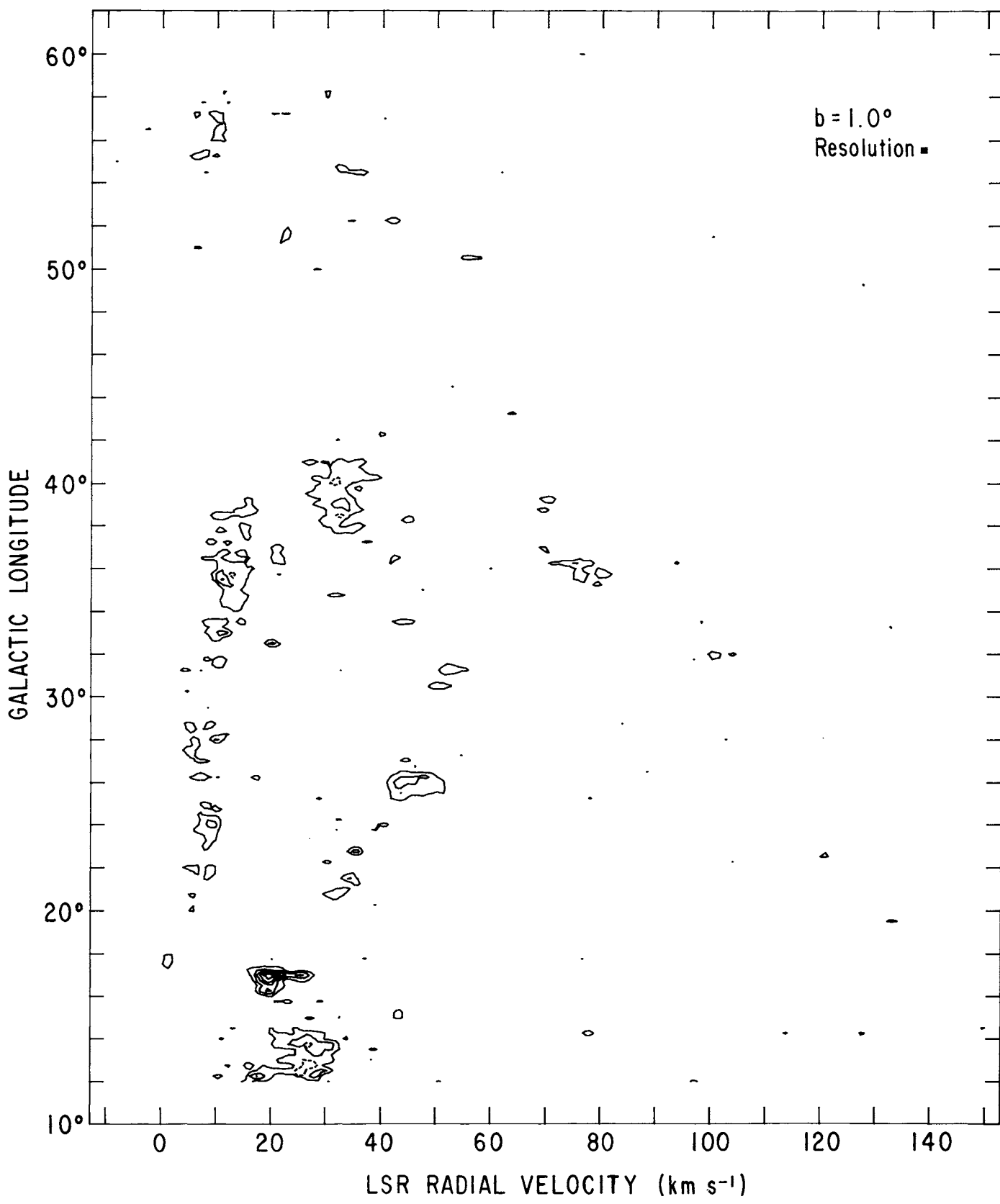


FIG. 5—Continued

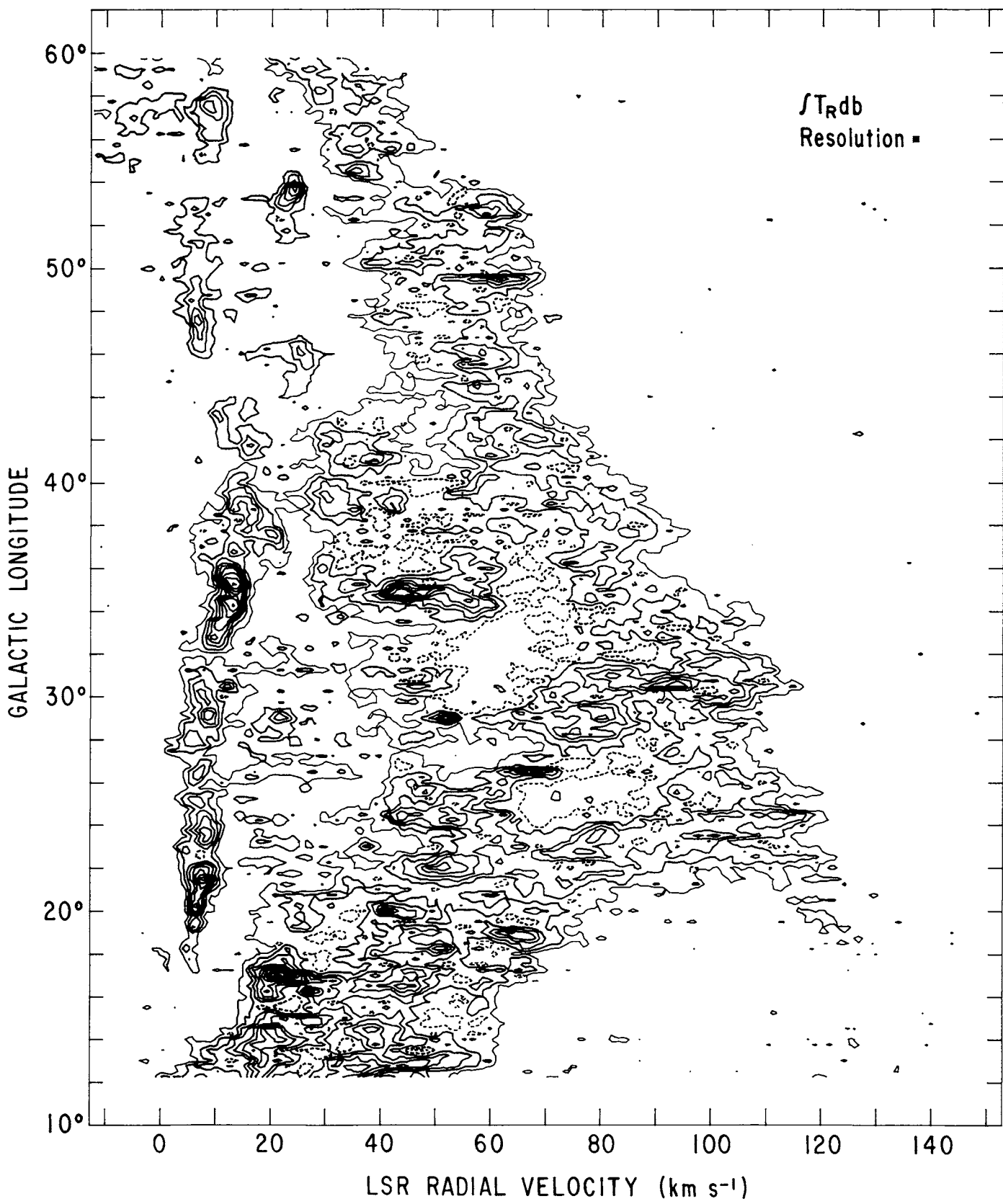


FIG. 6.—Longitude-velocity contour diagrams of CO emission integrated over latitude from  $-1^\circ$  to  $+1^\circ$ . Contours enclosing depressions (downgoing contours) are dotted. (a) The data at full resolution:  $0.25^\circ \times 1.3 \text{ km s}^{-1}$ . The contours are uniformly spaced at  $0.75, 1.50, \dots \text{K degrees of arc}$ . (b) The data smoothed to half the original resolution:  $0.5^\circ \times 2.6 \text{ km s}^{-1}$ . The contours are uniformly spaced at  $0.5, 1.0, \dots \text{K degrees of arc}$ . (c) The data smoothed to one-fourth the original resolution:  $1.0^\circ \times 5.2 \text{ km s}^{-1}$ . The contours are uniformly spaced at  $0.25, 0.50, \dots \text{K degrees of arc}$ .

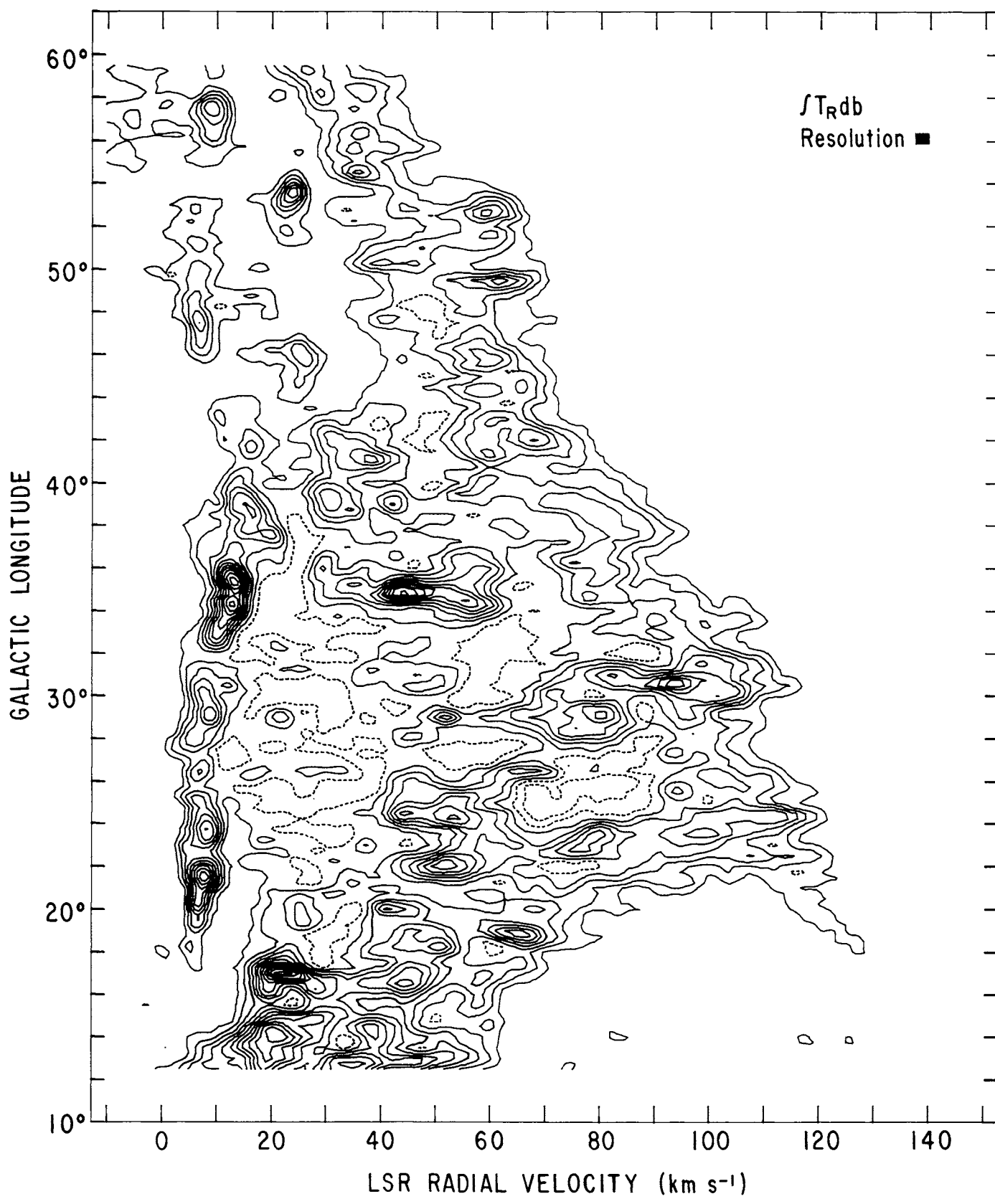


FIG. 6—Continued

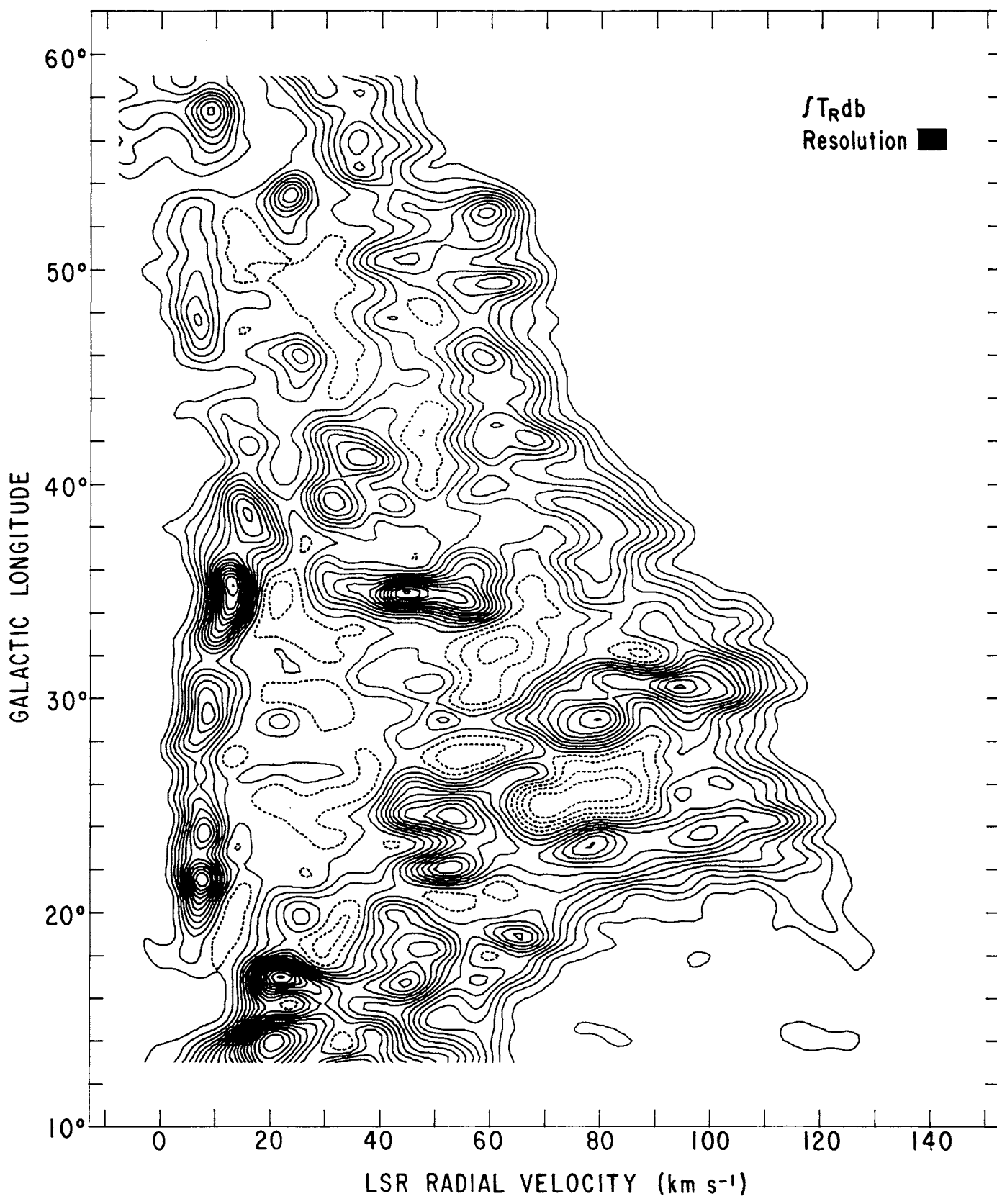


FIG. 6—Continued

the spectra had linear baselines removed and were smoothed to a velocity resolution of  $1.3 \text{ km s}^{-1}$ . The residual baseline, as observed in emission-free spectra at the upper and lower edges of the survey in latitude, is small compared with the noise.

Figure 4, the first of several contour diagrams of the data, is a spatial map that shows the CO emission integrated over the entire spectral range observed. The distant inner Galaxy appears here as a strip about  $1^\circ$  wide in latitude and, at the low longitudes where emission from the molecular ring is observed, slightly depressed below the  $b = 0^\circ$  plane. Local maxima at the tangent points, the classic signs of spiral arms on such "continuum" maps, appear for the three inner arms identified in Cohen *et al.* (1980), namely, the 4 kpc arm at  $l = 24^\circ$ , the Scutum arm at  $l \approx 30.5^\circ$ , and, weakly, the Sagittarius arm at  $l \approx 49.5^\circ$ . In spite of uncertainties that result from the high optical depth of CO in large clouds and other factors, the intensities on this map are probably the best available index of the column density of molecular matter and thus are the numbers to compare to  $\gamma$ -ray, IR, and other continuum data (see, for example, Myers *et al.* 1985).

A series of longitude-velocity diagrams, one for each latitude observed, is shown in Figure 5. The displacement of the inner Galactic arms (seen here at  $v > 20 \text{ km s}^{-1}$ ) below the  $b = 0^\circ$  plane is clearly illustrated by the difference between the  $b = +0.5^\circ$  and  $b = -0.5^\circ$  diagrams. The low intensity of the distant emission on the  $b = +1^\circ$  and  $b = -1^\circ$  maps demonstrates that very little molecular matter lies beyond the latitude range of the survey.

In addition to the arms, many individual clouds and cloud complexes stand out. The most conspicuous, the local, low-velocity feature which runs from  $l \approx 18^\circ$  to  $l = 40^\circ$  and extends well beyond the latitude edge of the present survey, has now been mapped more fully at low resolution (Dame and Thaddeus 1985) and identified as the Aquila Rift in the Milky

Way. A few other prominent objects seen on these maps are the molecular clouds associated with M17 ( $l \approx 14^\circ$  at  $20 \text{ km s}^{-1}$ ), W44 ( $l \approx 35^\circ$ ,  $b < 0^\circ$  at  $44 \text{ km s}^{-1}$ ), and W51 ( $l \approx 49^\circ$ ,  $b \approx -0.5^\circ$  at  $59 \text{ km s}^{-1}$ ).

The final contour plots are a set of summary  $l$ - $v$  diagrams representing the CO emission integrated over latitude. The first (Fig. 6a), at the highest spatial resolution for which our data are complete ( $0.25^\circ$ ) and smoothed (as are all the data here) to  $1.3 \text{ km s}^{-1}$ , is a quantitative representation of the same data shown in gray scale in Cohen *et al.* (1980). To improve the signal-to-noise ratio and emphasize the large-scale Galactic features, this diagram was smoothed in two steps to one-half and one-fourth the original resolution, i.e., to  $2.6 \text{ km s}^{-1}$  by  $0.5^\circ$  (Fig. 6b) and to  $5.2 \text{ km s}^{-1}$  by  $1.0^\circ$  (Fig. 6c). The sensitivity at the lower resolution is much better than in any published large-scale CO survey: each resolution element represents more than 50 of the original spectra for a total integration time of more than 10 hours, yet the resolution is still adequate to discern the major features noted in Cohen *et al.* (1980). For example, the large "holes," inside the loop of the Sagittarius arm ( $l = 42^\circ$ ,  $v = 48 \text{ km s}^{-1}$ ), between the Sagittarius and Scutum arms ( $l = 32^\circ$ ,  $v = 62 \text{ km s}^{-1}$ ), and between the Scutum and the 4 kpc arms ( $l = 25^\circ$ ,  $v = 75 \text{ km s}^{-1}$ ) become even more distinct when the signal-to-noise ratio is improved and the resolution smoothed to the scale of these largely empty areas.

Figure 7 is a graph of the CO emission integrated over both velocity and latitude as a function of Galactic longitude. The enhanced emission from the "molecular ring" region of the Galaxy ( $l < 40^\circ$ ) is dominated by four prominent peaks labeled A–D. An examination of the longitude-velocity diagrams reveals that peaks A and D are produced by relatively nearby, low-velocity clouds, while peaks B and C are produced by more distant, high-velocity clouds. Feature A corre-

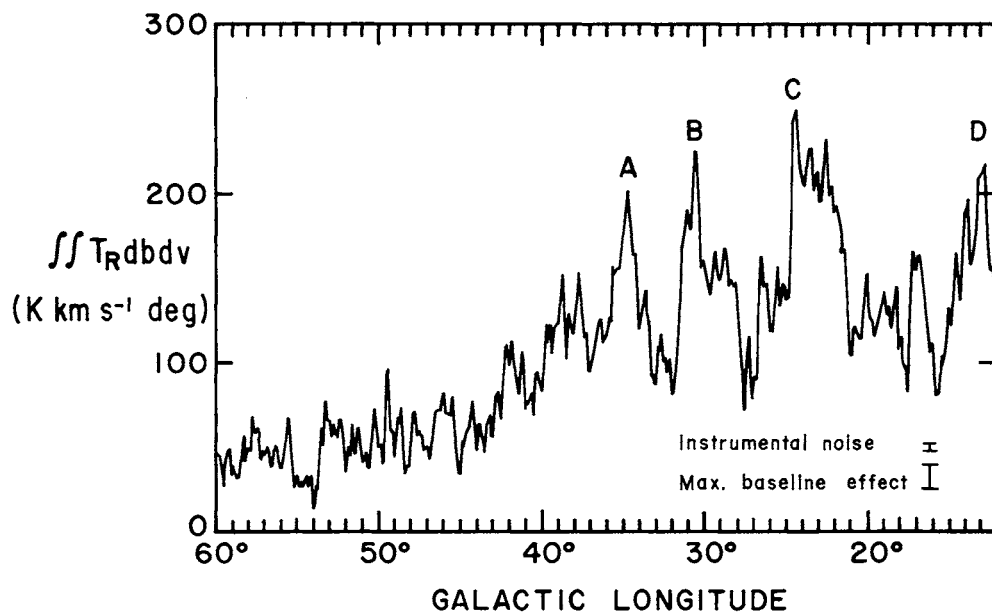


FIG. 7.—CO emission integrated over Galactic latitude from  $-1^\circ$  to  $+1^\circ$  and velocity from  $-13$  to  $153 \text{ km s}^{-1}$  as a function of Galactic longitude. The error bars represent our best  $1\sigma$  estimates of the contributions from receiver noise and baseline curvature. The letters A–D label prominent features discussed in the text.

sponds to a very large, CO-bright molecular complex associated with the supernova remnant W44 at a distance of 3 kpc. Feature *D* is produced primarily by the large molecular complex in the vicinity of M17 at 2 kpc ( $19 \text{ km s}^{-1}$ ), with smaller contributions from clouds at 4 and 6 kpc (35 and 50  $\text{km s}^{-1}$ ). Features *B* and *C* are produced by numerous, much more distant clouds spread along the tangent regions of the two major spiral arms of the inner Galaxy, the Scutum and 4 kpc arms. In both cases the intensity drops by almost a factor of 2 as our line of sight leaves the outer edge of the arm (i.e., toward higher longitudes), suggesting that the emission from the molecular ring derives mostly from the two spiral arms.

The data reported in this paper have been used in several studies. Cohen *et al.* (1980) used them to discuss the concentration of molecular clouds to spiral arms. Dame *et al.* (1986) extracted the largest molecular complexes from the

data and determined their locations and properties. Myers *et al.* (1986) compared the survey with IR and H II surveys to study star formation in the inner Galaxy. Thaddeus and Chanan (1985) used Dame's (1983) measurement of the thickness of the molecular layer to study the periodic perturbation of comets in the Oort cloud as the solar system oscillates about the Galactic plane. A complete analysis of the radial distribution of molecular clouds, including results from the recent Columbia Southern Hemisphere survey, will be published elsewhere.

We thank the many people who contributed to the design and construction of the 1.2 m telescope, including G. Chin, H.-I. Cong, J. Grange, D. Held, A. R. Kerr, D. Mumma, E. S. Palmer, and G. R. Tomasevich. A. Smith assisted greatly in the data reduction.

## APPENDIX A

### CALIBRATION

#### I. METHOD

At the Columbia telescope the absolute intensities of spectral lines are calibrated against a blackbody by the same "chopper wheel" method used at the NRAO 11 m and several other telescopes. Following Kutner (1978), the calibration formula is

$$T_{\text{line}} = (V_{\text{line}} / V_{\text{cal}}) W,$$

where  $T_{\text{line}}$  is the calibrated line temperature, corrected for antenna efficiency and atmospheric absorption;  $V_{\text{line}}$  is the receiver response to the source in volts;  $V_{\text{cal}} = V_{\text{chopper}} - V_{\text{sky}}$  is the difference in receiver output between an ambient temperature blackbody (the chopper wheel) and the sky at the source elevation; and  $W$  is a function given in Kutner (1978, his eq. [7]), approximately equal to the ambient temperature.

Specifically,  $W$  is a function of the following parameters:  $E$ , the source elevation;  $T_{\text{chopper}}$ , the temperature of the chopper wheel;  $g_i/g_s$ , the ratio of the receiver gains in the image and signal sidebands;  $T_{\text{oi}}, T_{\text{os}}$ , the effective temperatures of the atmospheric oxygen in the image and signal sidebands;  $T_w$ , the effective temperature of the atmospheric water;  $\tau_{\text{os}}, \tau_{\text{oi}}$ , the opacity per air mass of the oxygen in each sideband;  $\tau_w$ , the opacity per air mass of the water; and  $\eta_f$  ( $= \eta_{\text{source}} / \eta_{\text{sky}}$ ), the fraction of the forward beam on the source.

$V_{\text{line}}$  and  $E$  are accurately known. Because the entire telescope is in a temperature-controlled astrodome,  $T_{\text{chopper}}$  is known to within  $\pm 2$  K. The determination of the other parameters in the calibration equations is discussed below.

1. *Calibration signal,  $V_{\text{cal}}$ .*—The major difficulty in measuring  $V_{\text{cal}}$  is providing a well-matched blackbody load. We used a piece of Emerson and Cummin type AN72 Ecosorb. The reflection coefficient of this absorber is not specified at millimeter wavelengths, but the effects of reflections on the measurement of  $V_{\text{cal}}$  can be easily observed. When the position of a piece of Ecosorb held in front of the horn is varied by a wavelength, the receiver output varies by about 4%, but if the Ecosorb is tilted by more than  $10^\circ$  in any direction, the output varies by less than 0.5%. All observations at the Columbia telescope are made with the chopper blade bent by  $18^\circ$ .

2. *Sideband gain ratio,  $g_i/g_s$ .*—The gains of the receiver in each sideband were measured in the laboratory. With the local oscillator klystron set to 113.9 GHz, the gain from the resonant ring input through the 150 MHz IF output was found to be  $g_i = 64.7 \pm 0.5$  dB at 112.5 GHz (lower sideband) and  $g_s = 64.8 \pm 0.5$  dB at 115.3 GHz (upper sideband). We conclude that  $g_i/g_s = 1.0 \pm 0.1$ .

3. *Forward coupling efficiency,  $\eta_f$ .*—For sources larger than the main beam but smaller than a few degrees,  $\eta_f$  is roughly the fraction of the forward power in the main beam. (Most of the power is received either in the main beam or in distant sidelobes; nearby sidelobes contain only a few percent of the power.) Three effects remove power from the main beam: spillover of feed power around the secondary; scattering from the aperture blockage of the secondary mirror and its support structure; and diffraction through the finite aperture of the main mirror.

The spillover can be reliably calculated from the theoretical radiation pattern of the scalar feed horn; about 7% of the power goes around the secondary and 3% through a small hole in the center of the secondary. Some additional spillover results from power reflected from the secondary past the edge of the primary to the ground, but, estimated to be less than 1%, it was ignored. Thus, 90% of the horn power actually illuminates the main dish. A rough calculation of the effects of the blockage shows that diffraction and reflection by the support arms and the secondary scatter about 9% of the power into the sky at large angles and

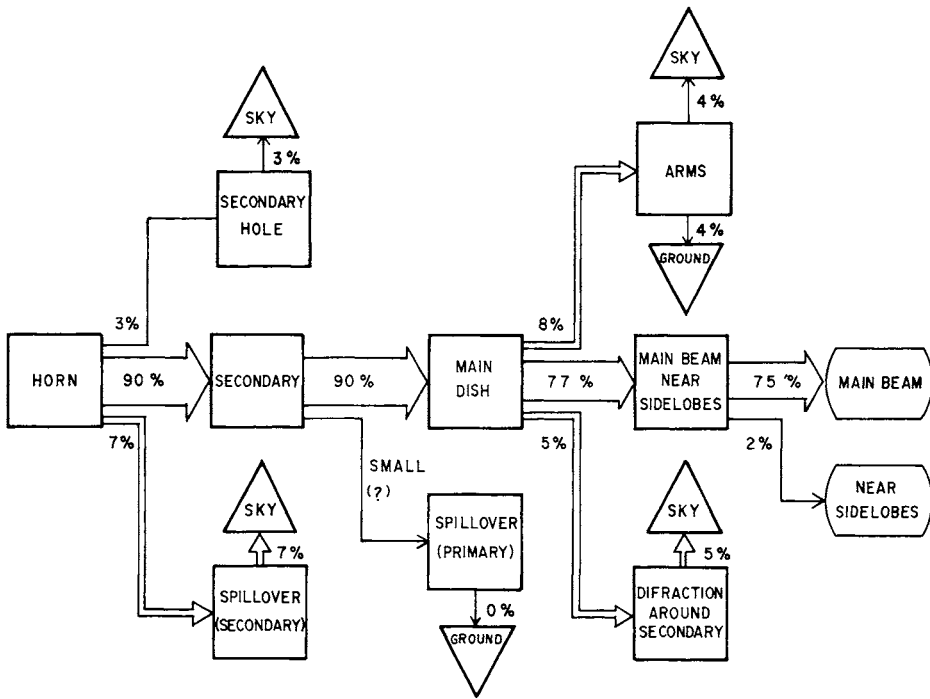


FIG. 8.—Schematic representation of sources of power loss from the main antenna beam. The pattern of the scalar feed horn was calculated with the computer code of Potter (1972); other contributions were from physical optics in the limit of a small blockage.

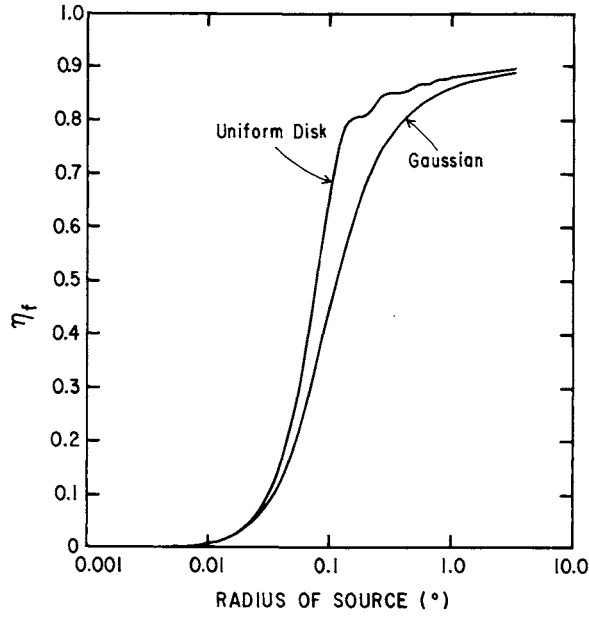


FIG. 9

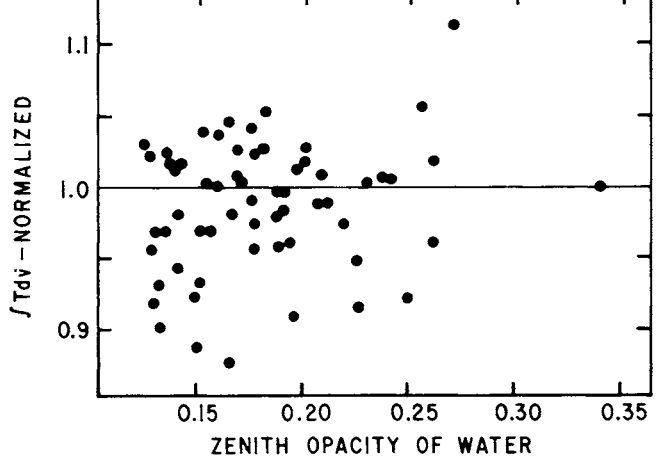


FIG. 10

FIG. 9.—Forward coupling efficiency vs. source size for both a disk-shaped source and a Gaussian source distribution. The parameter  $\eta_f$  is the efficiency by which  $T_A^*$  (measured directly by the chopper wheel calibration) must be divided to obtain the radiation temperature,  $T_R = \lambda 2I_r/2k$ , where  $I_r$  is the line intensity in standard units. In the notation of Kutner, Mundy, and Howard (1984),  $\eta_f = \eta_c \eta_{fss}$ , where  $\eta_c$  and  $\eta_{fss}$  are the coupling and forward spillover efficiencies. The efficiency  $\eta_f$  was calculated from scalar Kirchhoff diffraction theory and included diffraction from the main and secondary mirrors and the secondary-mirror support arms; the 90% limit at wide angles was derived from the calculated horn pattern. For the Gaussian distribution, the radius represents the half-width at half-maximum.

FIG. 10.—Variation in calibration with measured optical depth of atmospheric water vapor. Daily test observations of Orion A were integrated over velocity and normalized to the average value. The points include the normal range of weather conditions, temperatures from  $-13^\circ\text{C}$  to  $15^\circ\text{C}$ , relative humidities from 23% to 73%, and occasional cloudy days, but are somewhat biased toward lower elevations, 1.4–2.1 atmospheres. The standard deviation from the mean is 5%, and the peak deviation is 13%.

about 4% of the power into the ground. Finally, for the 13 dB edge illumination we used, diffraction from the primary aperture puts roughly 2% of the power into the near sidelobes (Goldsmith 1977). Adding these three effects, 96% of the power falls on the sky, and 75% remains in the main beam (Fig. 8). Thus, for a source filling the main beam,  $\eta_f = 0.75/0.96 = 0.78$ .

As a check and to determine how  $\eta_f$  varies with source size, a second estimate was made using scalar diffraction theory to calculate the antenna pattern (Cohen 1978) to 10° off-axis. For a uniform source that just fills the main beam this estimate yields  $\eta_f = 81\%$ , in good agreement with the previous result (Fig. 9). Since an estimate of  $\eta_f$  as a function of source size was useful, we used this second estimate to calibrate the data.

Most of our data required an additional correction to the efficiency. The pyramidal horn used as a feed before 1979 October, unlike the scalar horn used afterward, radiates a substantial fraction of power in distant sidelobes which are notoriously difficult to calculate. By comparing the antenna temperatures for the two horns, we determined that the spillover efficiency of the pyramidal horn is about 78%.

All our data were corrected for beam efficiency as if the source were a disk filling the main beam; specifically, a value of  $\eta_f = 0.81$  was used for the scalar feed and  $\eta_f = 0.69$  for the pyramidal horn. These values are thought to compensate reasonably well for power lost in distant sidelobes, yet are somewhat arbitrary and depend on the sizes of the sources as indicated in Figure 9.

**4. Effective oxygen temperatures,  $T_{os}$ ,  $T_{oi}$ , and opacities,  $\tau_{os}$ ,  $\tau_{oi}$ .**—The values used, calculated by the method of Meeks and Lilley (1963) for observations at 115.3 GHz in the upper sideband and for a standard winter atmosphere at 45° N latitude with a surface temperature of 0°C (Sissenwine 1969, Table 6), were  $T_{os} = 255$  K,  $T_{oi} = 254$  K,  $\tau_{os} = 0.21$ , and  $\tau_{oi} = 0.10$ . These values could be slightly improved by using Kutner's equations (2) and (3), resulting in weather-dependent changes of less than 0.04 in  $\tau_{oi}$  and  $\tau_{os}$  and 5°C in  $T_{os}$  and  $T_{oi}$ , giving total errors of less than 10% in the final calibration (see Kutner's Table 1). In fact, the actual errors are undoubtedly smaller because errors in the O<sub>2</sub> opacity will be largely canceled by corresponding errors in the water opacity as measured by antenna tipping.

**5. Effective temperature and opacity of water,  $T_w$  and  $\tau_w$ .**—These are determined from the antenna tippings done at least once every six hours.

## II. ACCURACY

We estimate that the calibration is accurate to within about 15%, with three roughly equal sources of error: receiver calibration, atmospheric model, and the calculation of  $\eta_f$ . For an individual source, the rms variation in calibration is 5% (Fig. 10).

Figure 11, which shows a complete set of the survey spectra, appears at the end of this paper.

## REFERENCES

- Altenhoff, W. J., Downes, D., Goad, L., Maxwell, A., and Rhinehart, R. 1970, *Astr. Ap. Suppl.*, **1**, 319.  
 Burton, W. B., and Gordon, M. A. 1978, *Astr. Ap.*, **63**, 7.  
 Burton, W. B., Gordon, M. A., Bania, T. M., and Lockman, F. J. 1975, *Ap. J.*, **202**, 30.  
 Cohen, R. S. 1978, Ph.D. thesis, Columbia University (published as NASA Tech. Memo. 78071).  
 Cohen, R. S., Cong, H.-I., Dame, T. M., and Thaddeus, P. 1980, *Ap. J. (Letters)*, **239**, L53.  
 Cohen, R. S., and Thaddeus, P. 1977, *Ap. J. (Letters)*, **217**, L155.  
 Cong, H.-I., Kerr, A. R., and Mattauch, R. J. 1979, *IEEE Trans. MTT*, **27**, 245.  
 Dame, T. M. 1983, Ph.D. thesis, Columbia University (published as NASA Tech. Paper 2288).  
 Dame, T. M., Elmegreen, B. G., Cohen, R. S., and Thaddeus, P. 1986, *Ap. J.*, in press.  
 Dame, T. M., and Thaddeus, P. 1985, *Ap. J.*, **297**, 751.  
 Frerking, M. A. 1980, private communication.  
 Goldsmith, P. F. 1977, *Bell System Tech. J.*, **56**, 1483.  
 Kutner, M. L. 1978, *Ap. Letters*, **19**, 81.  
 Kutner, M. L., Mundy, L., and Howard, R. J. 1984, *Ap. J.*, **283**, 890.  
 Kutner, M. L., and Ulich, B. L. 1981, *Ap. J.*, **250**, 341.  
 Linsky, J. L. 1973, *Solar Phys.*, **28**, 409.  
 Liszt, H. S., Burton, W. B., and Xiang, D.-L. 1984, *Astr. Ap.*, **140**, 303.  
 Mauzy, B. 1974, *256-Channel Filter Receivers* (Electronics Div. Internal Rep. No. 146; Charlottesville: NRAO).  
 Meeks, M. L., and Lilley, A. E. 1963, *J. Geophys. Res.*, **68**, 6.  
 Myers, P. C., Dame, T. M., Thaddeus, P., Cohen, R. S., Silverberg, R. F., Dwek, E., and Hauser, M. G. 1986, *Ap. J.*, **301**, 398.  
 Pace, C., and Payne, J. 1973, *A 512-Channel Integrator and Multiplexer* (Electronics Div. Internal Rep. No. 134; Charlottesville: NRAO).  
 Potter, P. D. 1972, in NASA Tech. Rept. JPL-TR-32-1526, **13**, 92.  
 Sanders, D. B., Solomon, P. M., and Scoville, N. Z. 1984, *Ap. J.*, **276**, 182.  
 Schwartz, P. R., Wilson, W. J., and Epstein, E. E. 1973, *Ap. J.*, **186**, 529.  
 Scoville, N. Z., and Solomon, P. M. 1975, *Ap. J. (Letters)*, **199**, L105.  
 Sissenwine, N. 1969, in *World Survey of Climatology*, Vol. 4, *Climate of the Free Atmosphere*, ed. D. F. Rex (Amsterdam: Elsevier), p. 5.  
 Solomon, P. M., Sanders, D. B., and Rivolo, A. R. 1985, *Ap. J. (Letters)*, **292**, L19.  
 Stark, A. A. 1983, private communication.  
 Thaddeus, P., and Chanan, G. A. 1985, *Nature*, **314**, 73.  
 Ulich, B. L., and Haas, R. W. 1976, *Ap. J. Suppl.*, **30**, 247.

R. S. COHEN, T. M. DAME, and P. THADDEUS: Goddard Institute for Space Studies, 2880 Broadway, New York, NY 10025

(This Page Intentionally Left Blank)

FIGURE 11

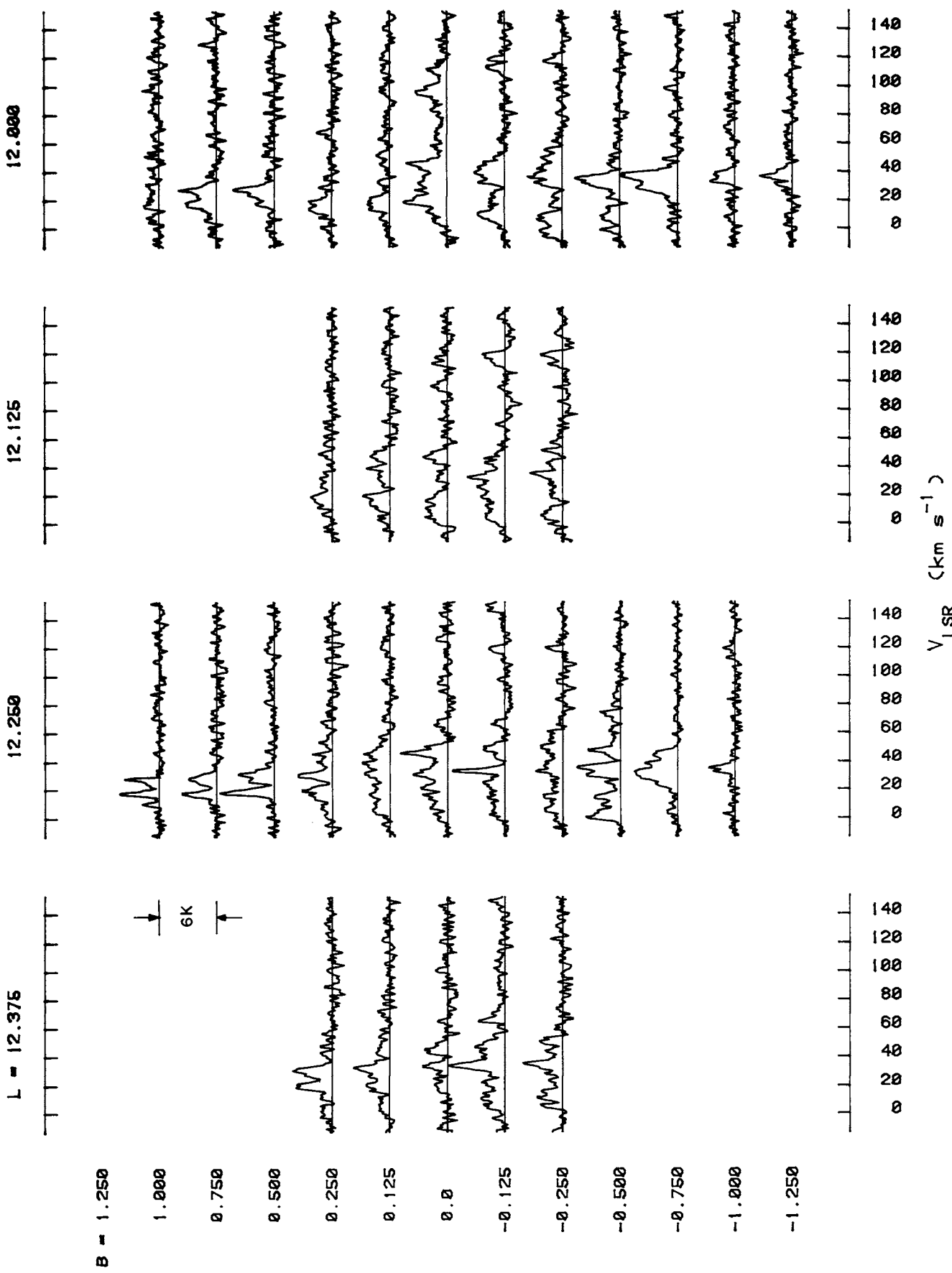


Fig. 11.—Spectra of the survey ordered according to Galactic longitude and latitude. Each spectrum consists of 256 channels of  $0.65 \text{ km s}^{-1}$  width; all have a linear baseline removed and were smoothed to a velocity resolution of  $1.3 \text{ km s}^{-1}$  (2 channels). Emission is in units of radiation temperature, i.e., antenna temperature corrected for atmospheric absorption and main beam efficiency.

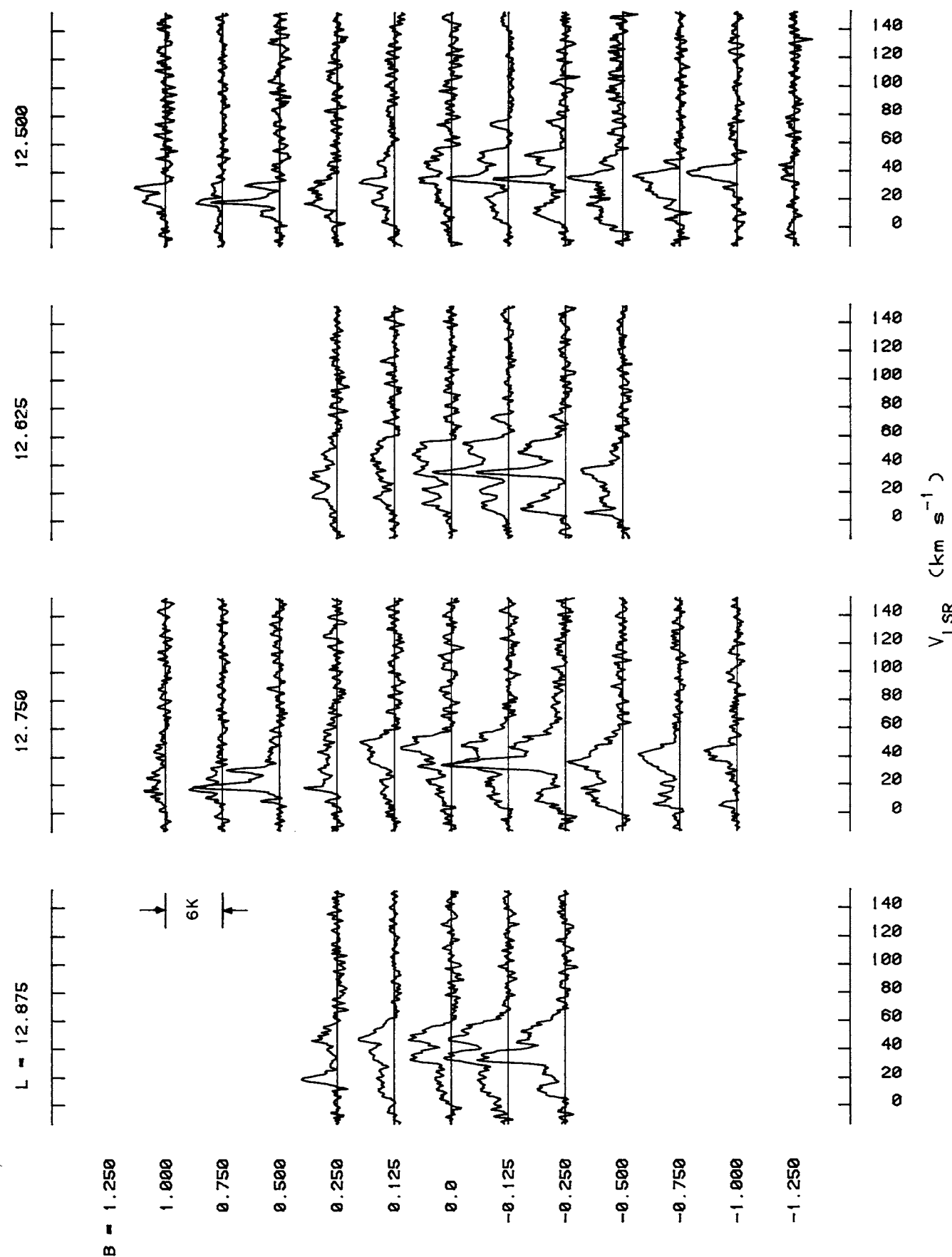


FIG. 11.—Continued

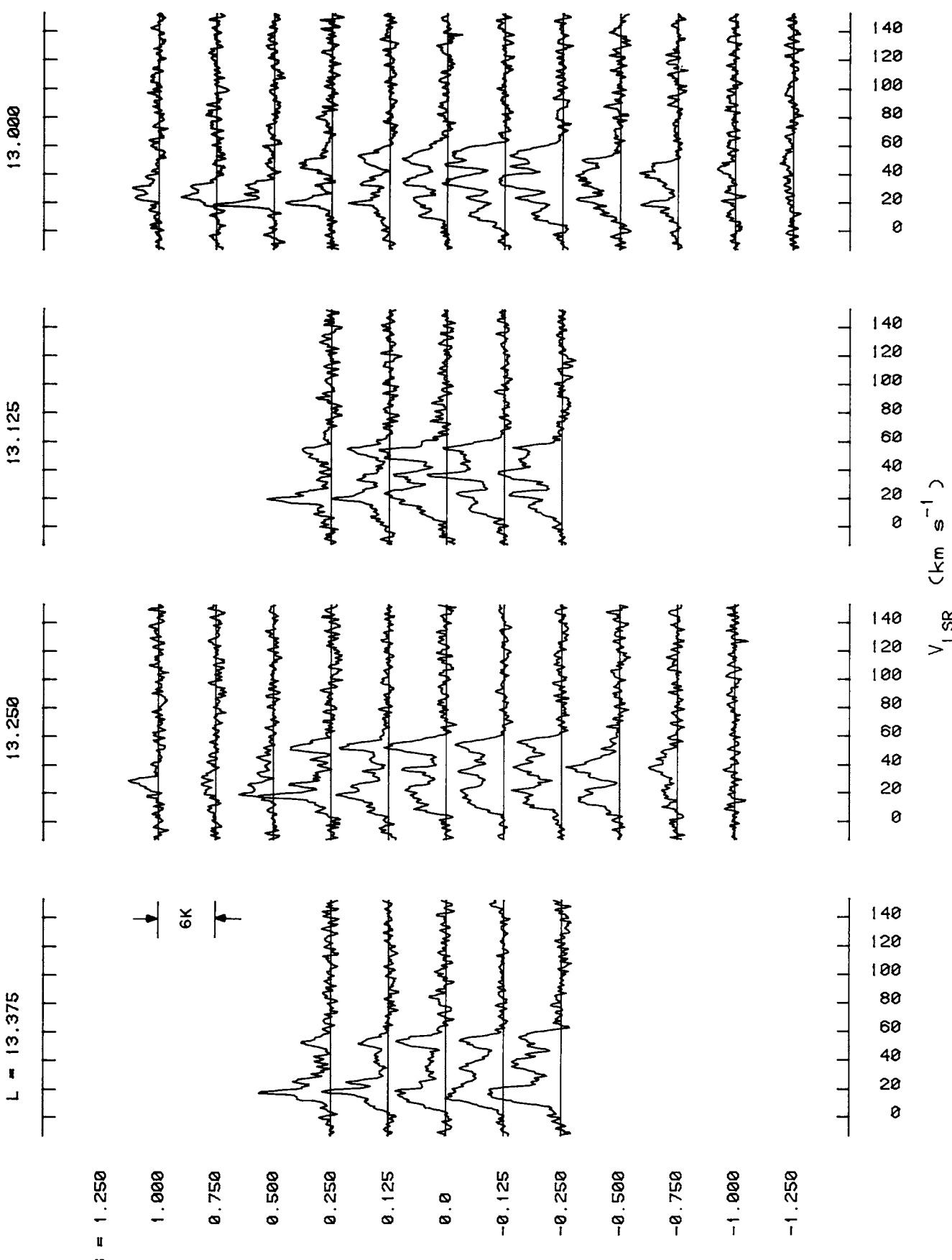


FIG. 11—Continued

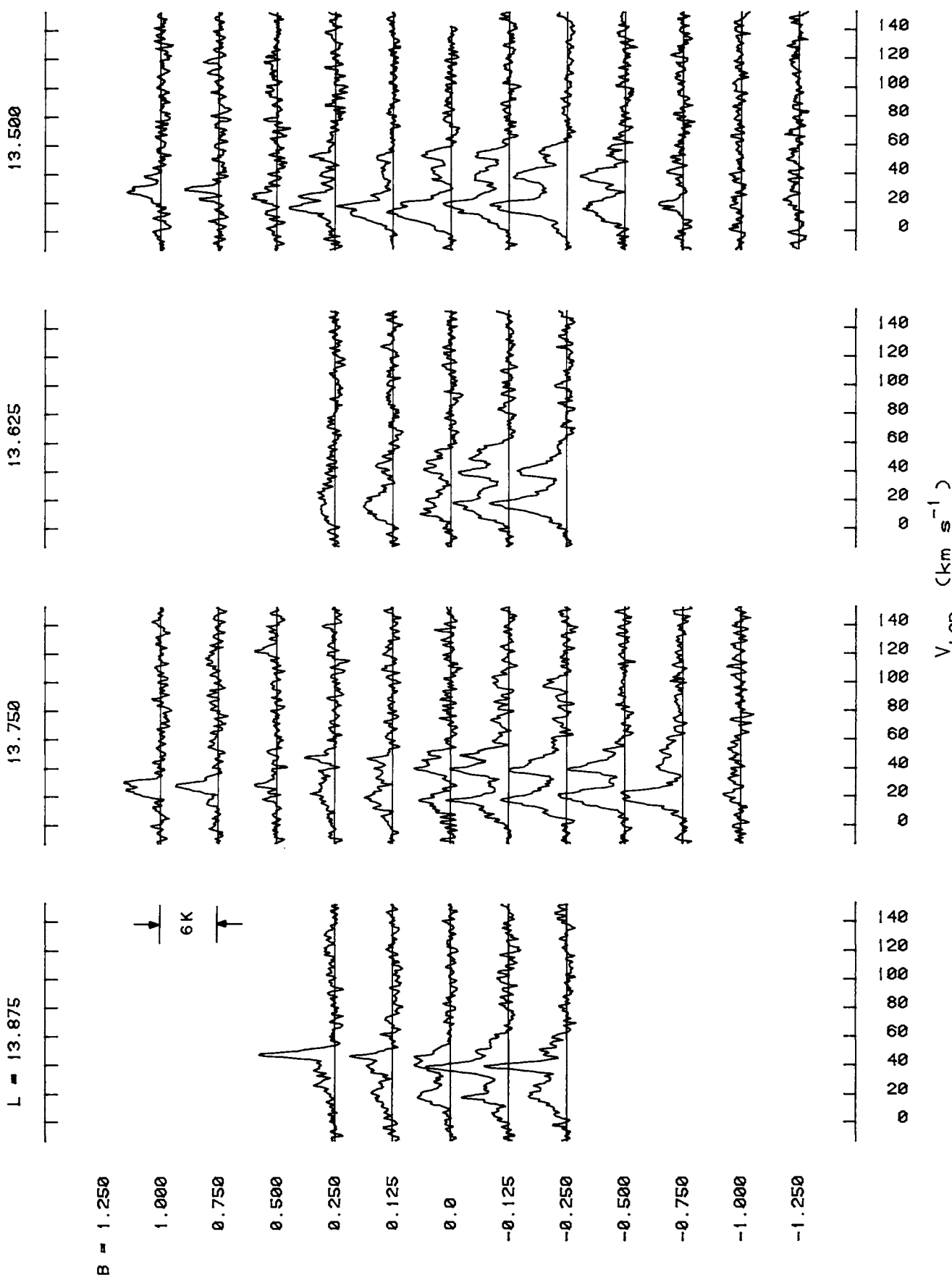


FIG. 11—Continued

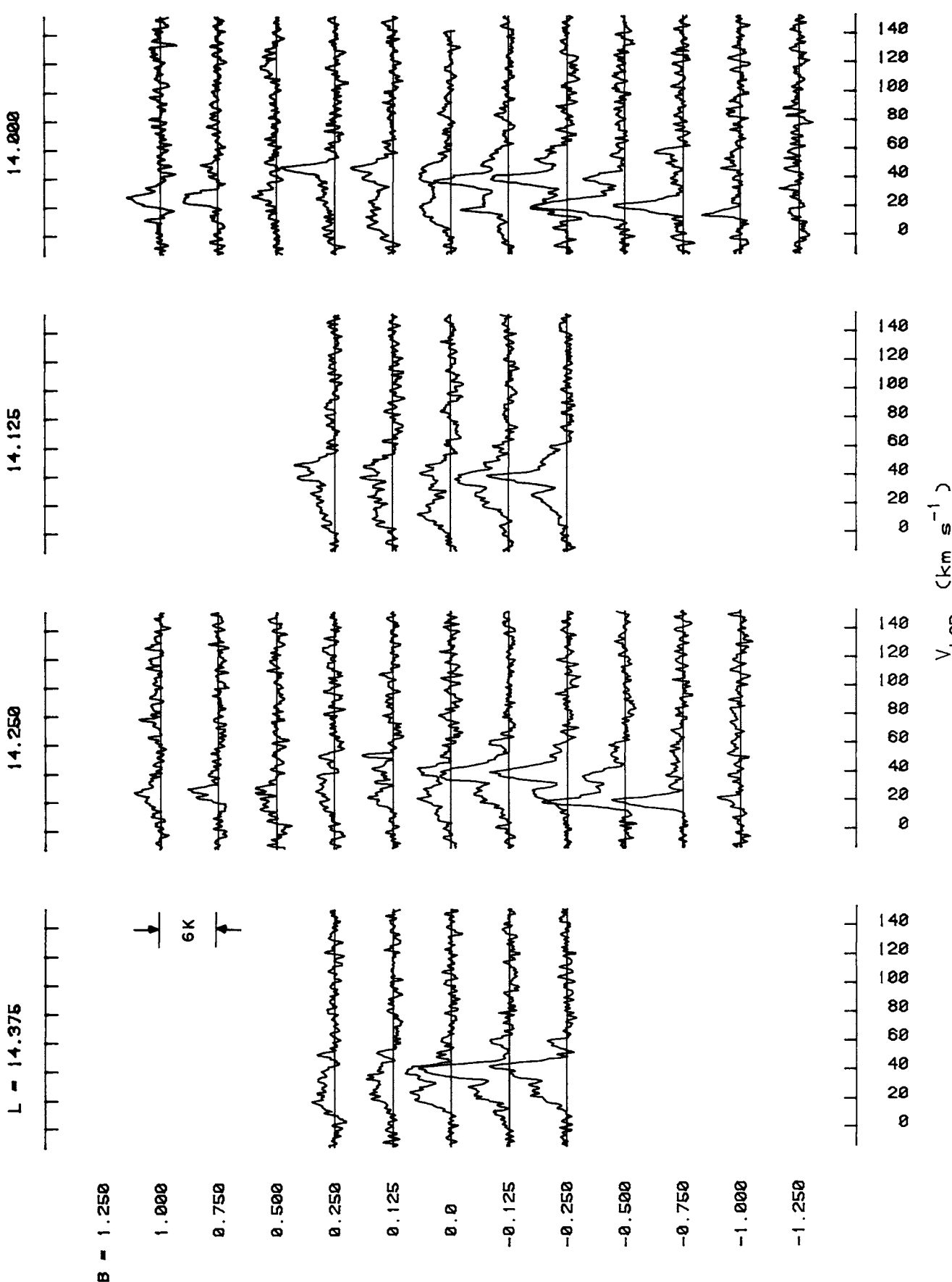


FIG. 11—Continued

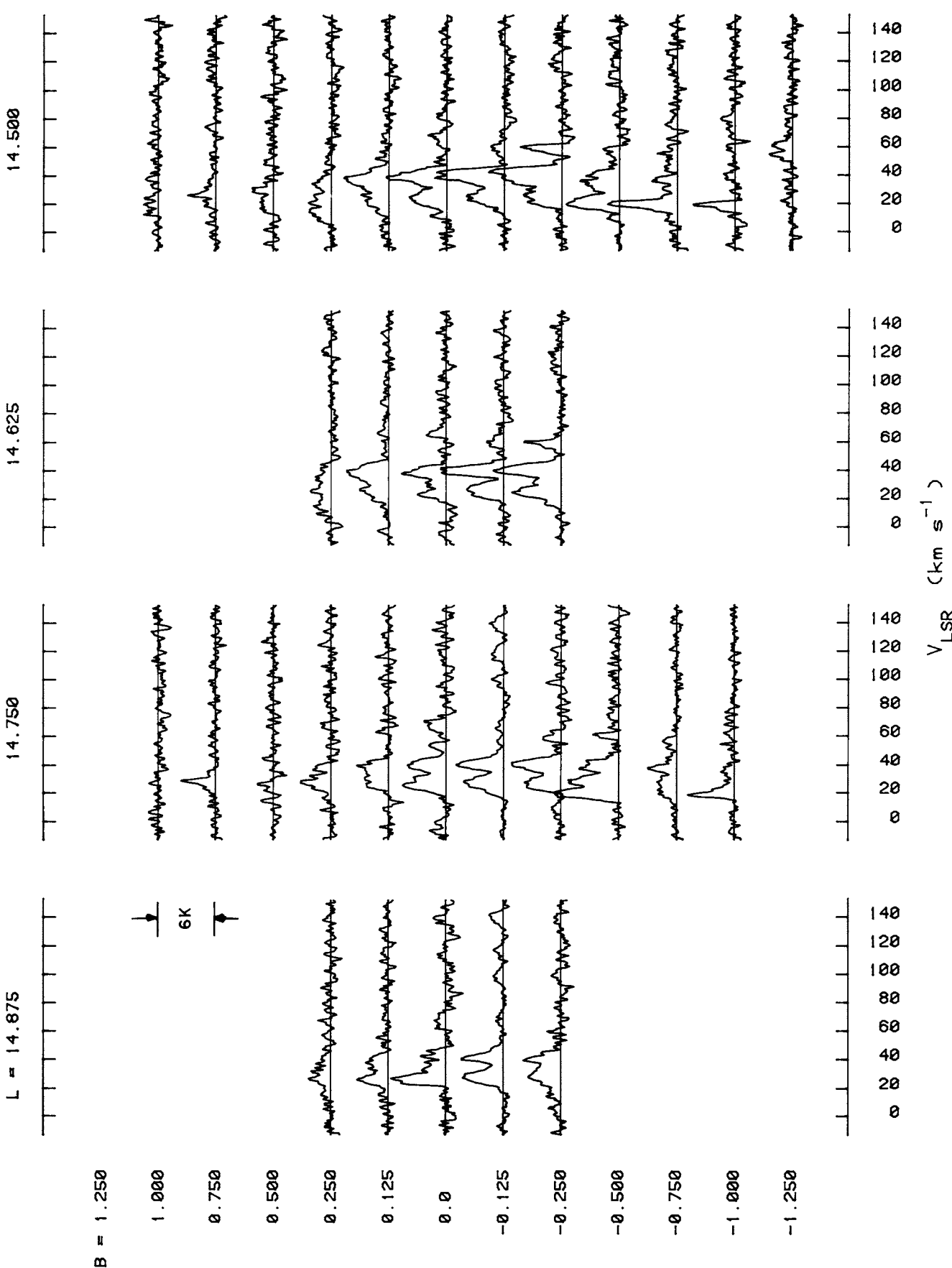


FIG. 11—Continued

15.000

15.125

15.250

 $L = 15.375$  $B = 1.250$ 

1.000



0.750



0.500



0.250



0.125



0.0



-0.125



-0.250



-0.500



-0.750



-1.000



-1.250

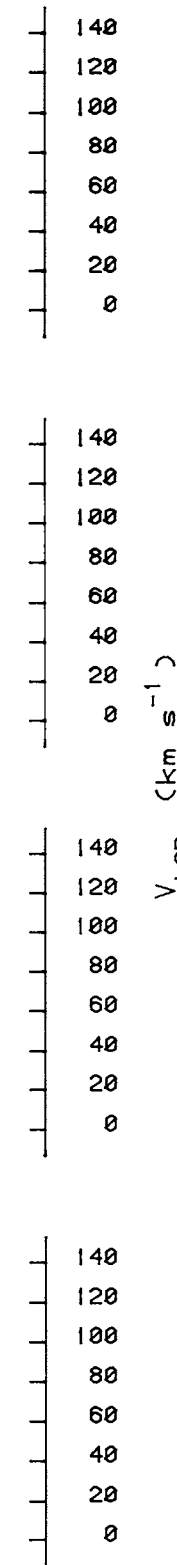
 $V_{\text{LSR}}$  ( $\text{km s}^{-1}$ )

FIG. 11—Continued

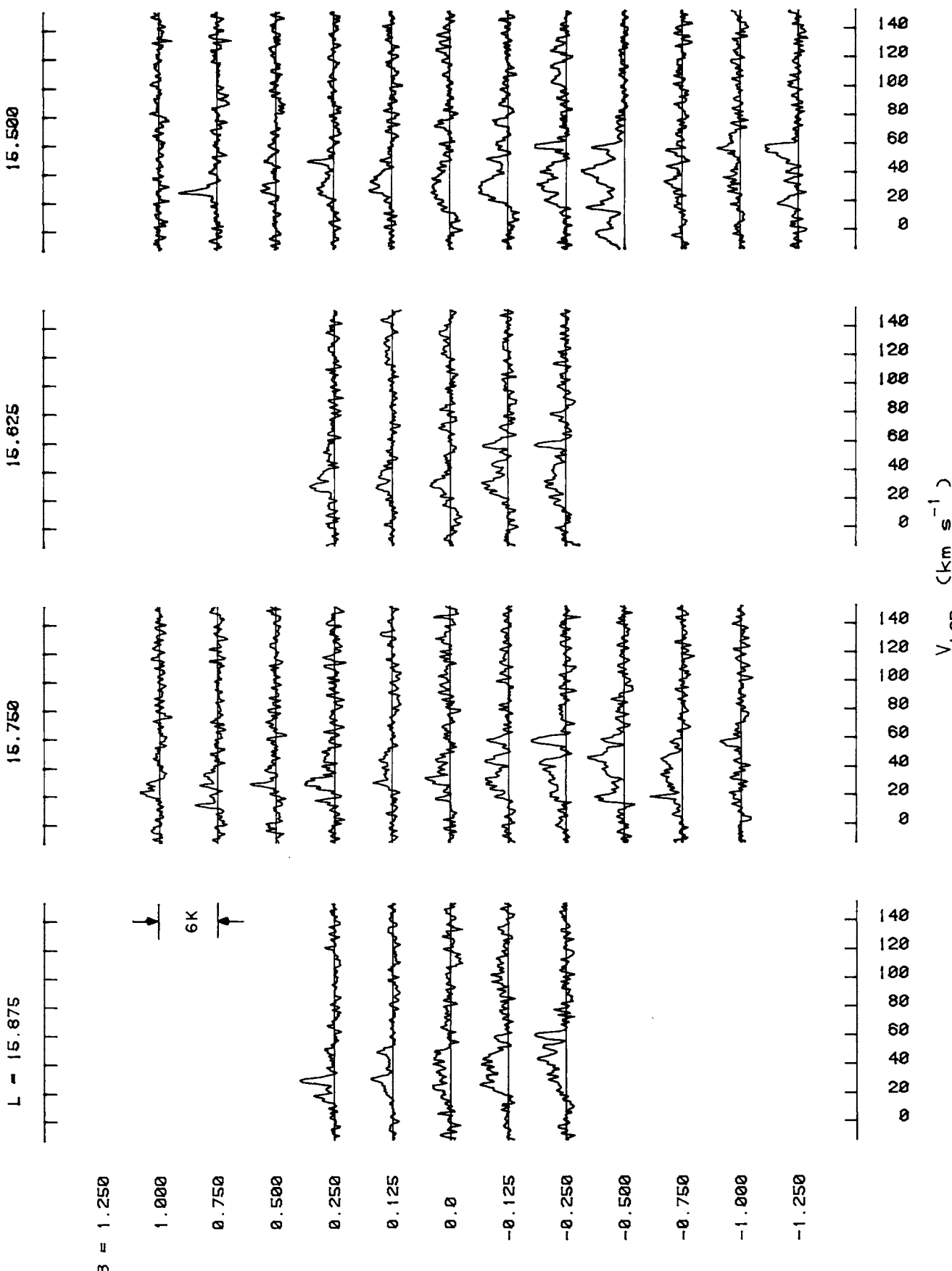


FIG. 11—Continued

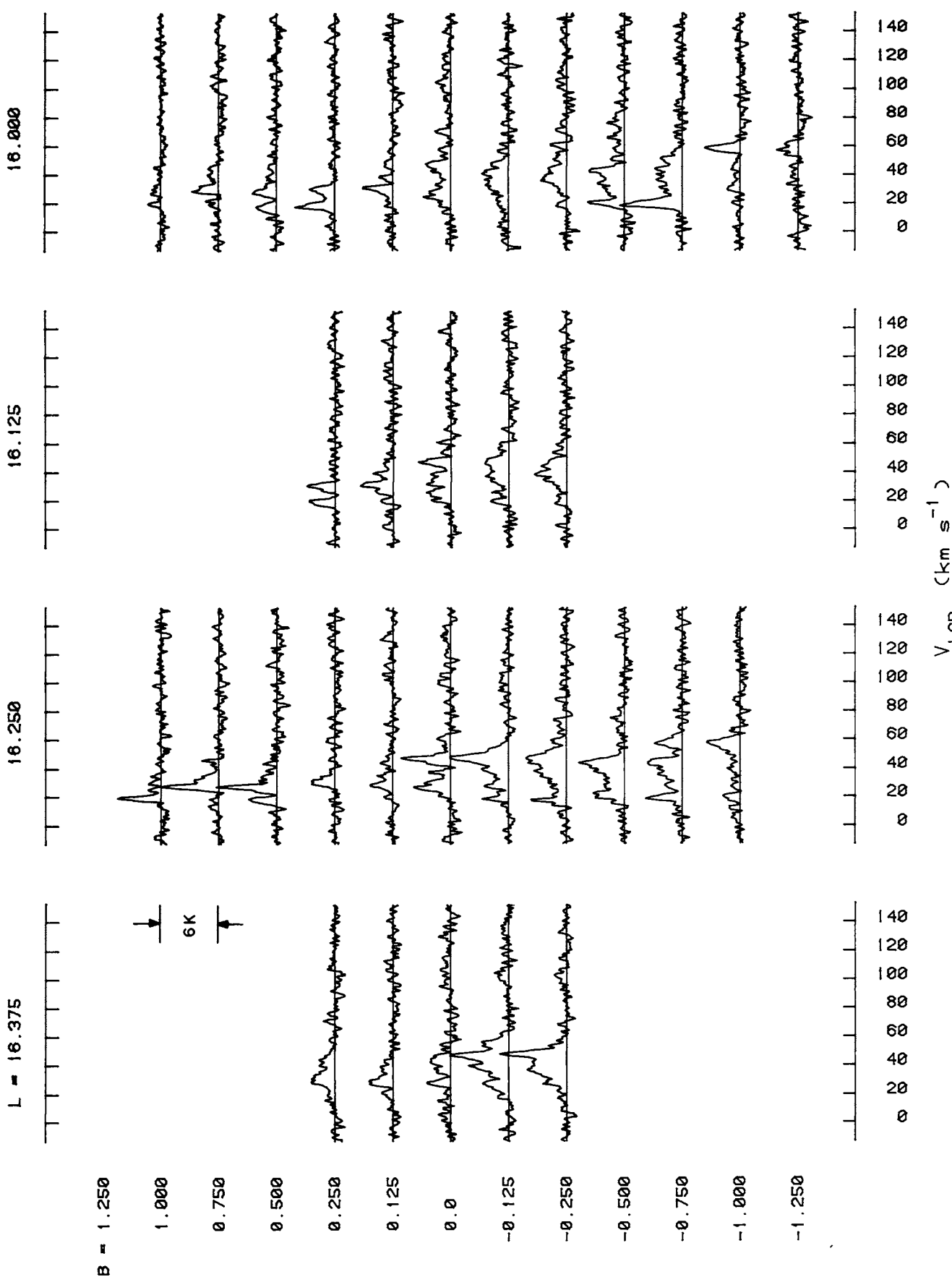


FIG. 11—Continued

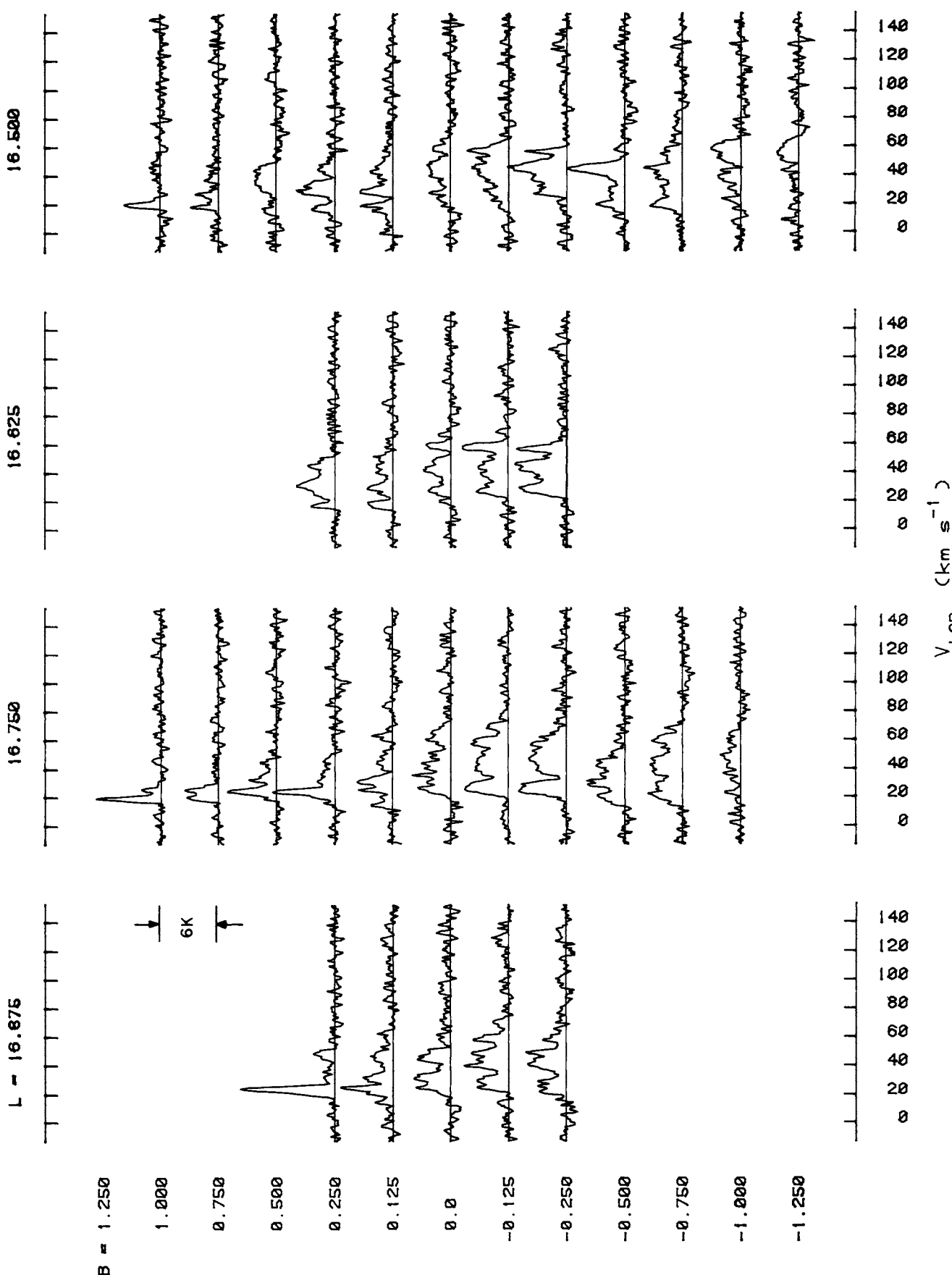
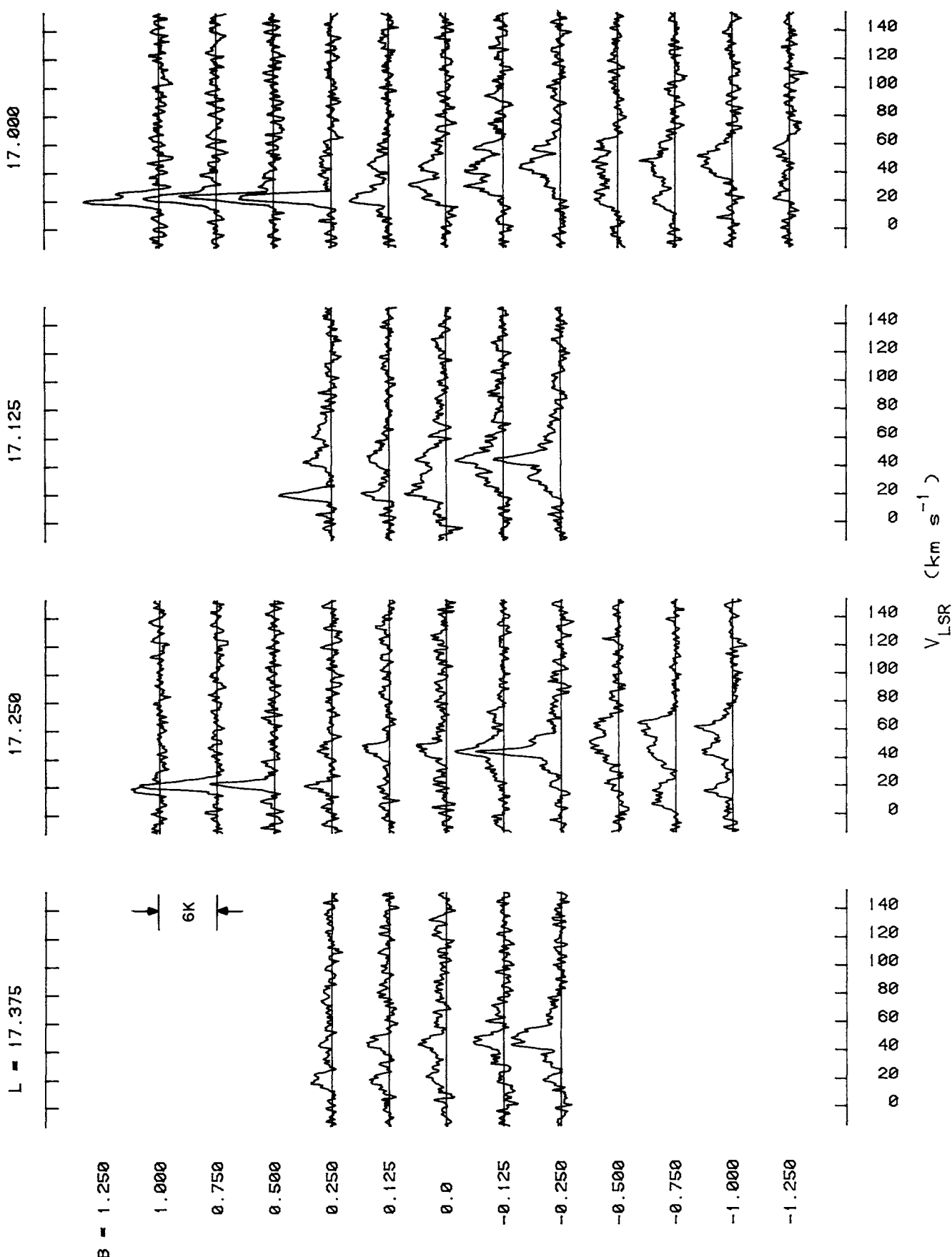


FIG. 11—Continued



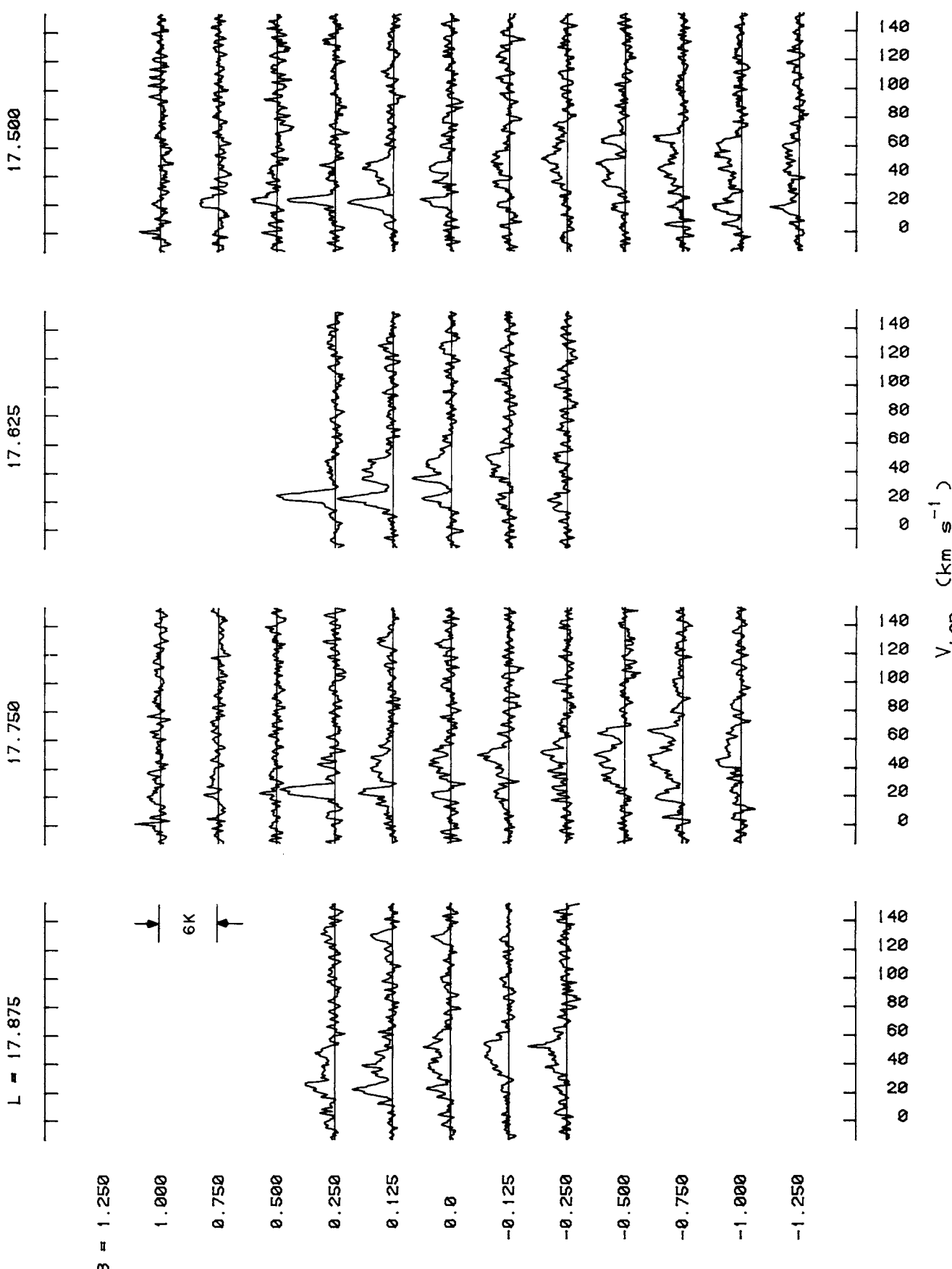


FIG. 11—Continued

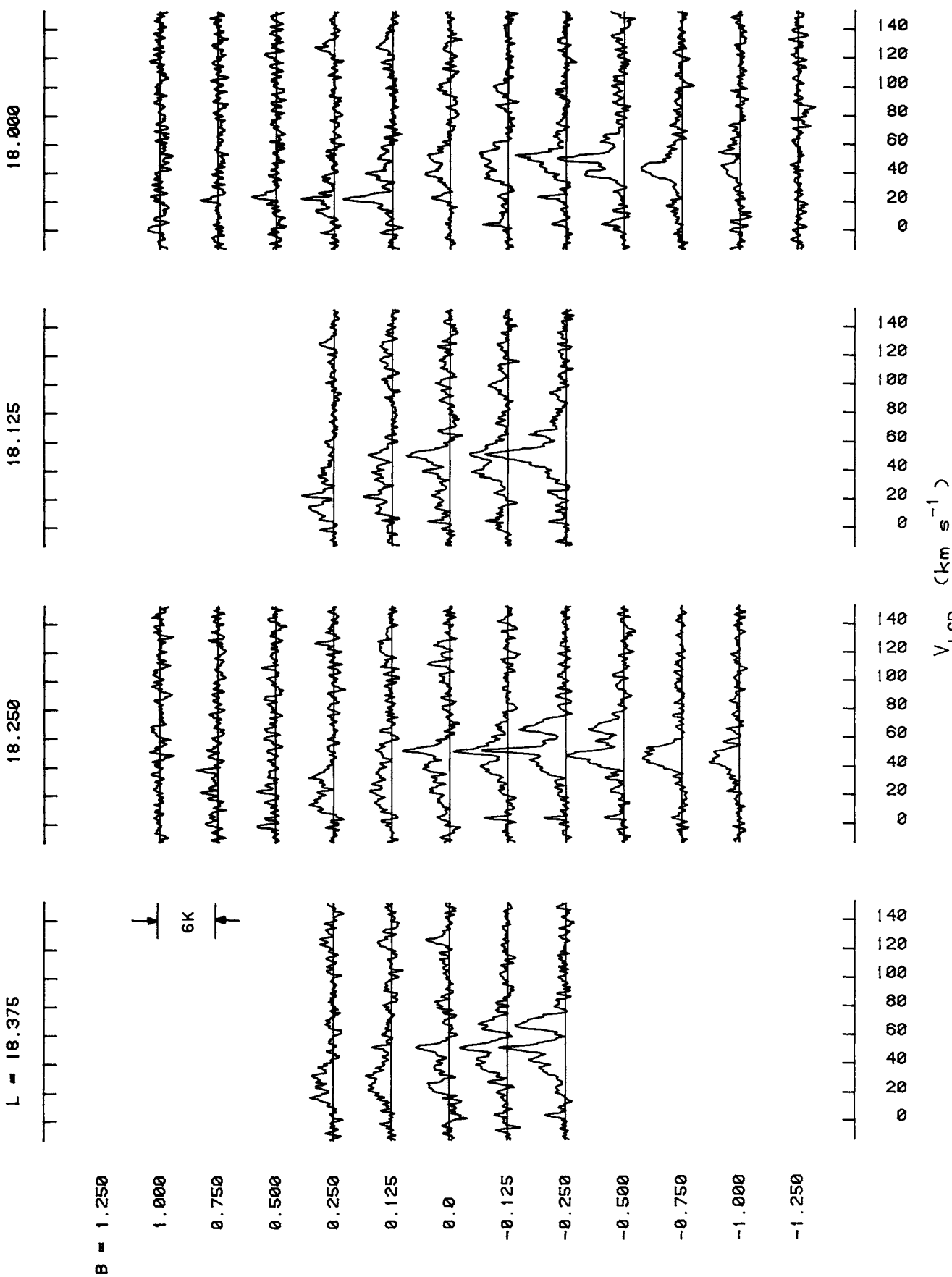


FIG. 11.—Continued

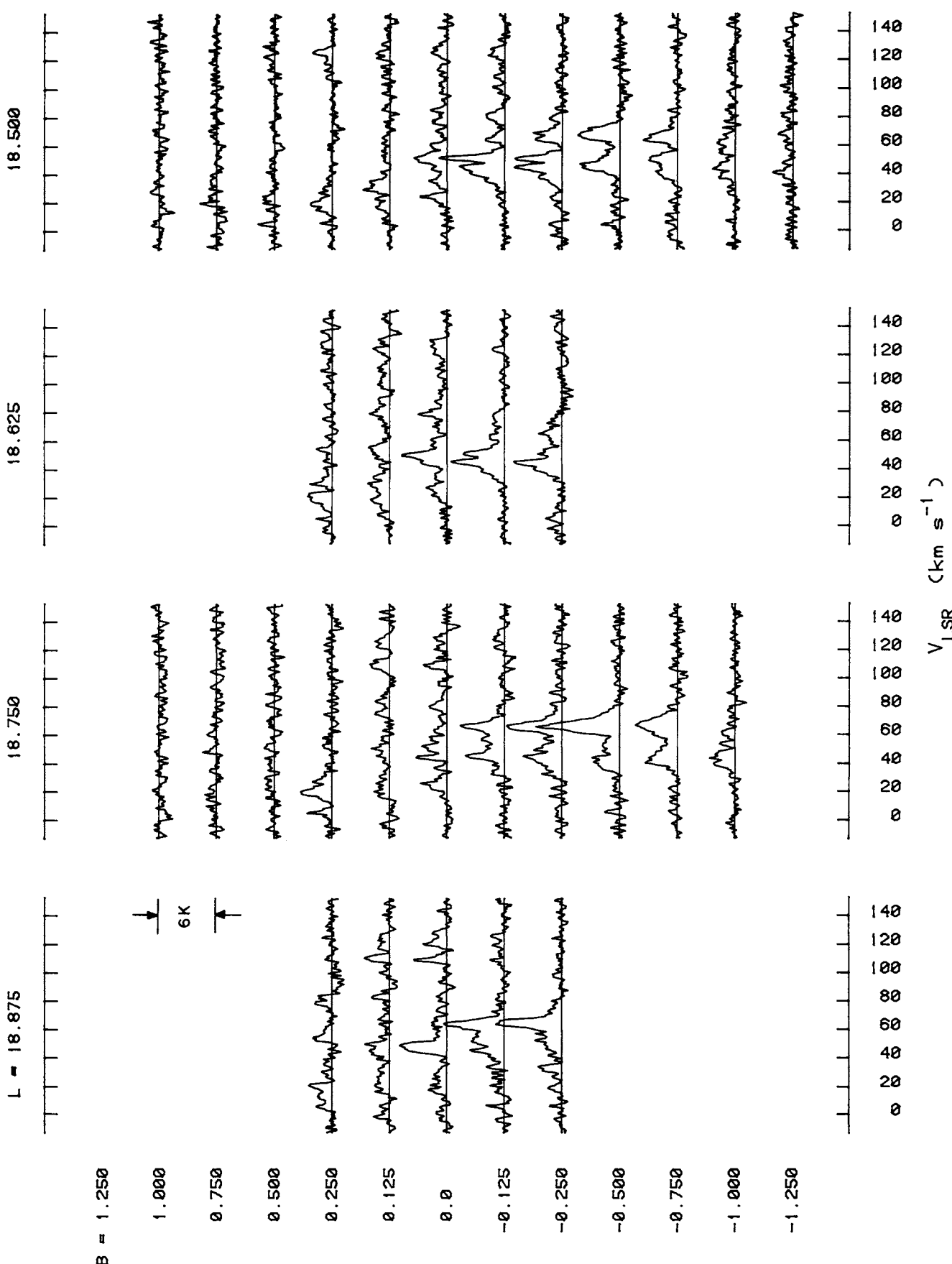


FIG. 11—Continued

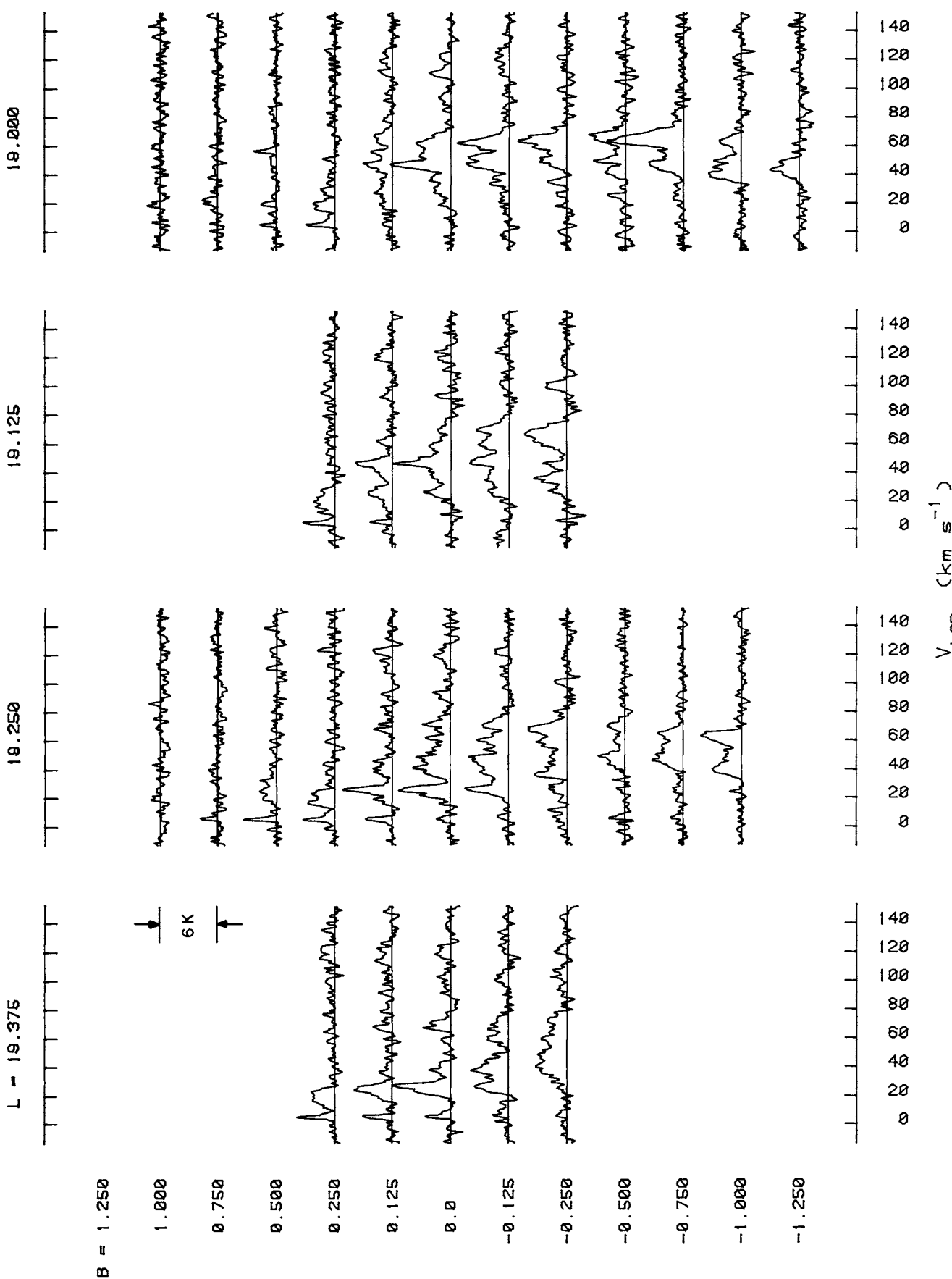


FIG. 11.—Continued

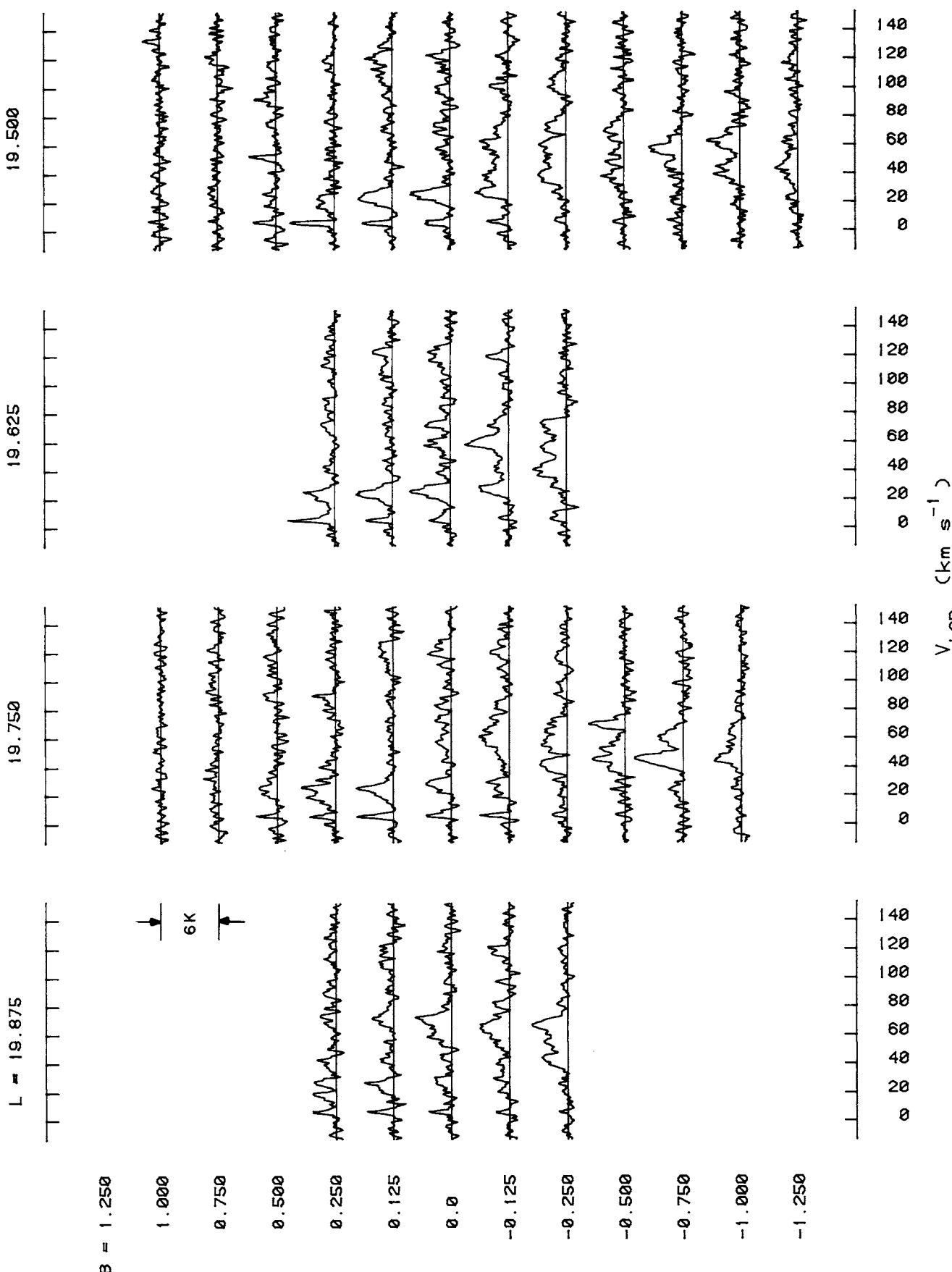


FIG. 11—Continued

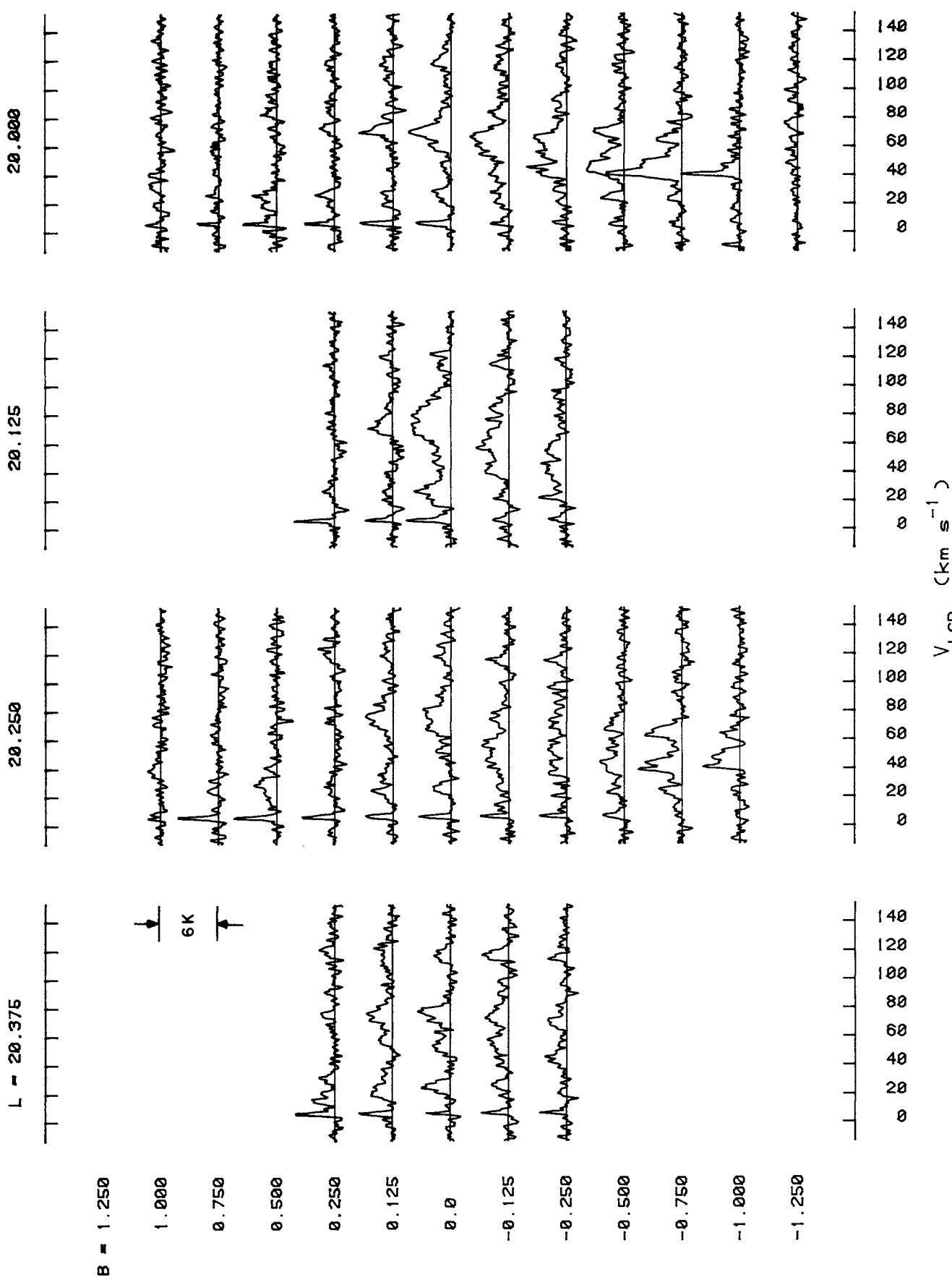


FIG. 11—Continued

20.500

20.625

20.750

L = 20.875

 $B = 1.250$ 

1.000

0.750

0.500

0.250

0.125

0.0

-0.125

-0.250

-0.500

-0.750

-1.000

-1.250

add emission

add absorption

6K

140

120

100

80

60

40

20

0

20

40

60

80

100

120

140

160

180

200

220

240

260

280

300

320

340

360

380

400

420

440

460

480

500

520

540

560

580

600

620

640

660

680

700

720

740

760

780

800

820

840

860

880

900

FIG. 11—Continued

21.000

21.125

21.250

L = 21.375

B = 1.250

1.000

0.750

0.500

0.250

0.125

0.0

-0.125

-0.250

-0.500

-0.750

-1.000

-1.250

V<sub>LSR</sub> (km s<sup>-1</sup>)140  
120  
100  
80  
60  
40  
20  
0140  
120  
100  
80  
60  
40  
20  
0140  
120  
100  
80  
60  
40  
20  
0140  
120  
100  
80  
60  
40  
20  
0140  
120  
100  
80  
60  
40  
20  
0140  
120  
100  
80  
60  
40  
20  
0140  
120  
100  
80  
60  
40  
20  
0140  
120  
100  
80  
60  
40  
20  
0

FIG. 11—Continued

21.500

21.750

21.750

L = 21.875

 $B = 1.250$ 

1.000

0.750

0.500

0.250

0.125

0.0

-0.125

-0.250

-0.500

-0.750

-1.000

-1.250



6K

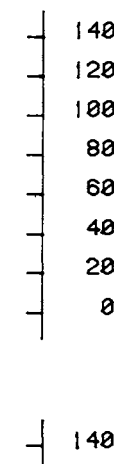
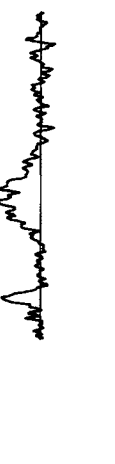
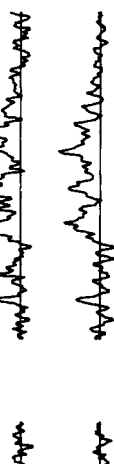
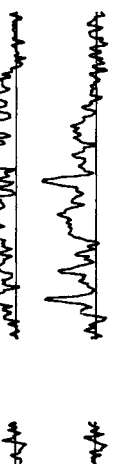
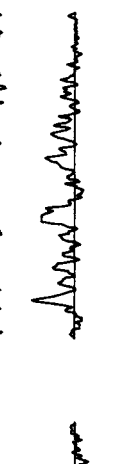
 $V_{\text{LSR}}$  ( $\text{km s}^{-1}$ )

FIG. 11—Continued

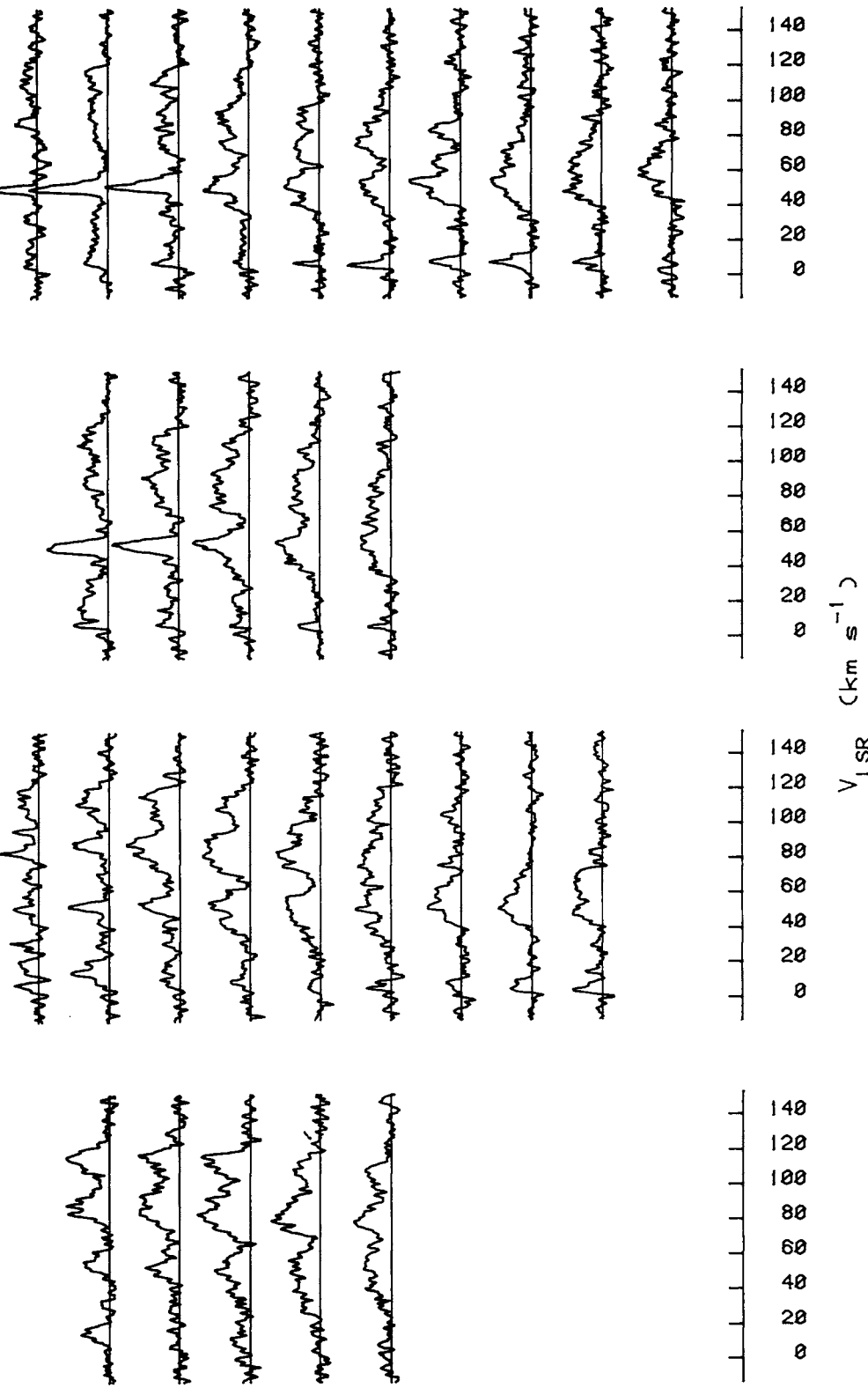
$B = 1.250$  $1.000$  $0.750$  $0.500$  $0.250$  $0.125$  $0.0$  $-0.125$  $-0.250$  $-0.500$  $-0.750$  $-1.000$  $-1.250$  $\downarrow$   
 $6K$  $\downarrow$   
 $6K$  $\downarrow$   
 $6K$ 

FIG. 11.—Continued

$B = 1.250$ 

1.000

6K

0.750

1.000

0.750

6K

0.500

1.000

0.750

6K

0.250

1.000

0.750

6K

0.125

1.000

0.750

6K

0.0

1.000

0.750

6K

-0.125

1.000

0.750

6K

-0.250

1.000

0.750

6K

-0.500

1.000

0.750

6K

-0.750

1.000

0.750

6K

-1.000

1.000

0.750

6K

-1.250

1.000

0.750

6K

-1.500

1.000

0.750

6K

-1.750

1.000

0.750

6K

 $V_{\text{LSR}}$  (km s<sup>-1</sup>)

140

120

100

80

60

40

20

0

140

120

100

80

60

40

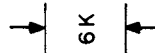
20

0

FIG. 11—Continued

$B = 1.250$ 

1.000



6K

0.750



0.500



0.250



0.125



0.0



-0.125



-0.250



-0.500



-0.750



-1.000



-1.250



744

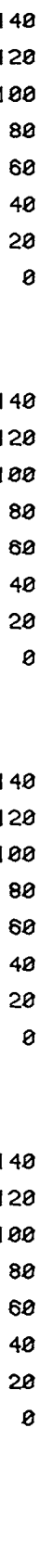
 $V_{\text{LSR}}$  (km s $^{-1}$ )

FIG. 11.—Continued

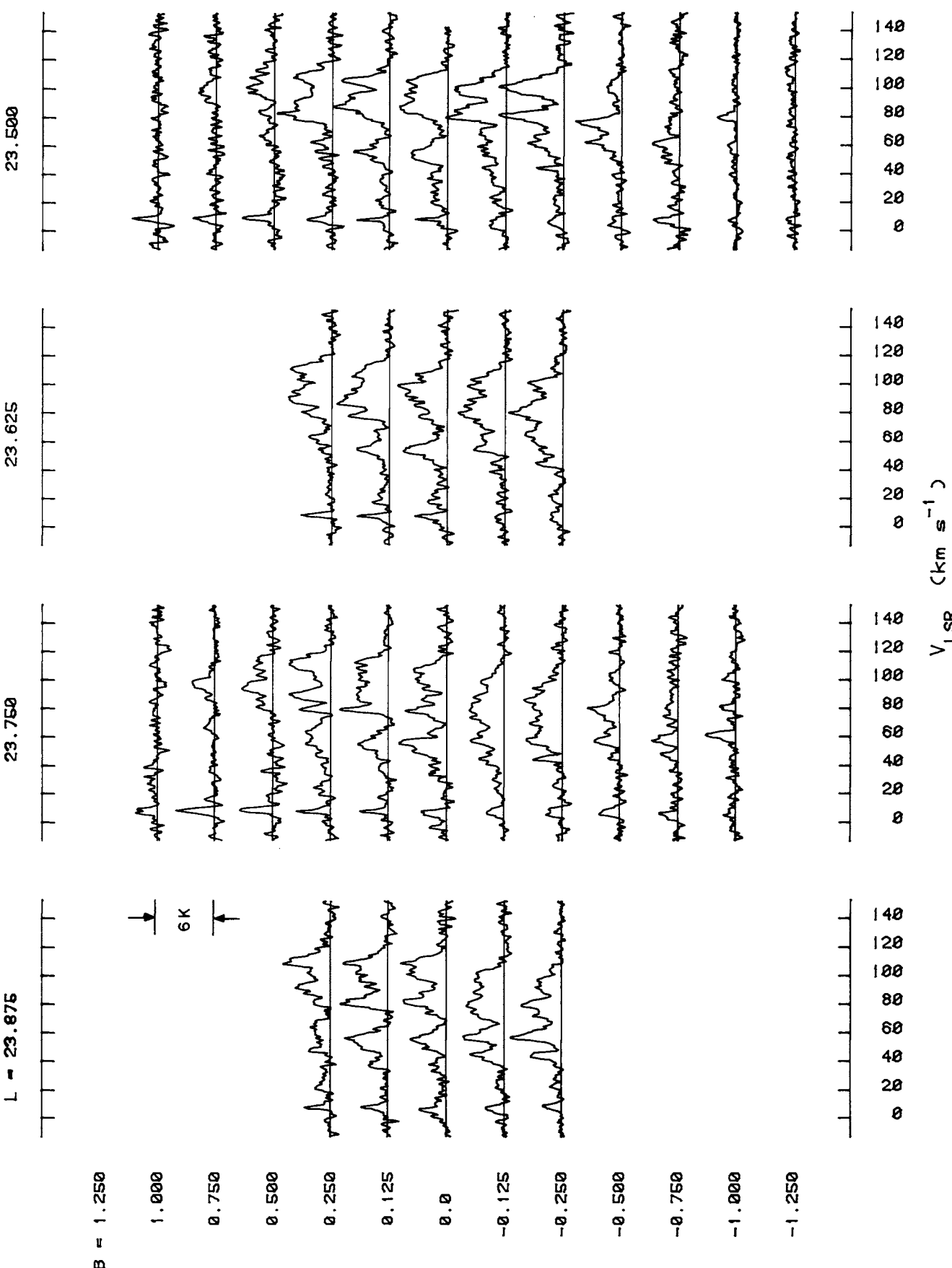


FIG. 11—Continued

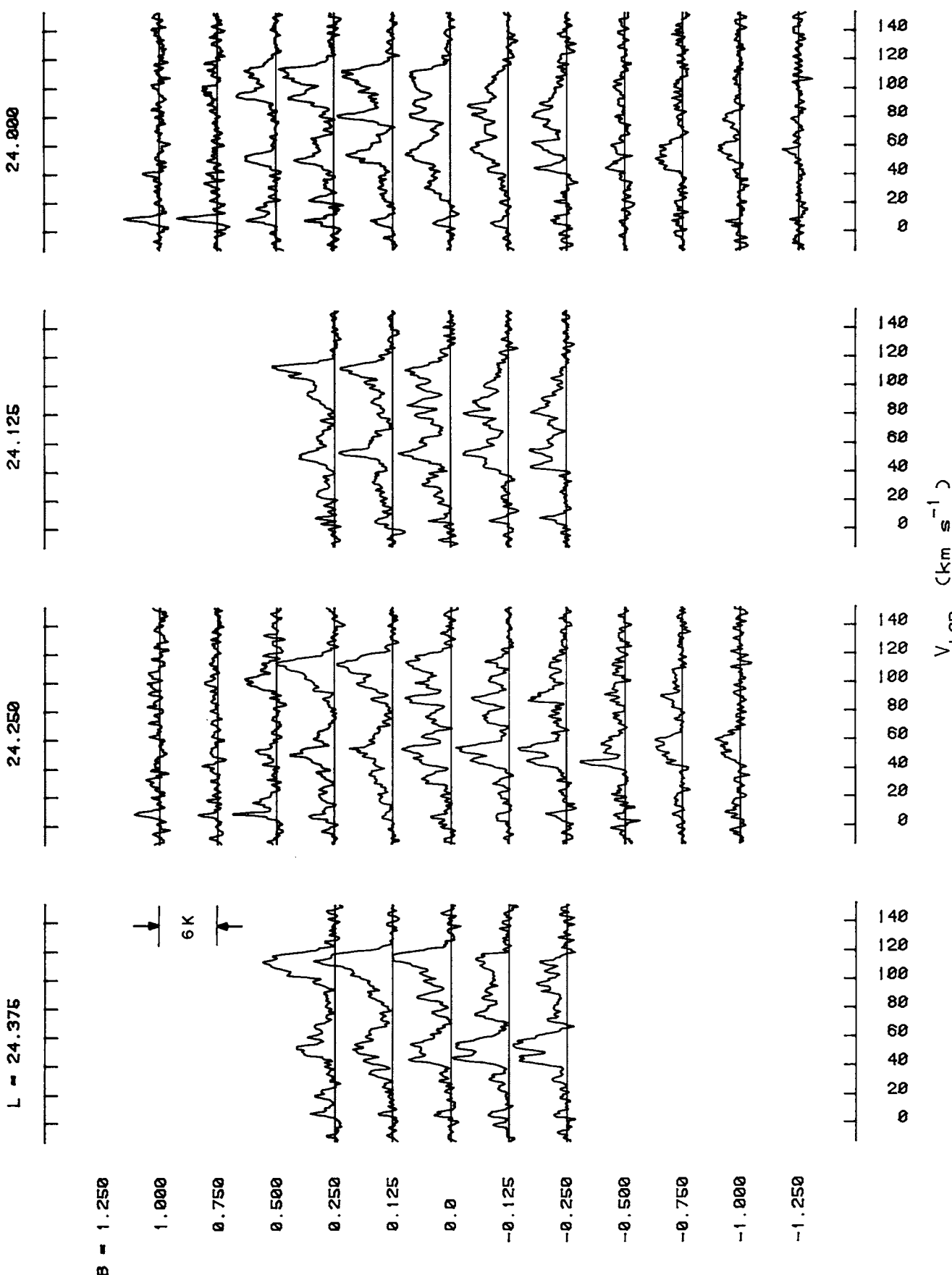


FIG. 11.—Continued

$B = 1.250$ 

1.000

0.750

0.500

0.250

0.125

0.0

-0.125

-0.250

-0.500

-0.750

-1.000

-1.250

 $\rightarrow$   
6K $V_{\text{LSR}}$  (km s<sup>-1</sup>)

FIG. 11—Continued

25.200

25.125

25.250

L = 25.375

 $B = 1.250$ 

1.000

0.750

0.500

0.250

0.125

0.0

-0.125

-0.250

-0.500

-0.750

-1.000

-1.250

1.000

6K

1.000

1.000

1.000

1.000

1.000

1.000

1.000

1.000

1.000

1.000

1.000

1.000

1.000

 $V_{\text{LSR}}$  ( $\text{km s}^{-1}$ )

FIG. 11—Continued

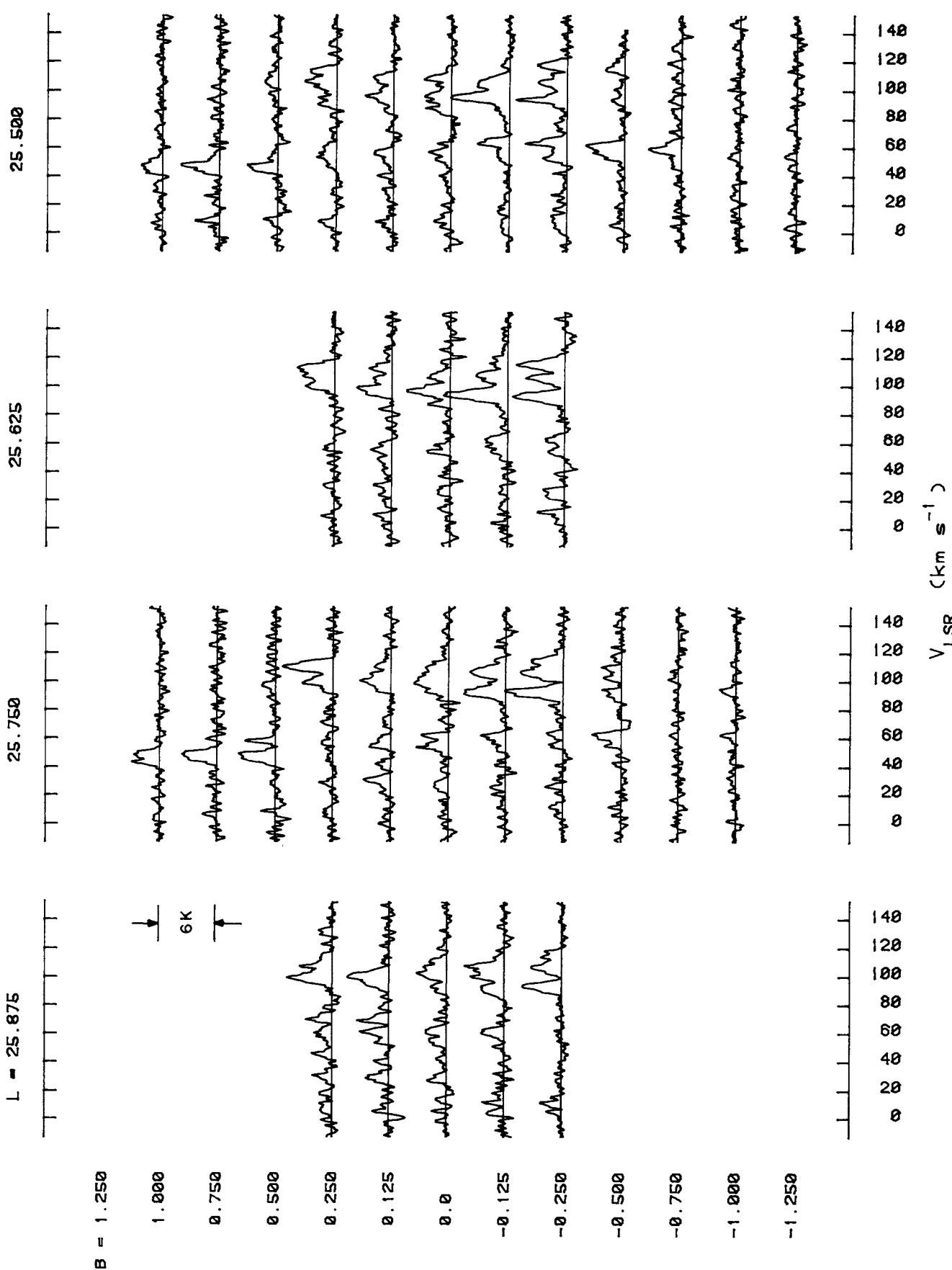


FIG. 11—Continued

26.000

26.125

26.250

L = 26.375

 $B = 1.250$ 

1.000

0.750

0.500

0.250

0.125

0.0

-0.125

-0.250

-0.500

-0.750

-1.000

-1.250

140  
120  
100  
80  
60  
40  
20  
0140  
120  
100  
80  
60  
40  
20  
0140  
120  
100  
80  
60  
40  
20  
0 $V_{\text{LSR}}$  (km s<sup>-1</sup>)140  
120  
100  
80  
60  
40  
20  
0140  
120  
100  
80  
60  
40  
20  
0140  
120  
100  
80  
60  
40  
20  
0

FIG. 11—Continued

$B = 1.250$ 

1.000

6K

0.750

0.500

0.250

0.125

0.0

-0.125

-0.250

-0.500

-0.750

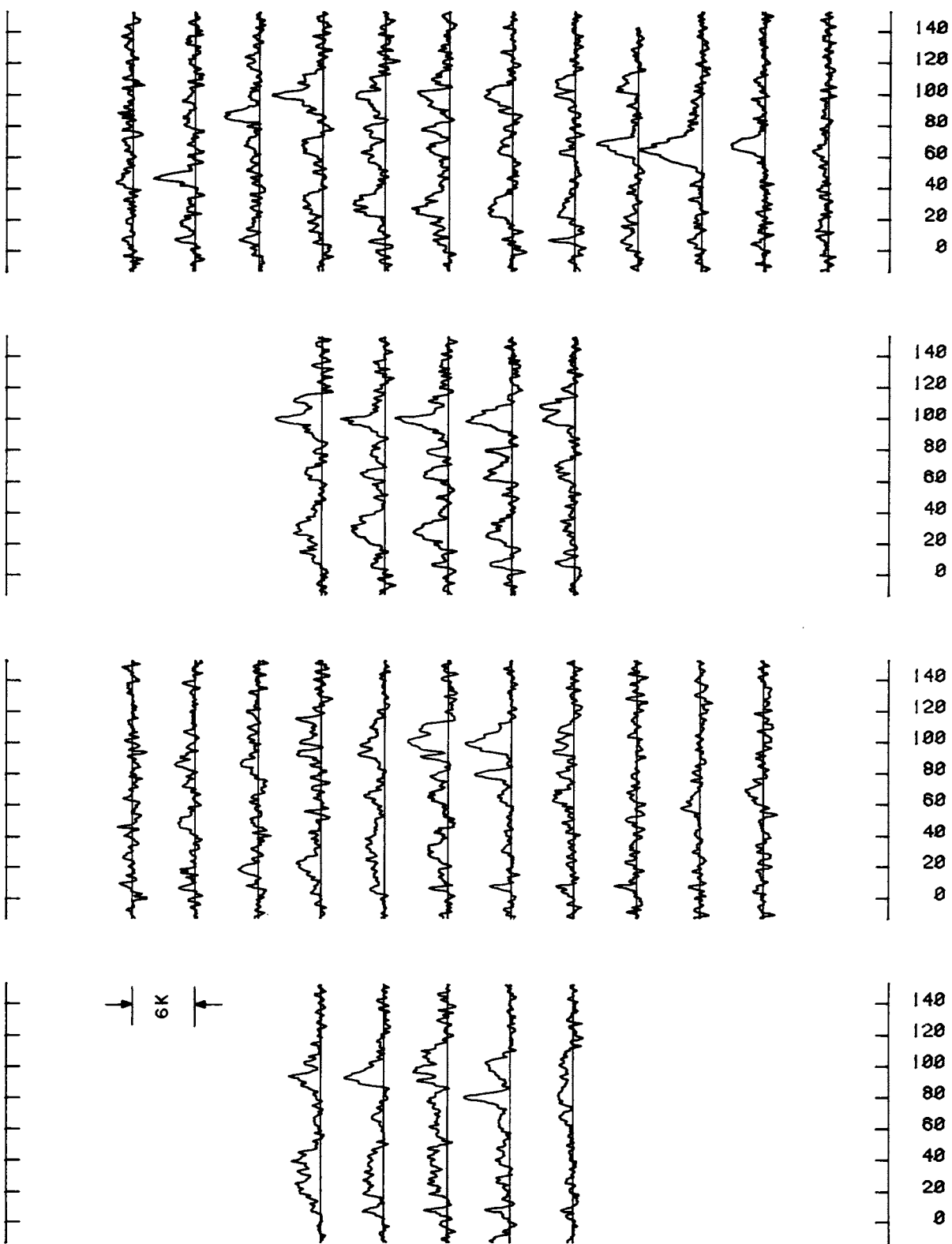
-1.000

-1.250

751

 $V_{\text{LSR}}$  ( $\text{km s}^{-1}$ )

FIG. 11—Continued



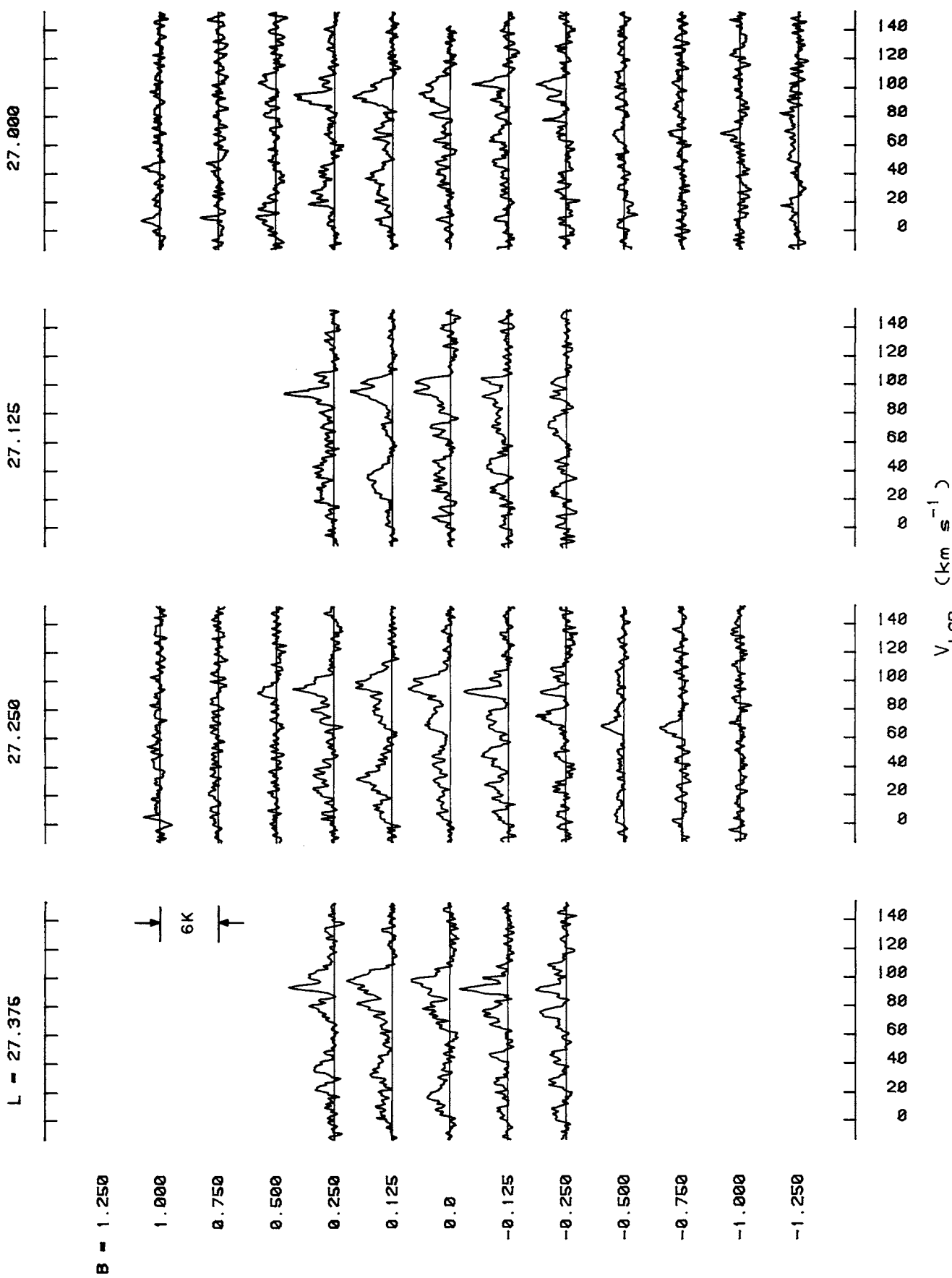


FIG. 11—Continued

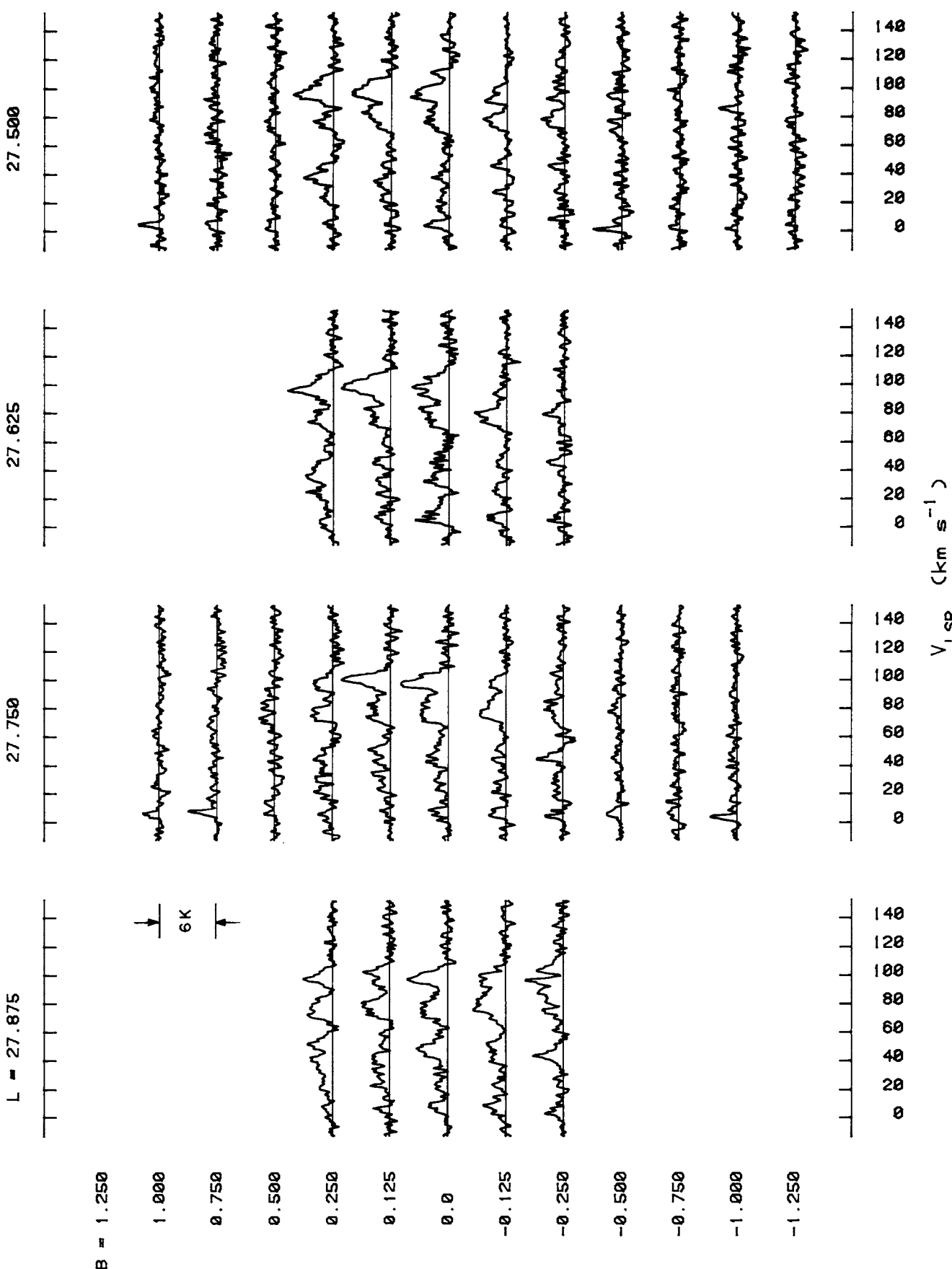


FIG. 11—Continued

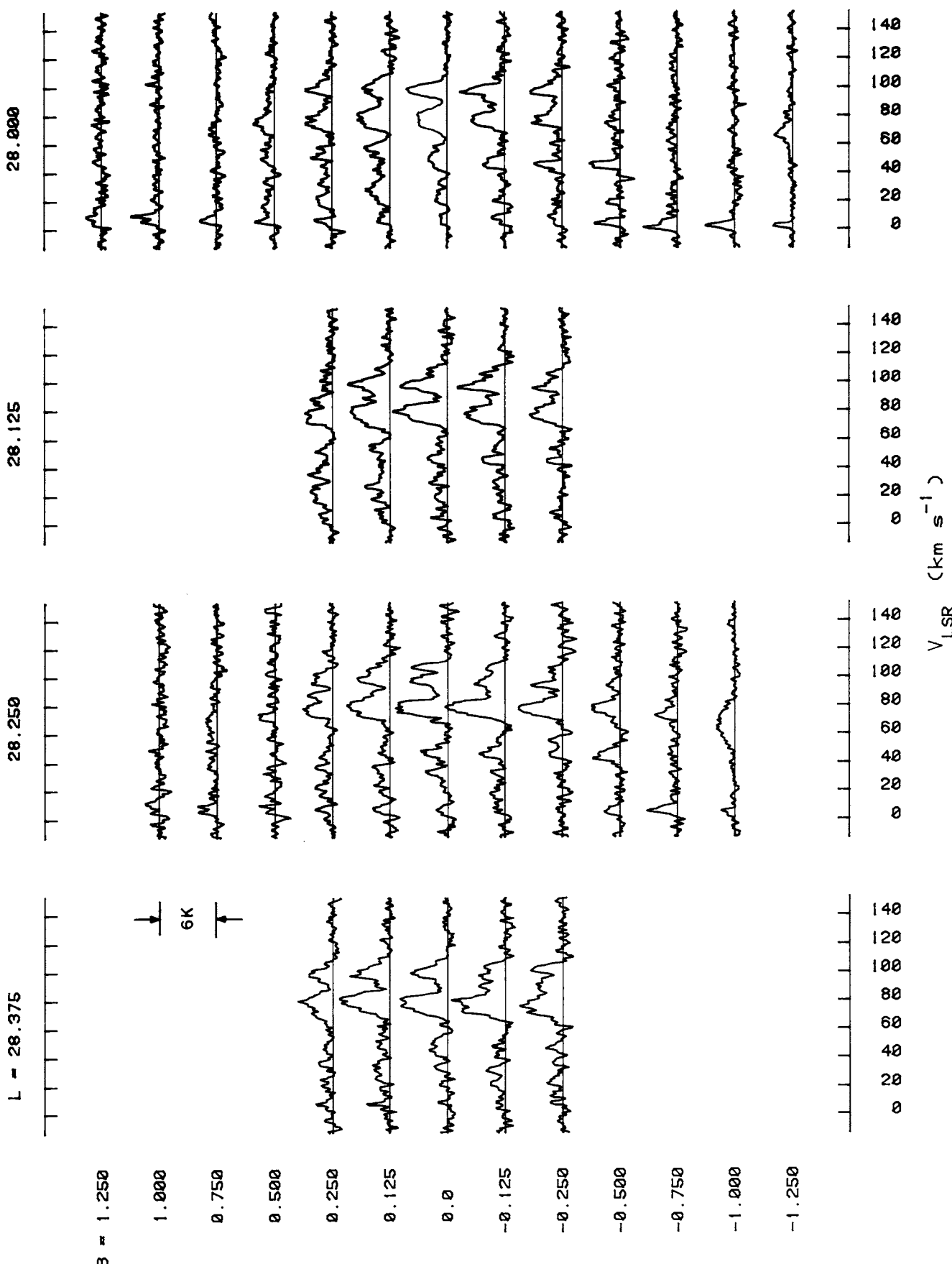


FIG. 11—Continued

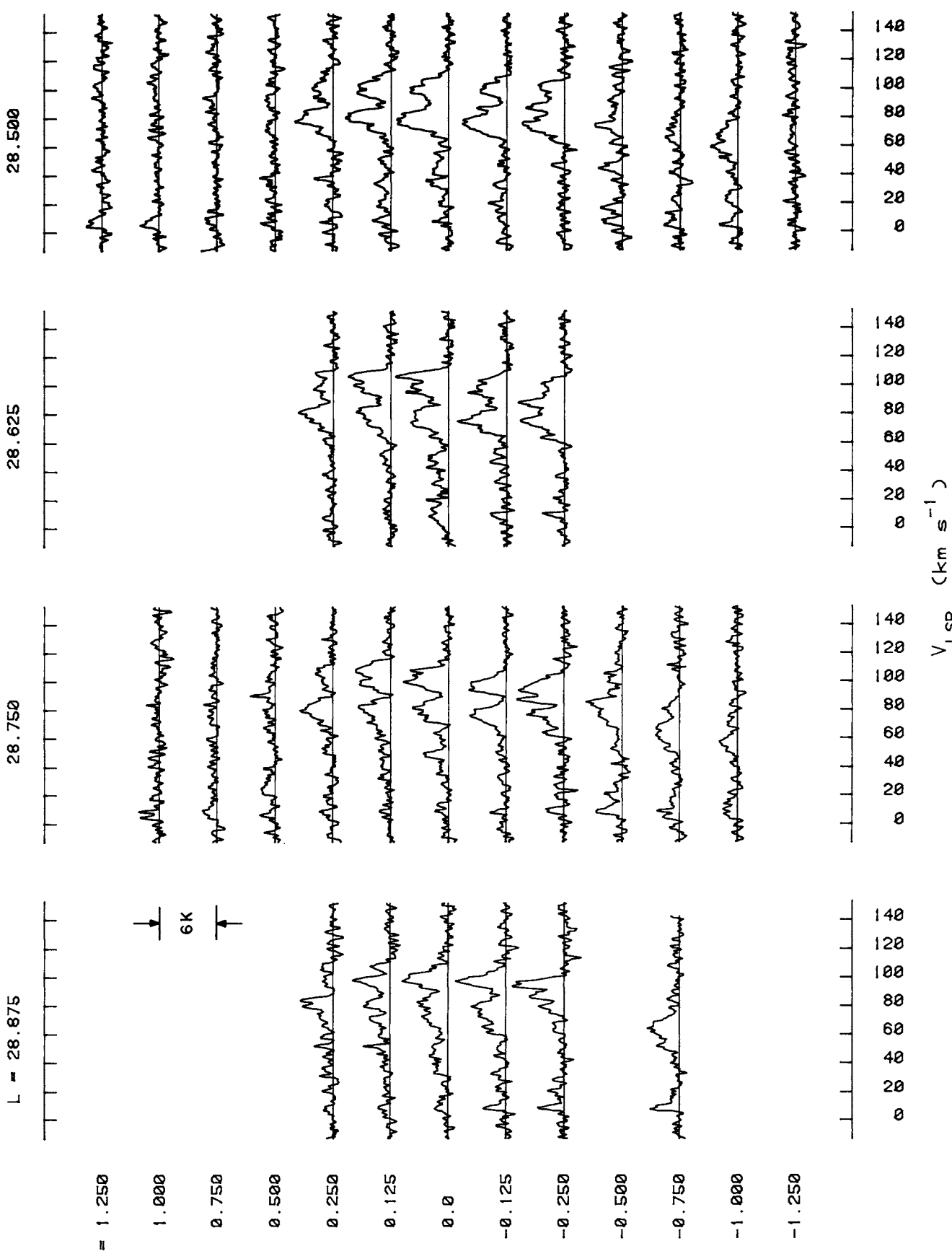


FIG. 11—Continued

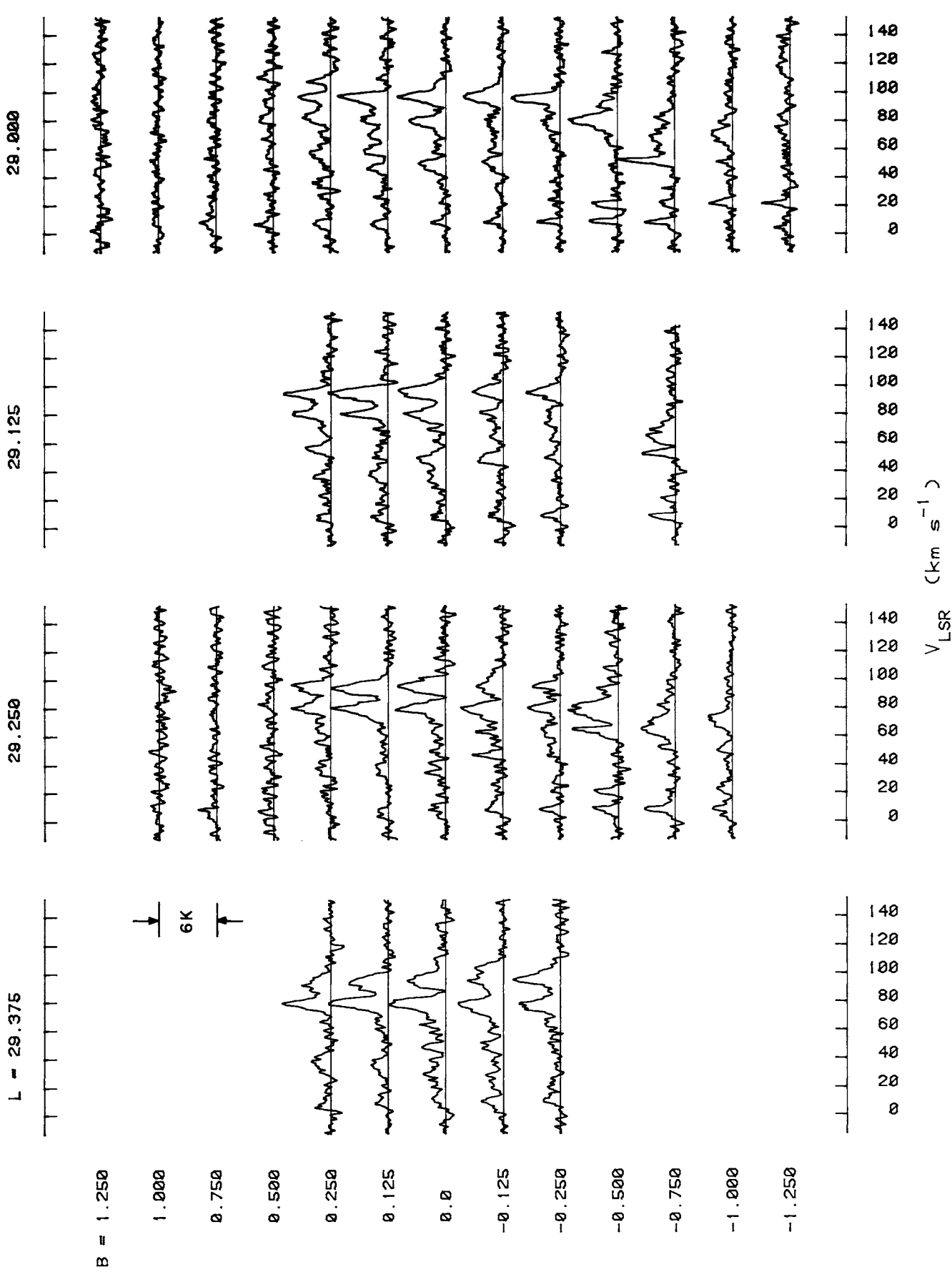


FIG. 11—Continued

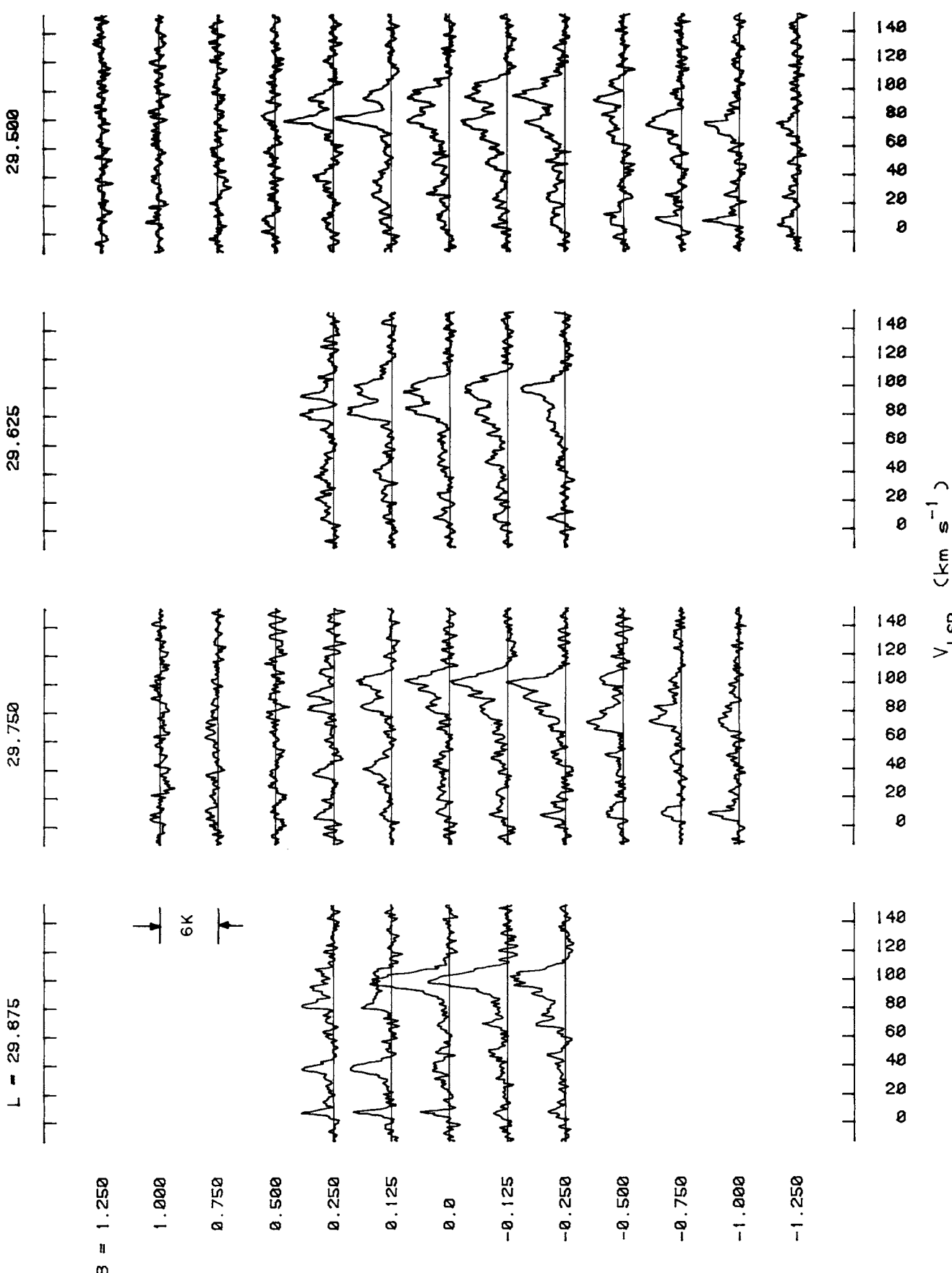


FIG. 11—Continued

30.000

30.125

30.250

L = 30.375

B = 1.250

1.000

0.750

0.500

0.250

0.125

0.0

-0.125

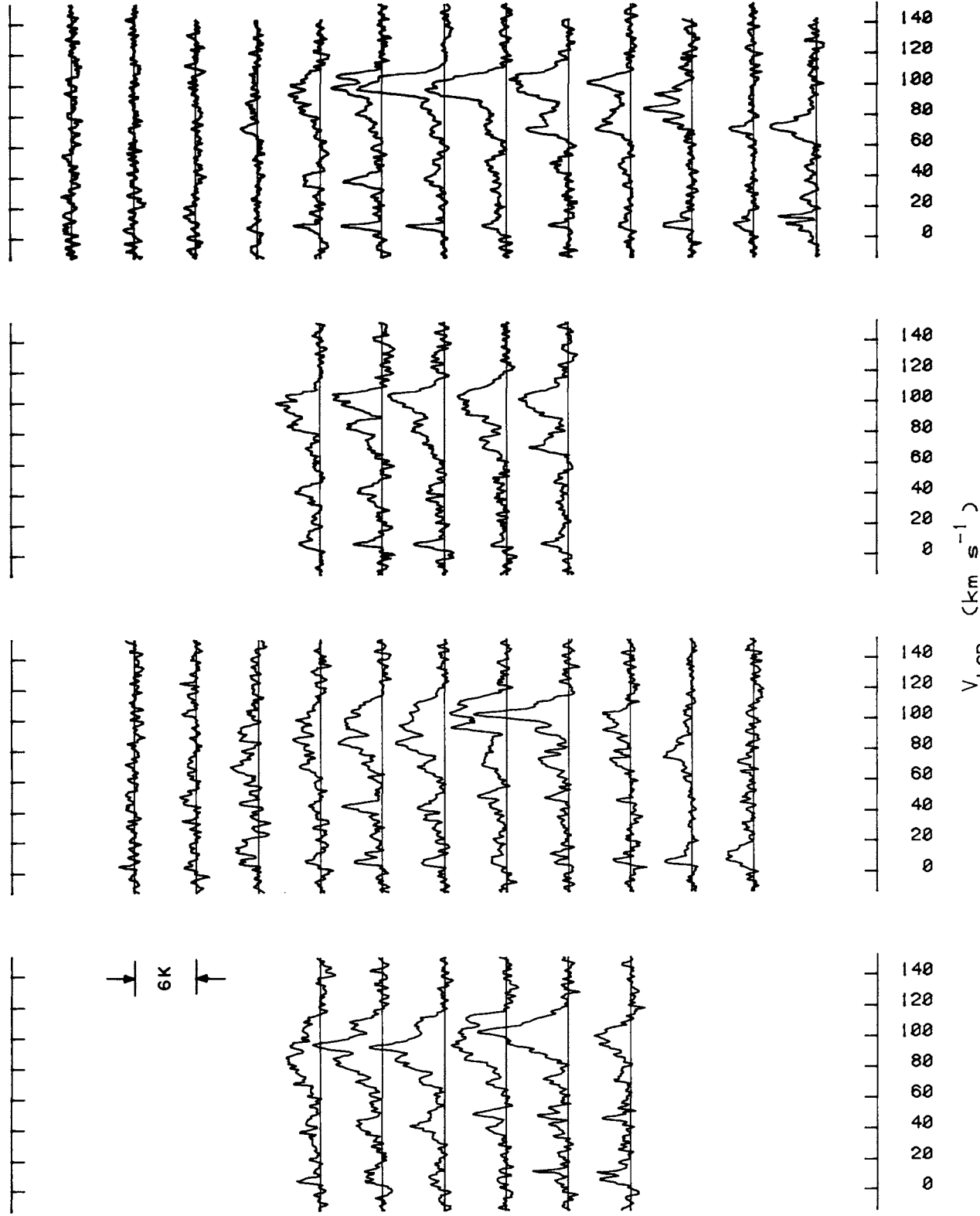
-0.250

-0.500

-0.750

-1.000

-1.250

V<sub>LSR</sub> (km s<sup>-1</sup>)140  
120  
100  
80  
60  
40  
20  
0140  
120  
100  
80  
60  
40  
20  
0140  
120  
100  
80  
60  
40  
20  
0

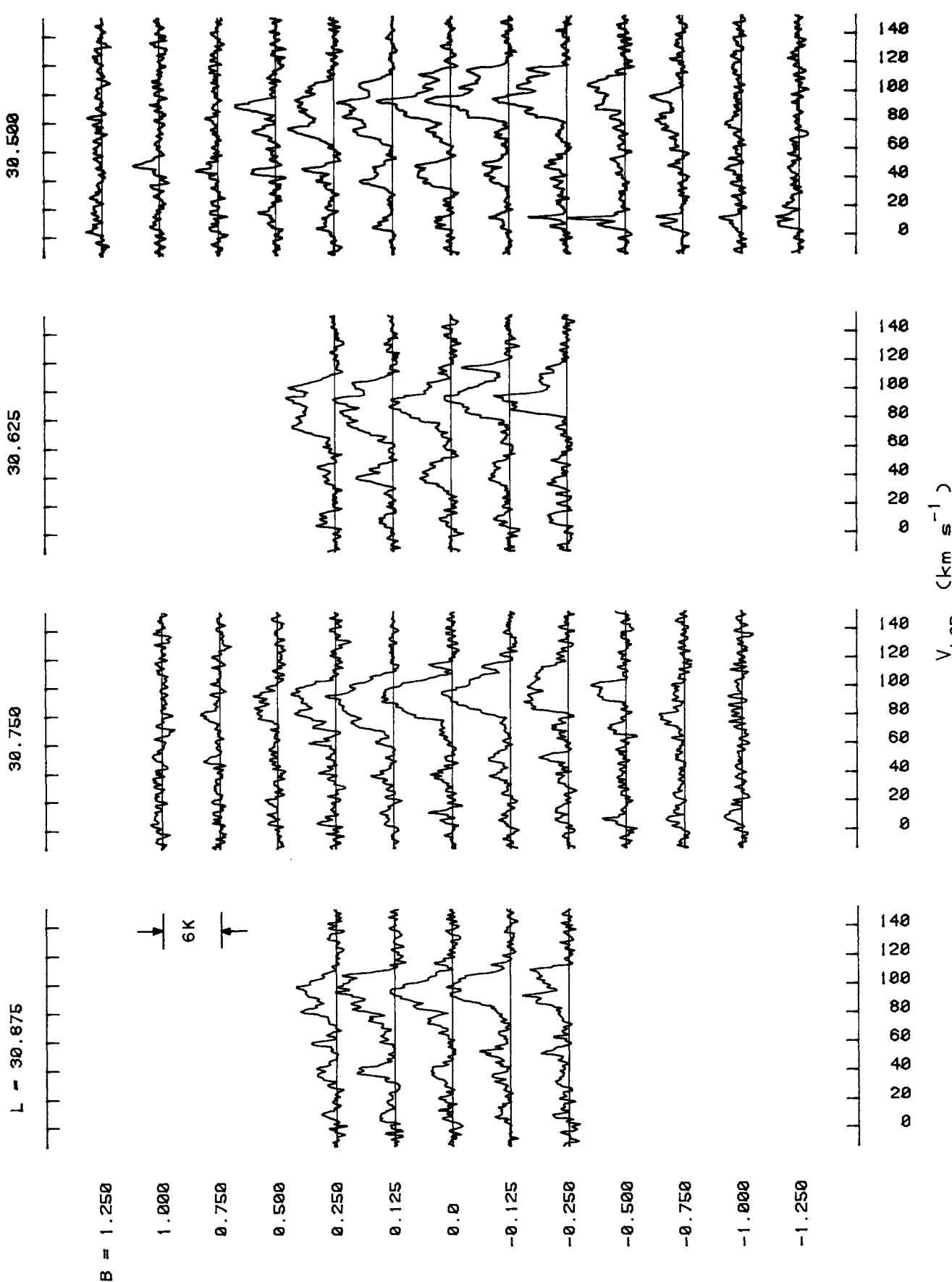


FIG. 11—Continued

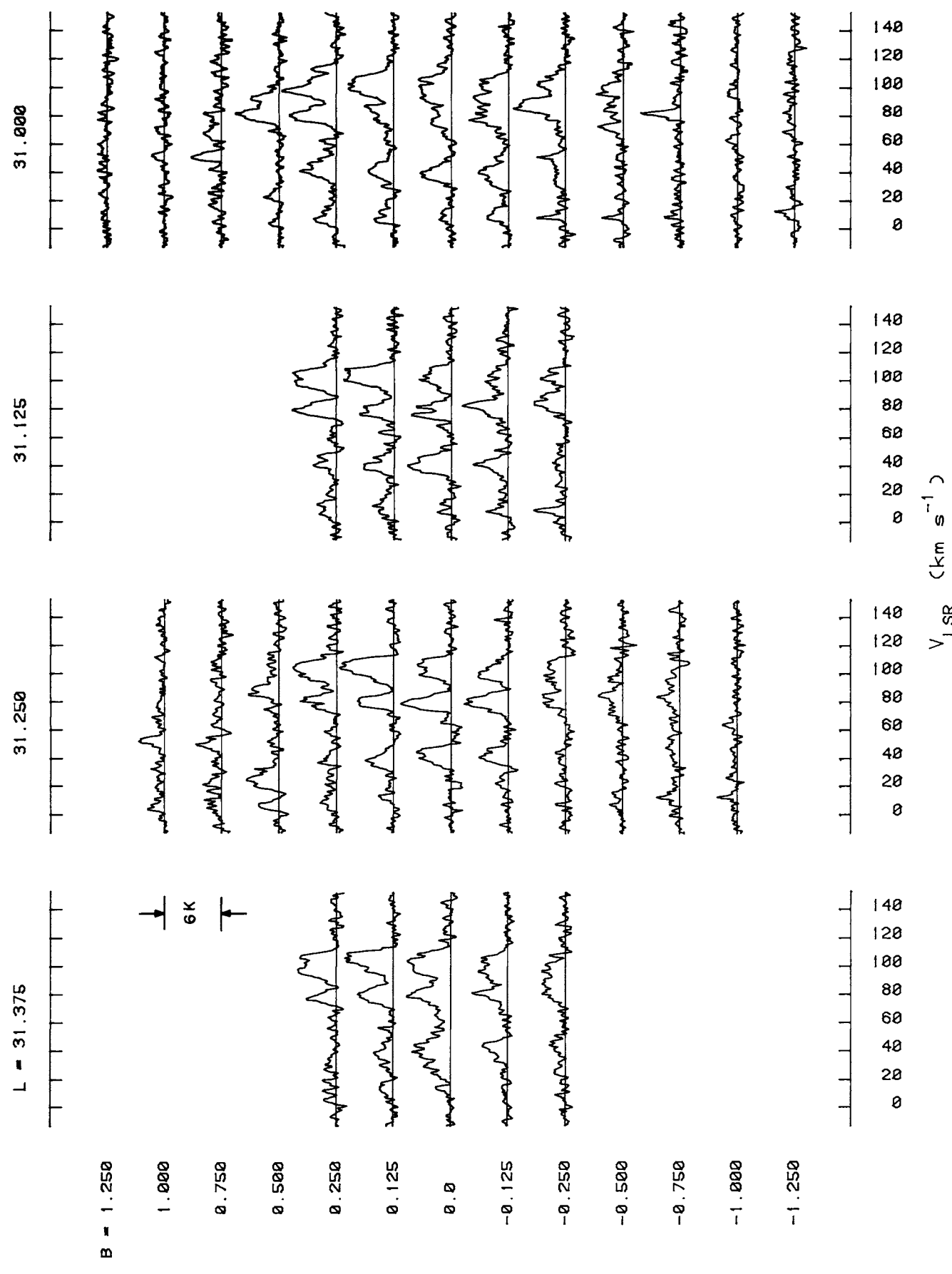


FIG. 11—Continued

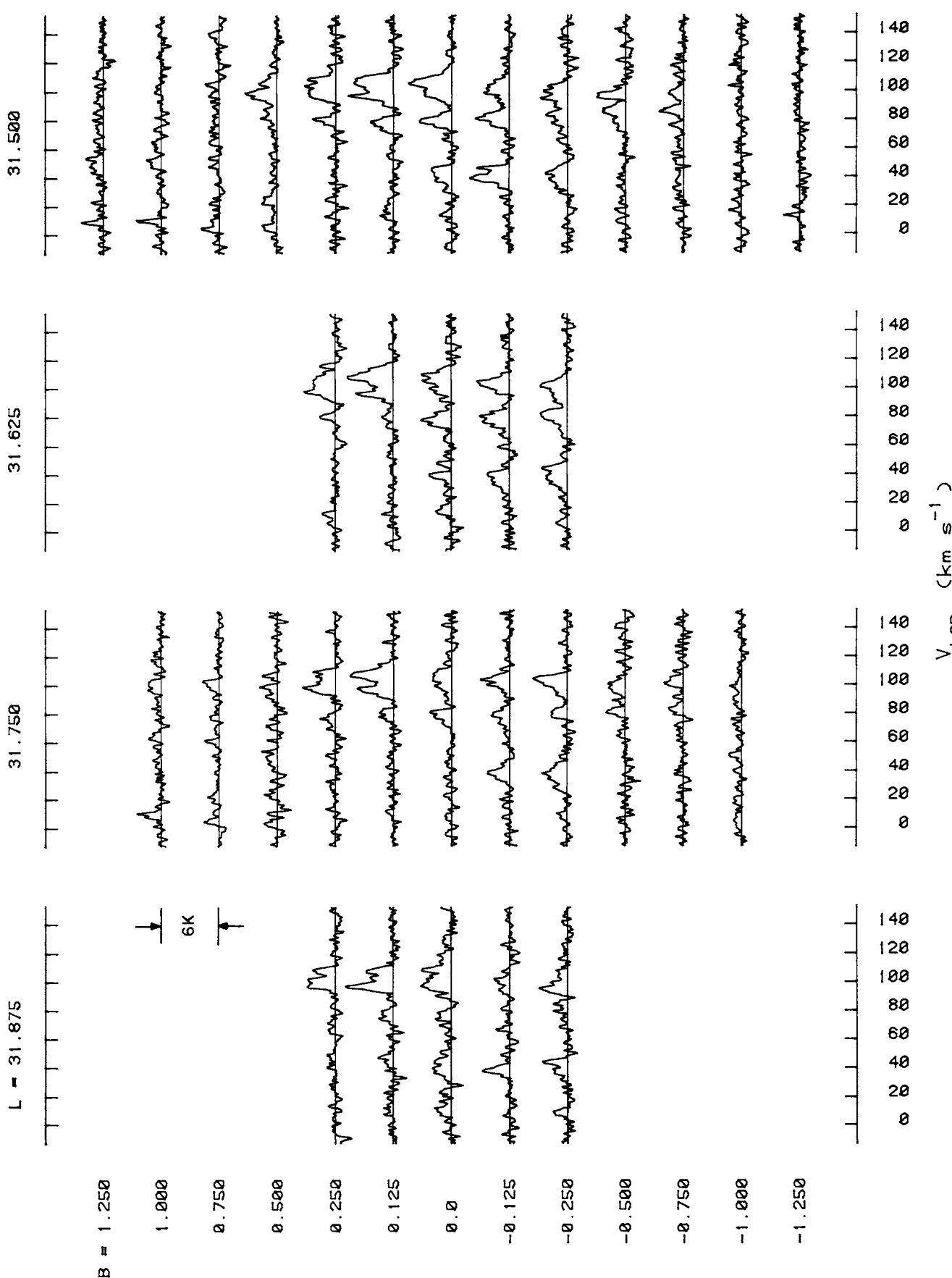


FIG. 11.—Continued

$B = 1.250$ 

1.000



0.750



0.500



0.250



0.125



0.0



-0.125



-0.250



-0.500



-0.750



-1.000



-1.250

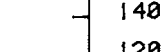
 $V_{\text{LSR}}$  ( $\text{km s}^{-1}$ )140  
120  
100  
80  
60  
40  
20  
0140  
120  
100  
80  
60  
40  
20  
0140  
120  
100  
80  
60  
40  
20  
0140  
120  
100  
80  
60  
40  
20  
0

FIG. 11.—Continued

32.500

32.625

32.750

L = 32.875

B = 1.250

1.000

0.750

0.500

0.250

0.125

0.0

-0.125

-0.250

-0.500

-0.750

-1.000

-1.250

763

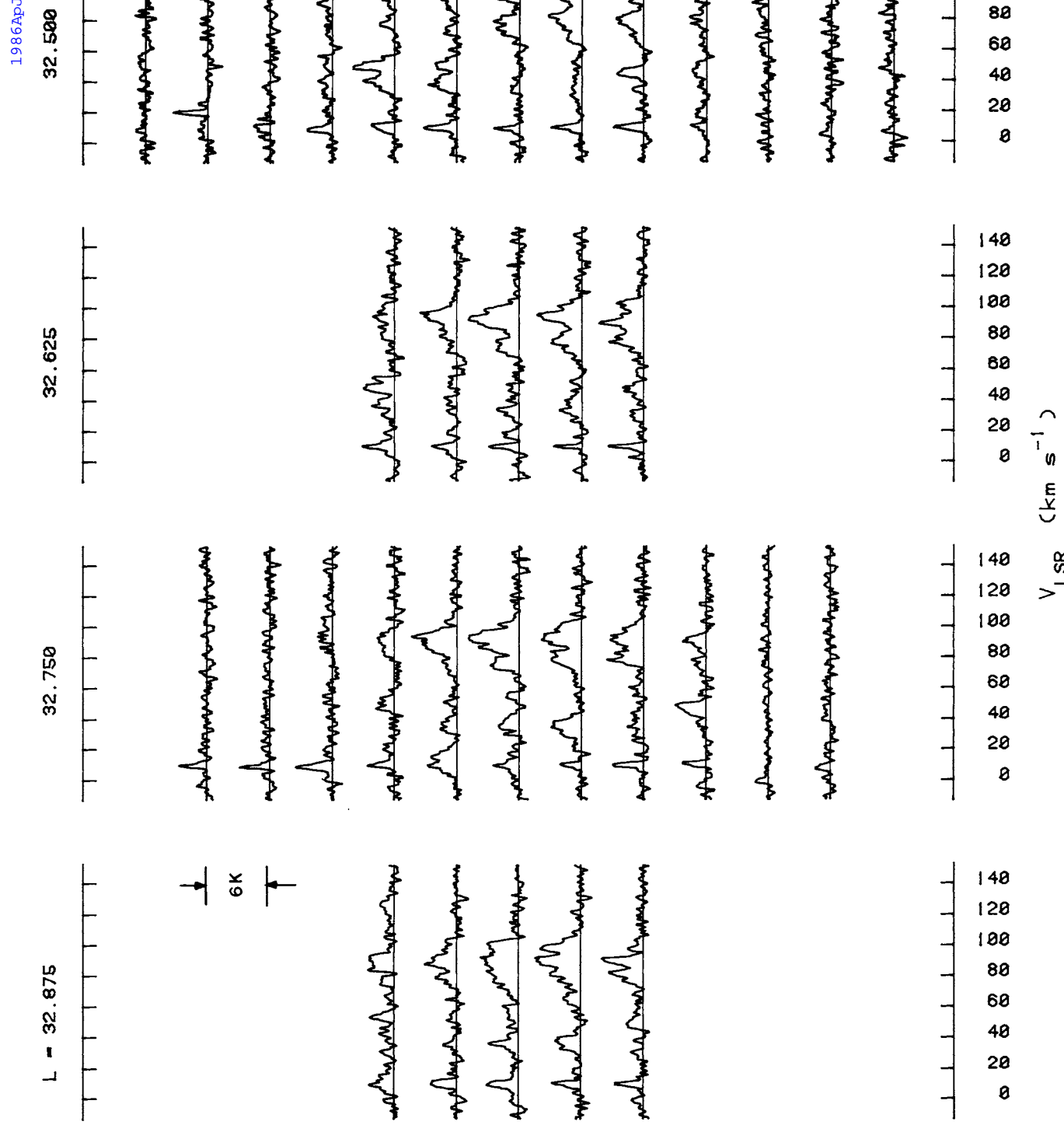

 $V_{\text{LSR}}$  ( $\text{km s}^{-1}$ )

FIG. 11—Continued

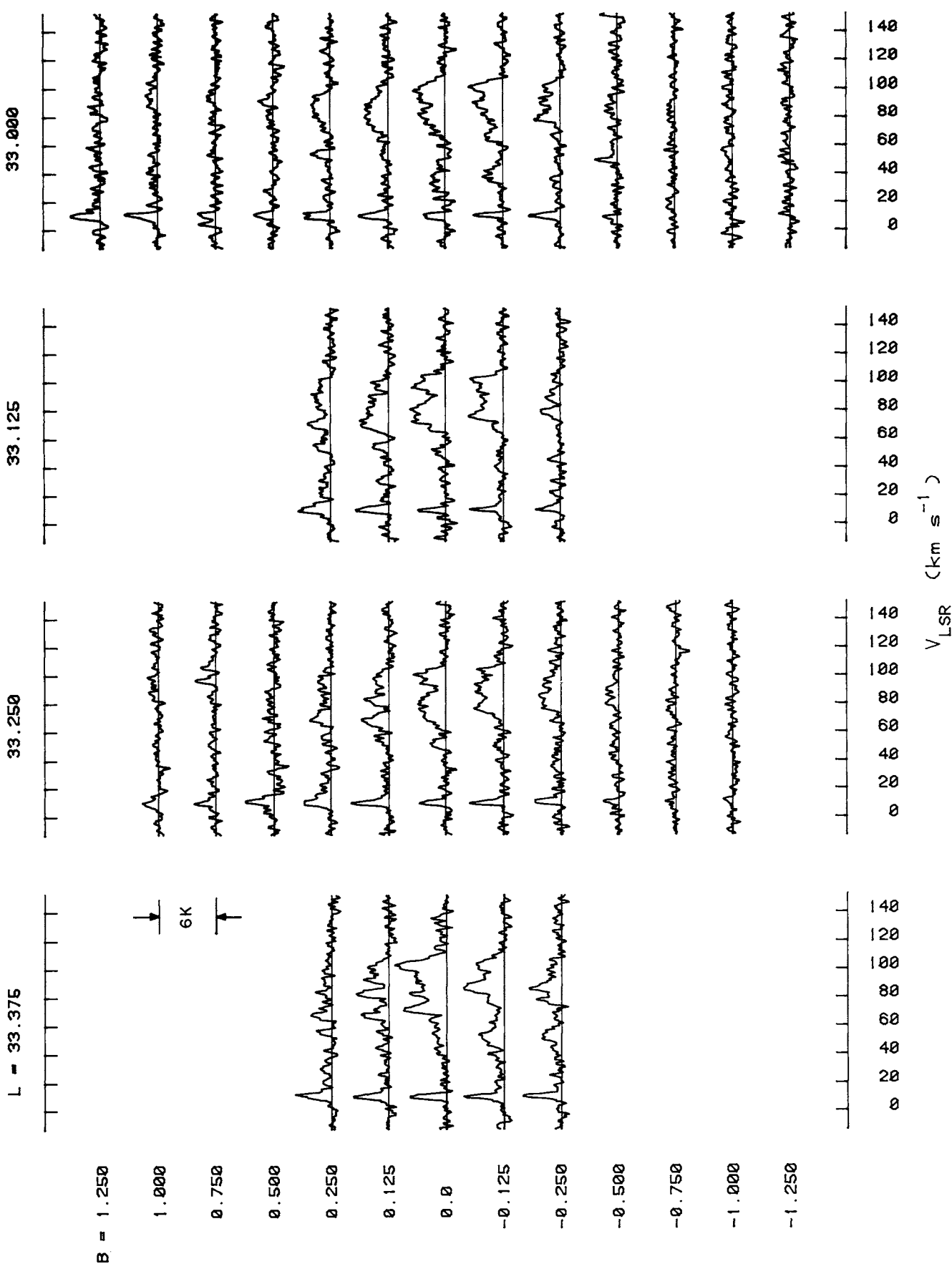


FIG. 11—Continued

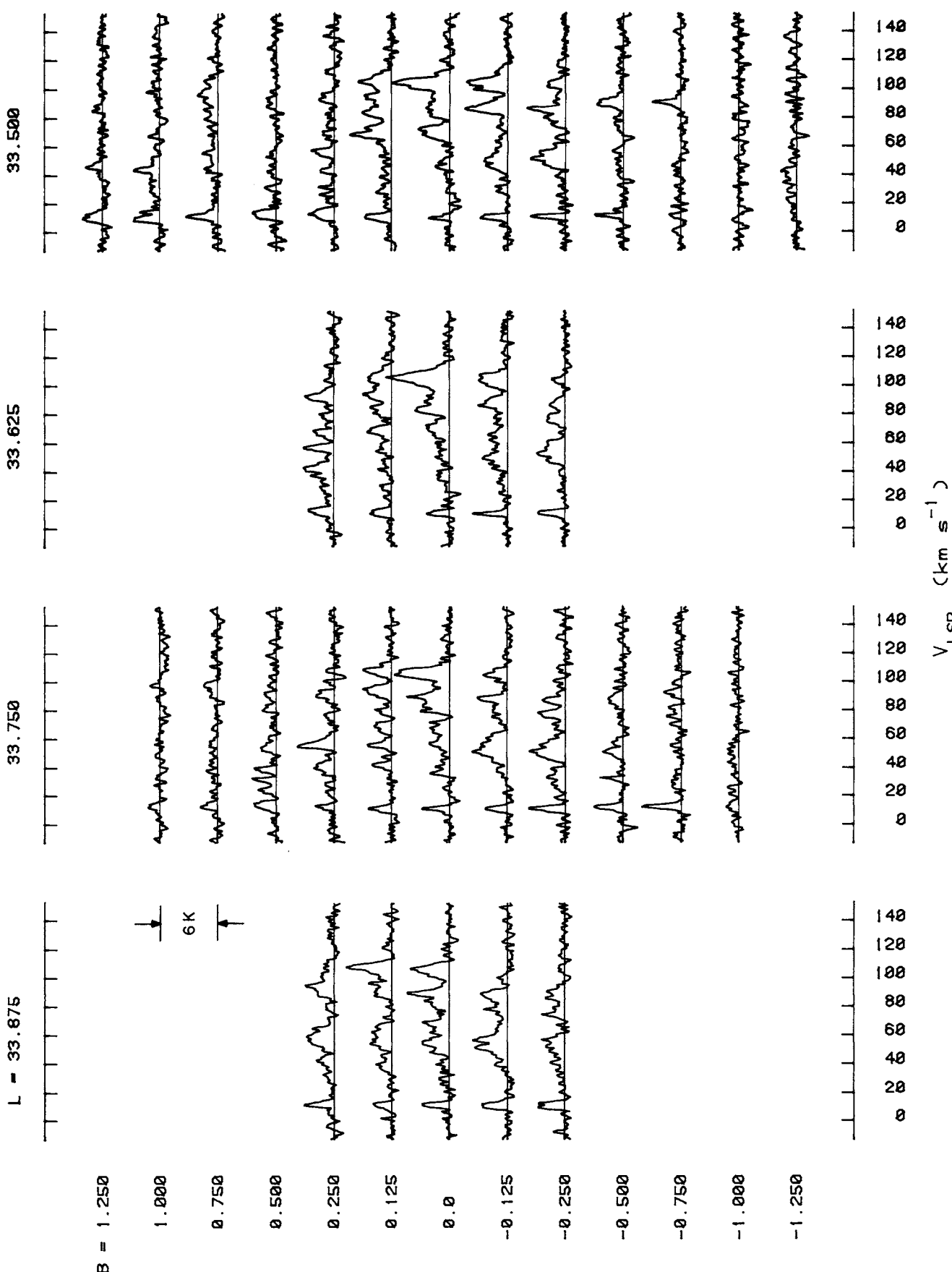


FIG. 11—Continued

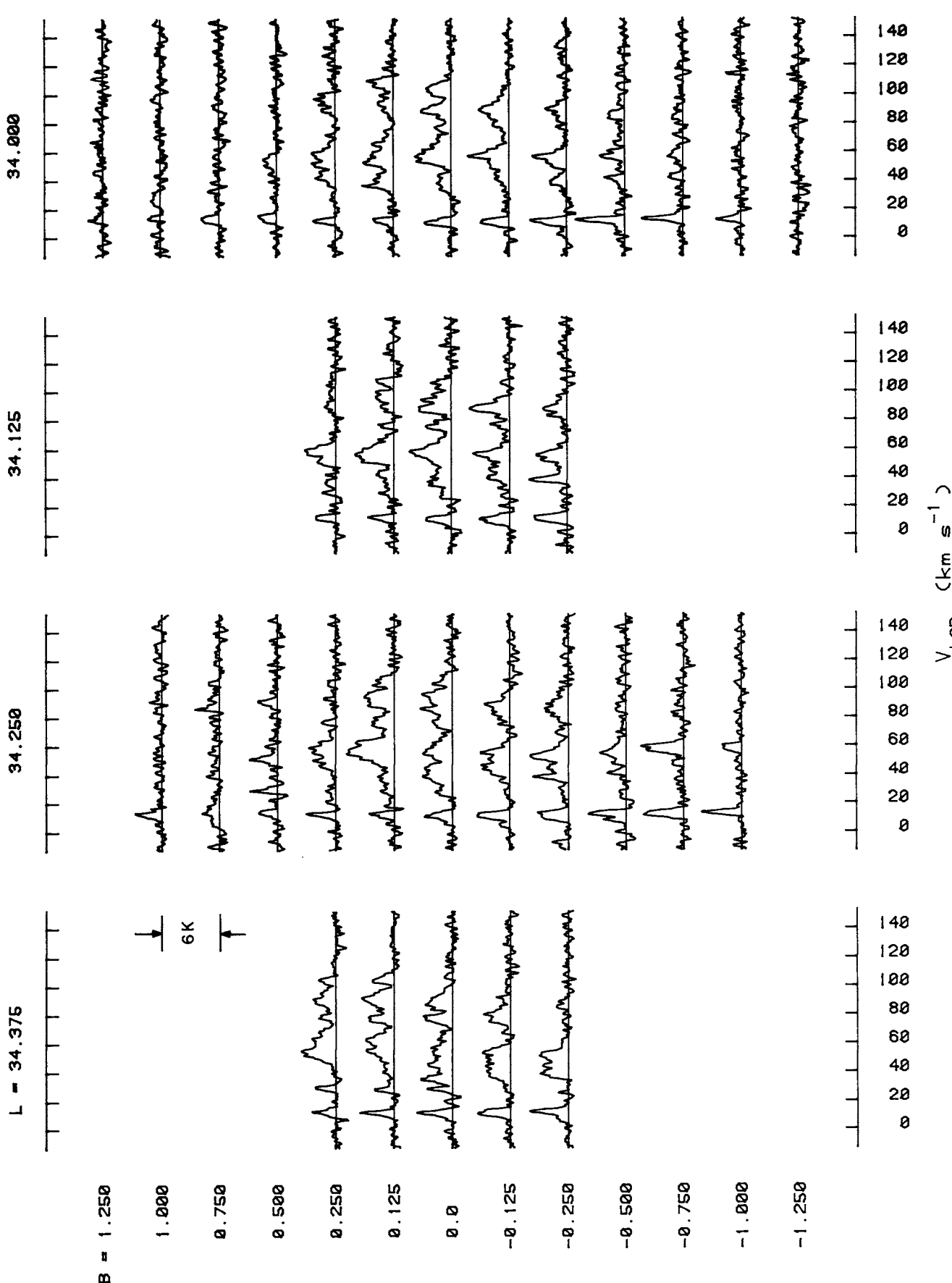


FIG. 11—Continued

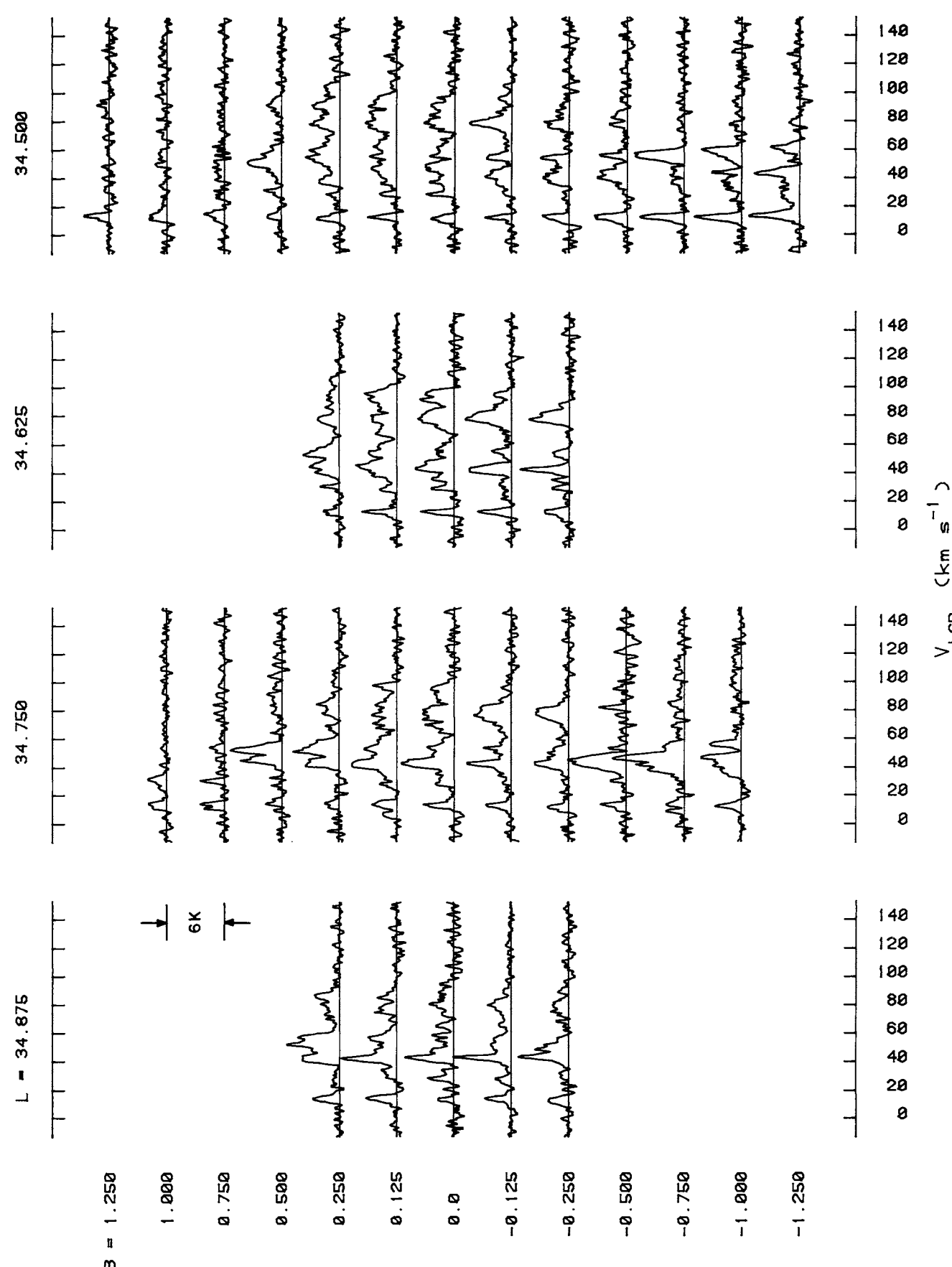


FIG. 11—Continued

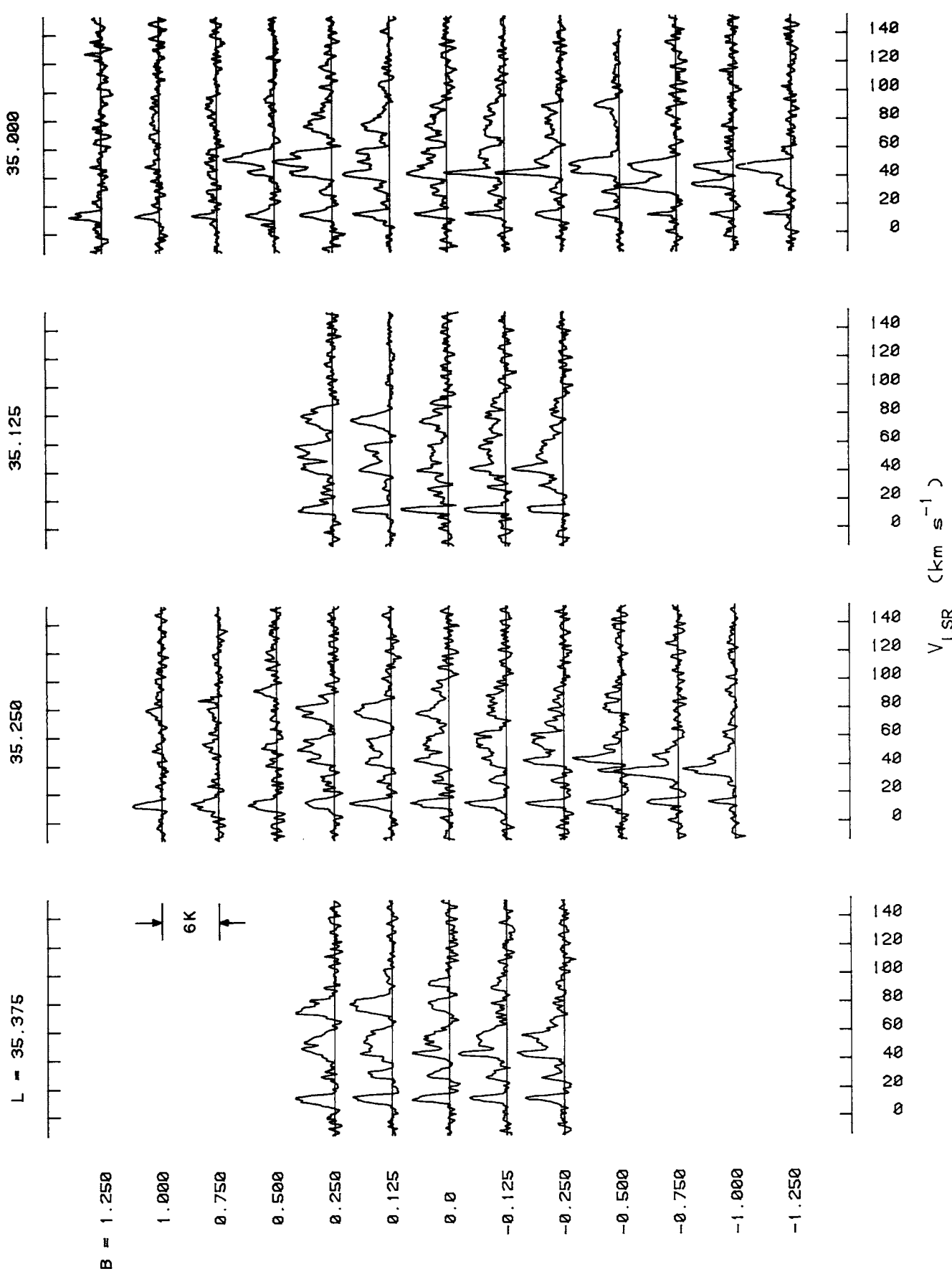


FIG. 11—Continued

35.500

35.625

35.750

L = 35.875

B = 1.250

1.000

 $\frac{1}{6K}$ 

0.750

0.500

0.250

0.125

0.0

-0.125

-0.250

-0.500

-0.750

-1.000

-1.250

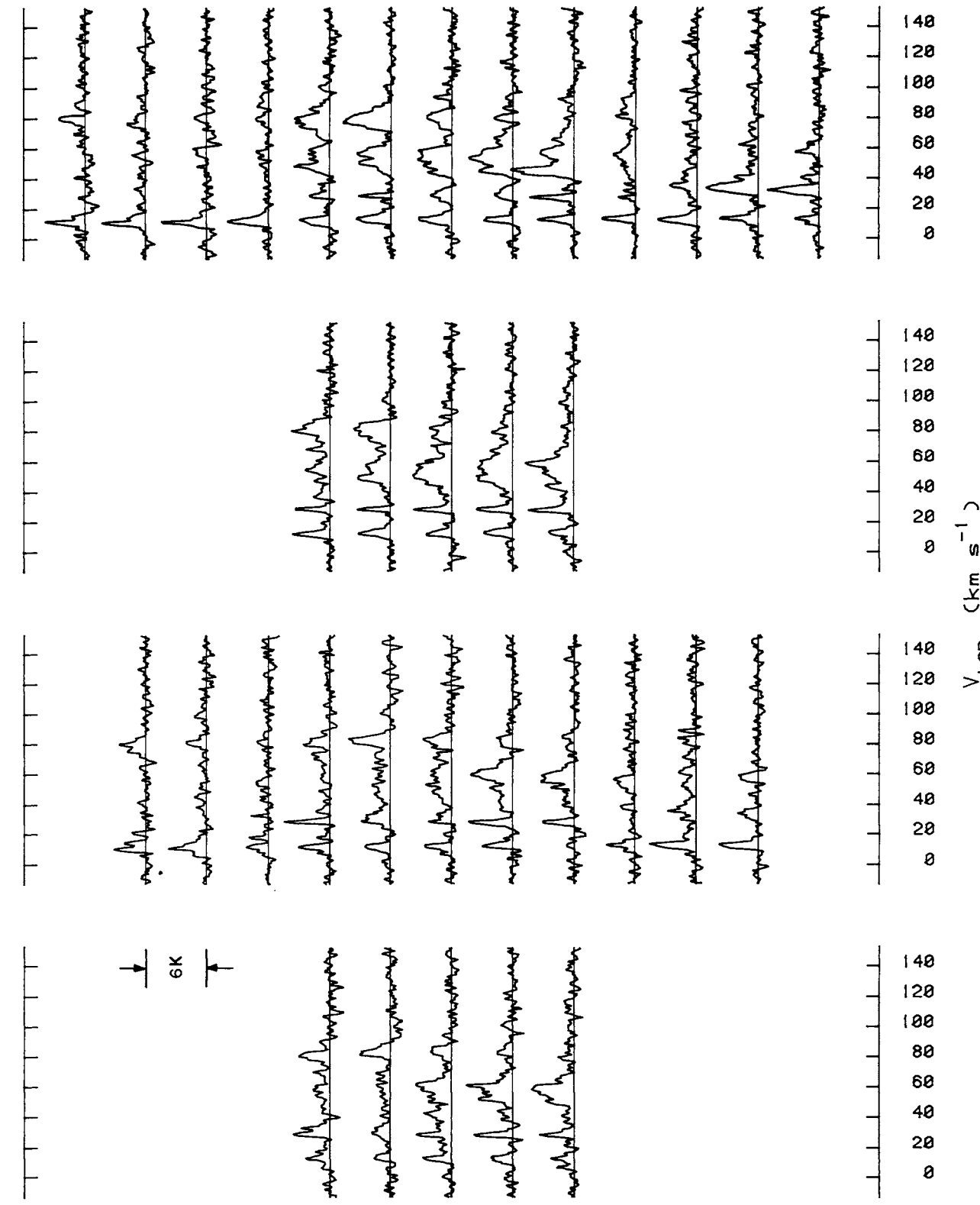
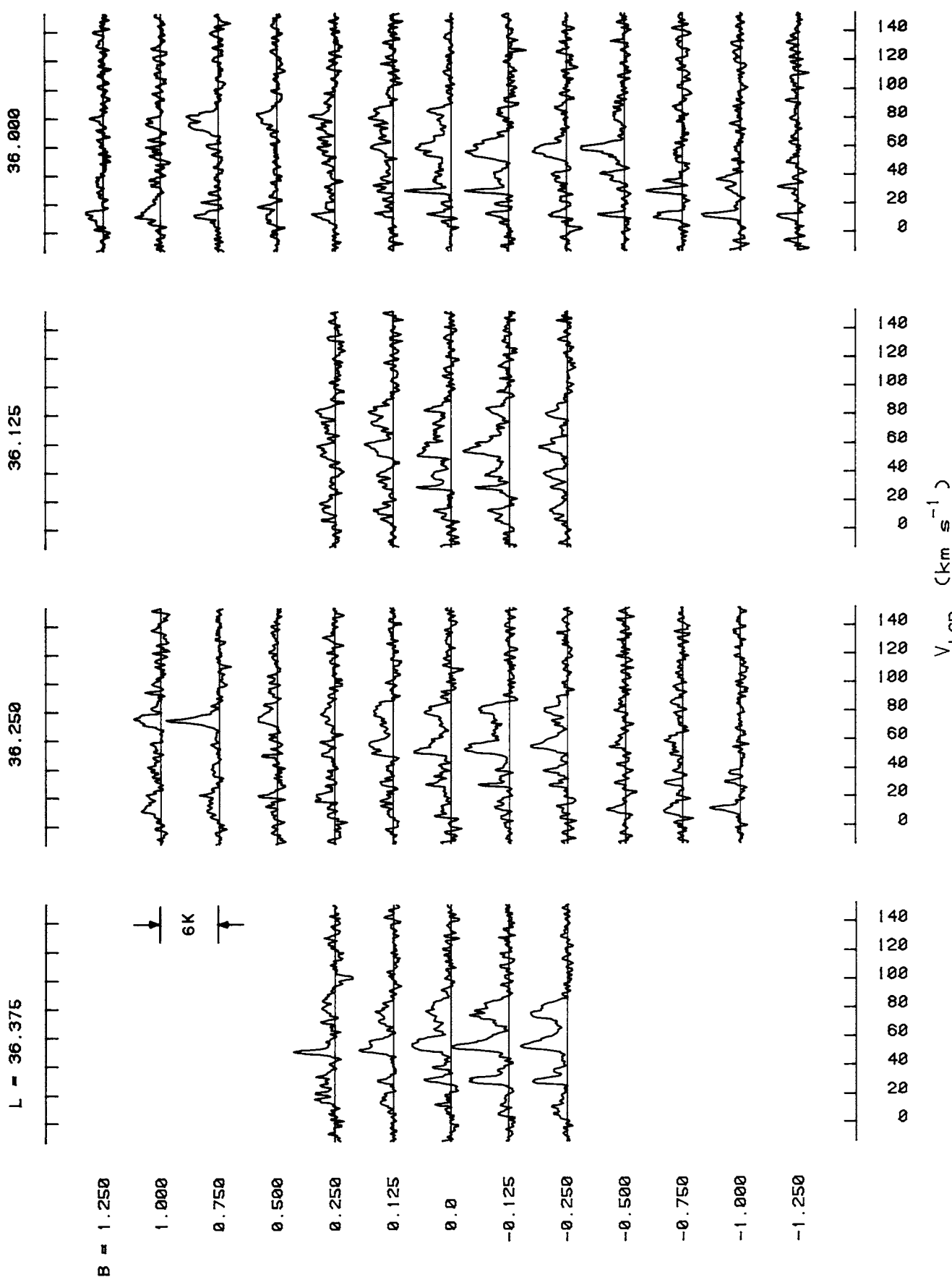


FIG. 11—Continued



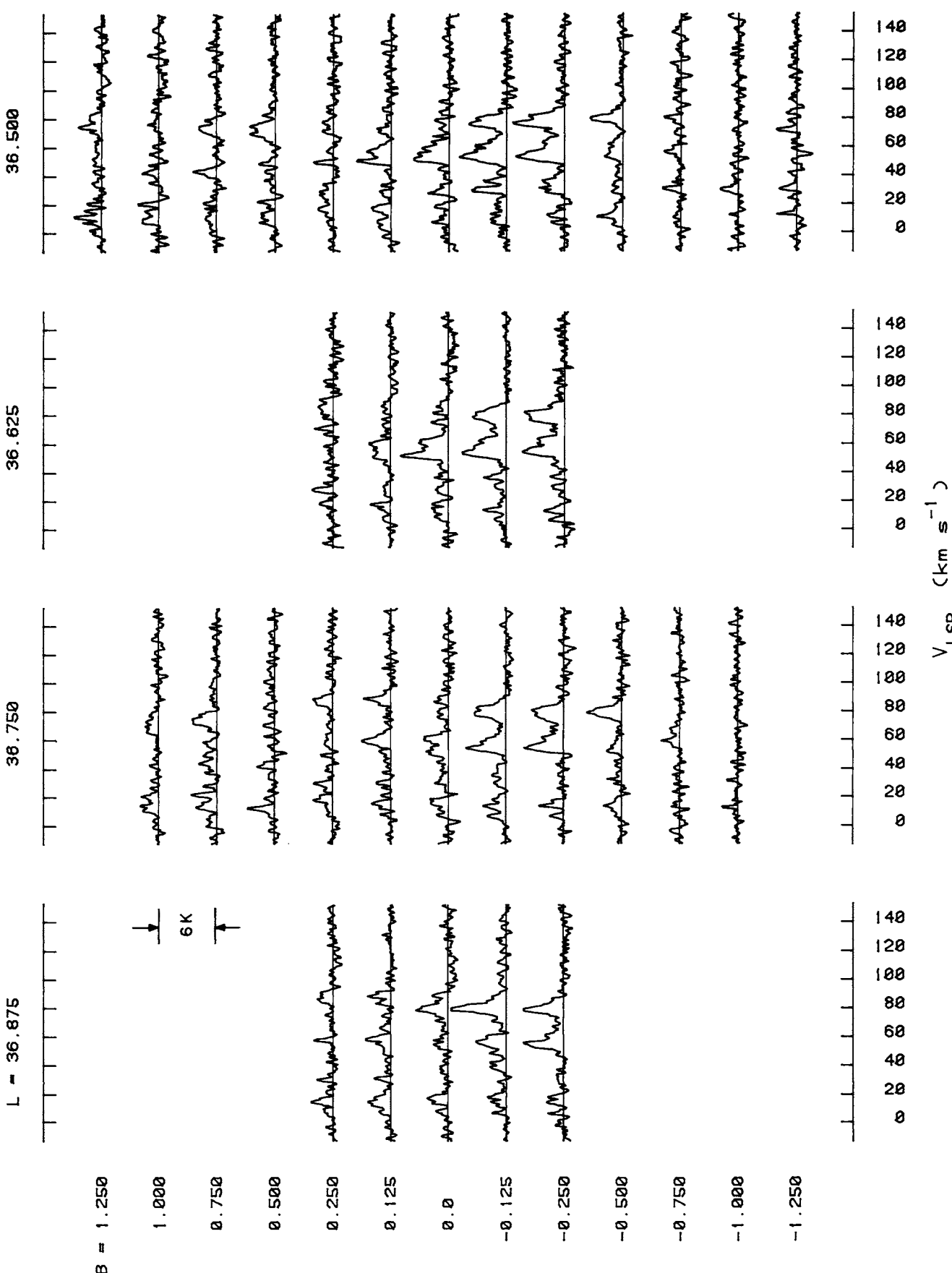


FIG. 11—Continued

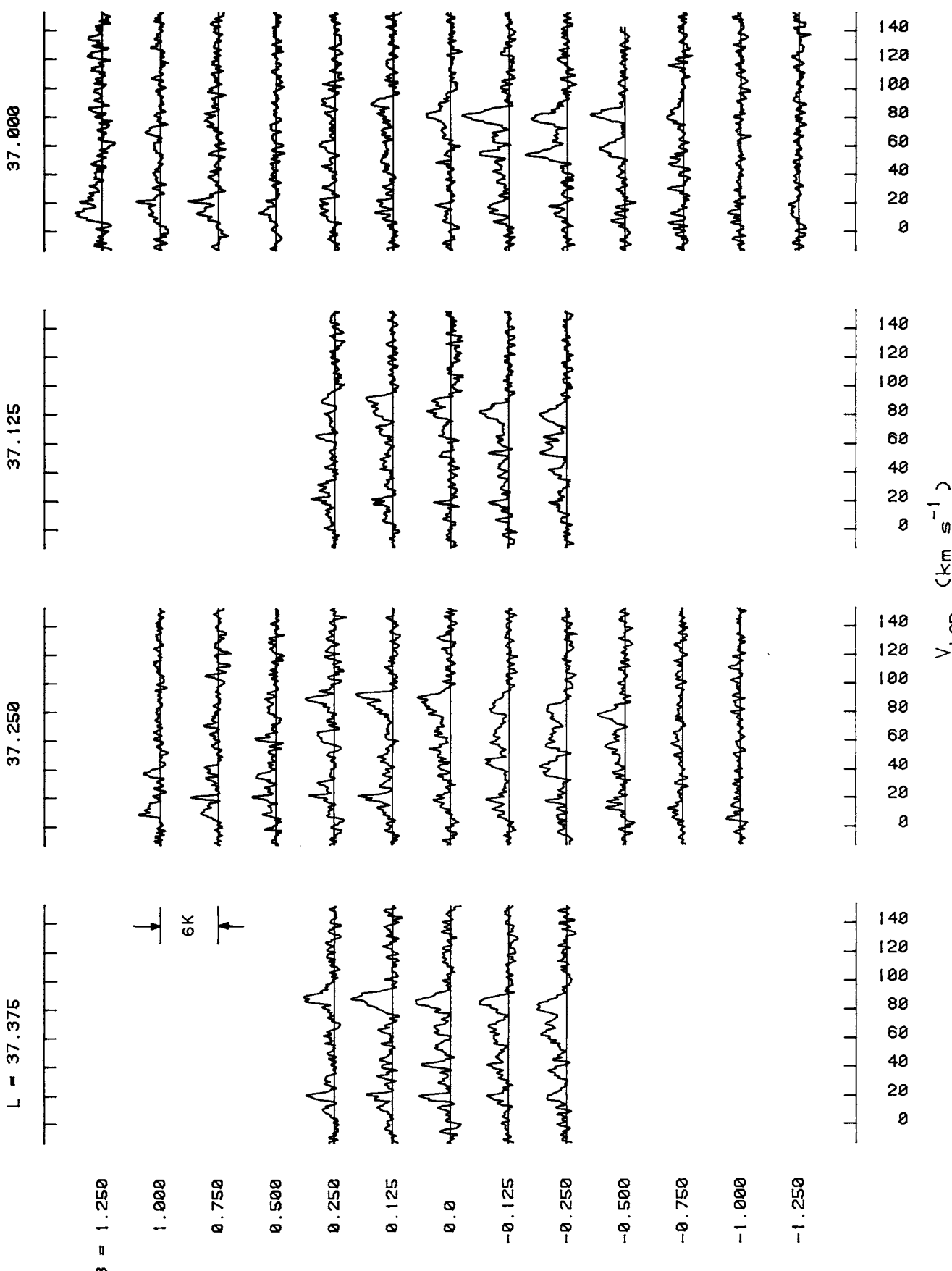
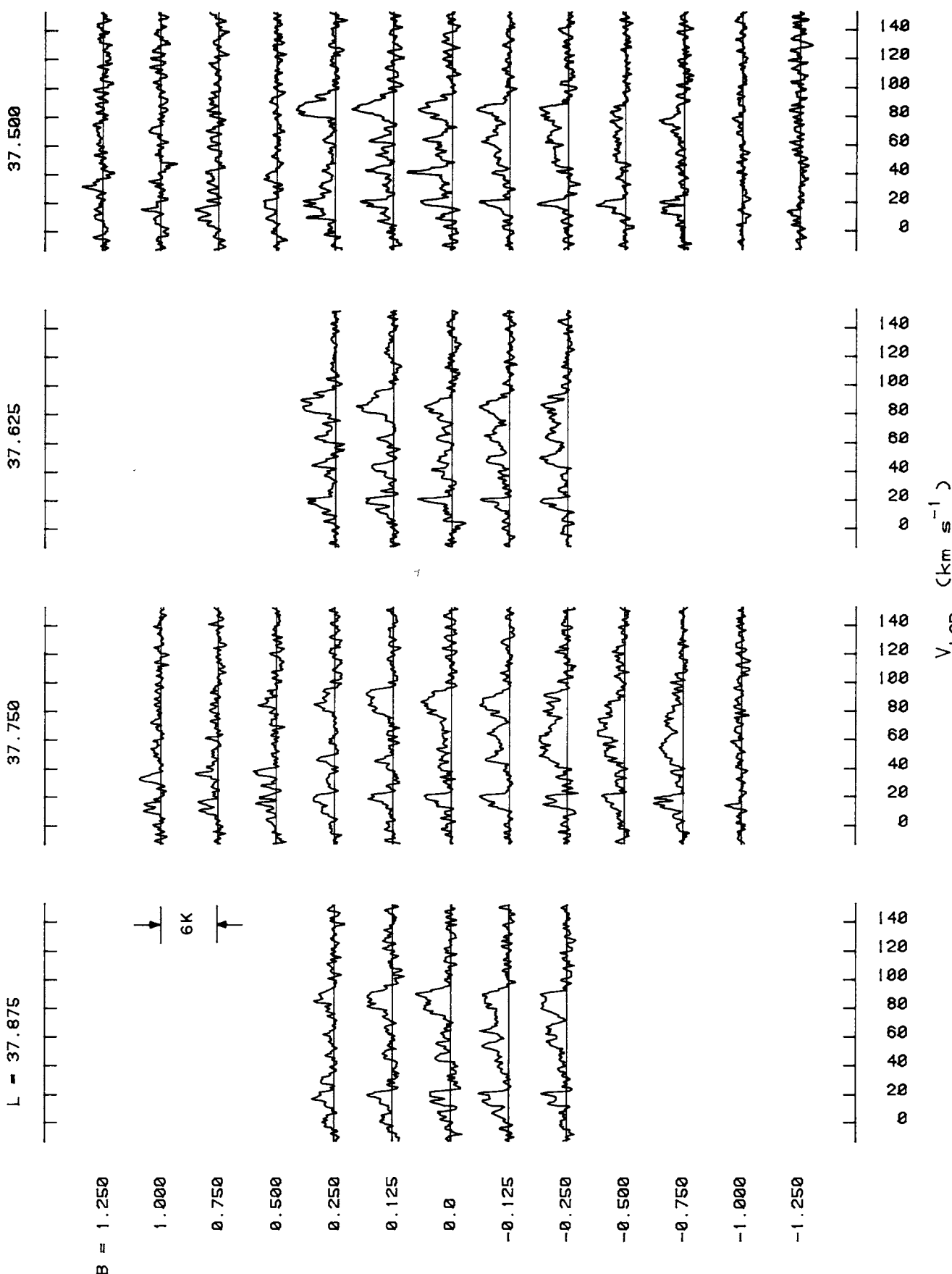


FIG. 11—Continued



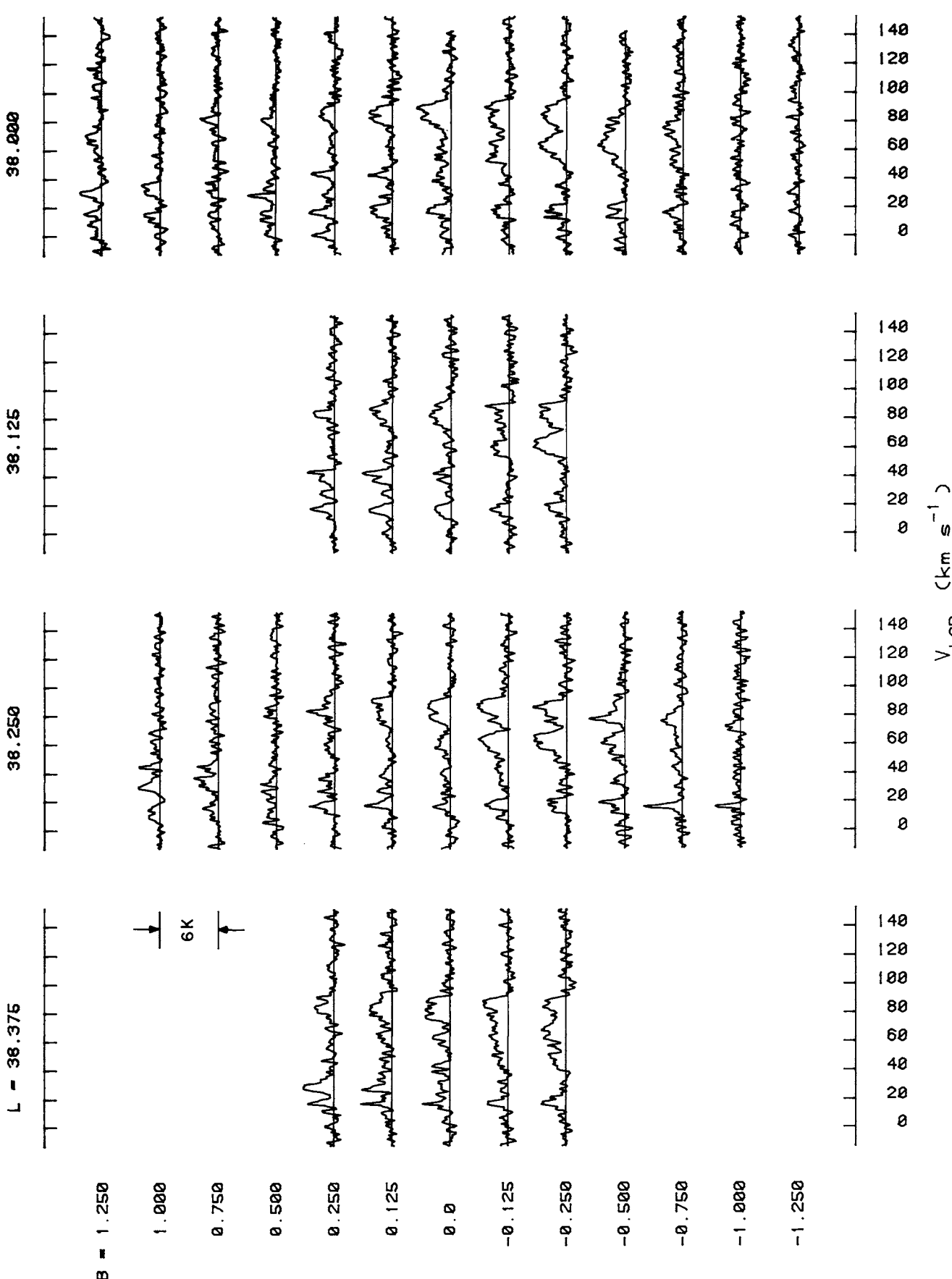


FIG. 11.—Continued

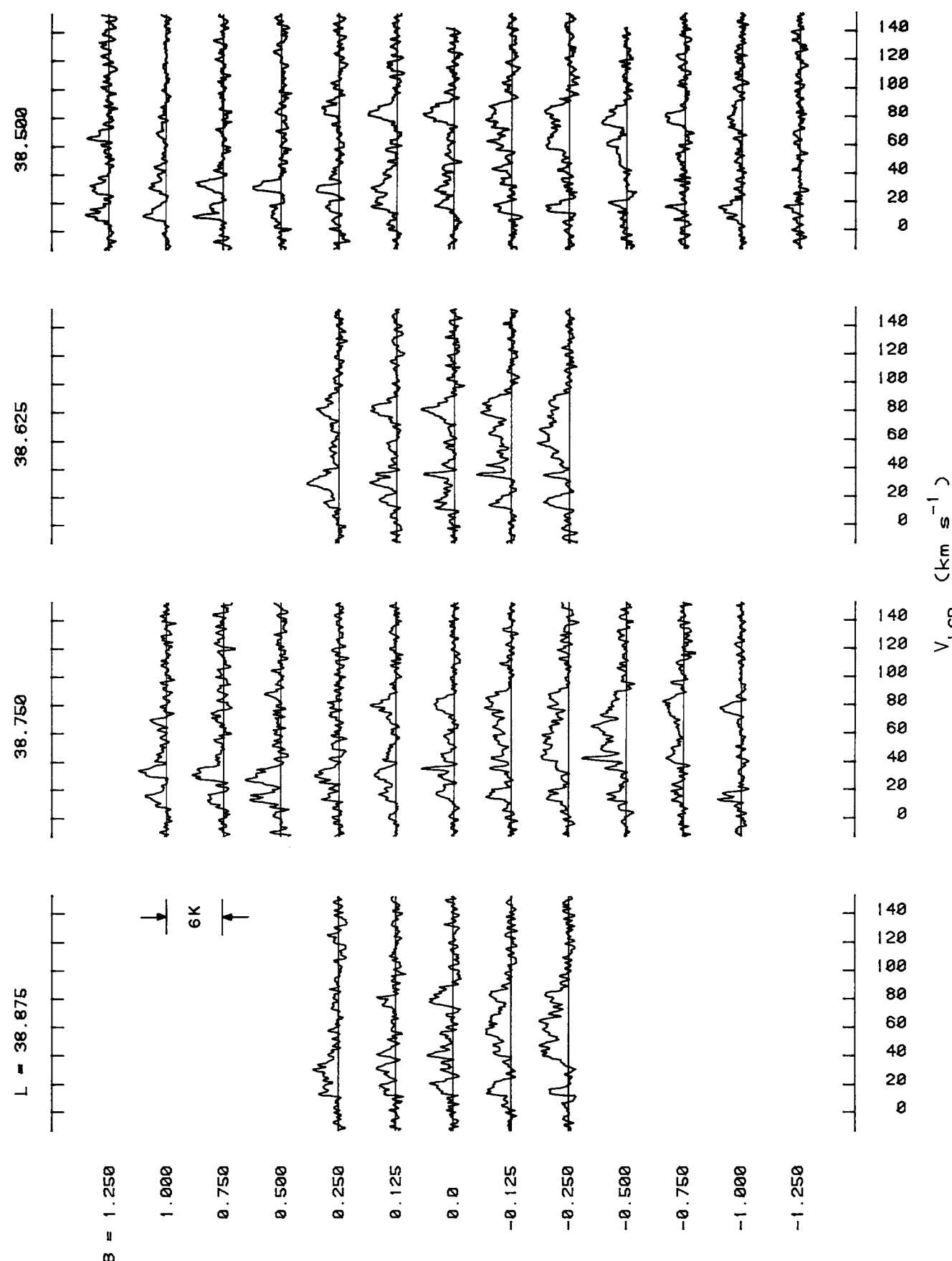


FIG. 11—Continued

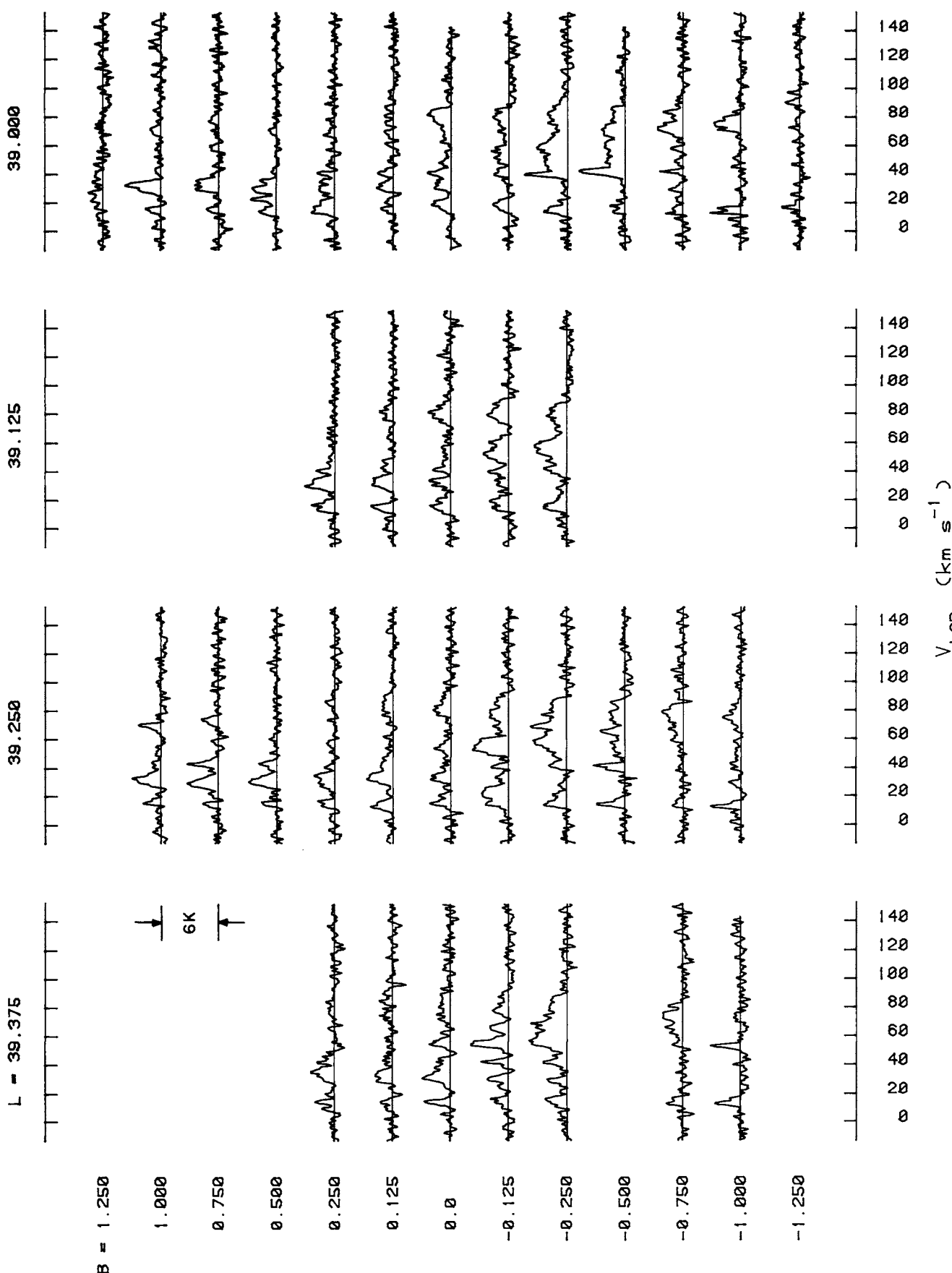


FIG. 11—Continued

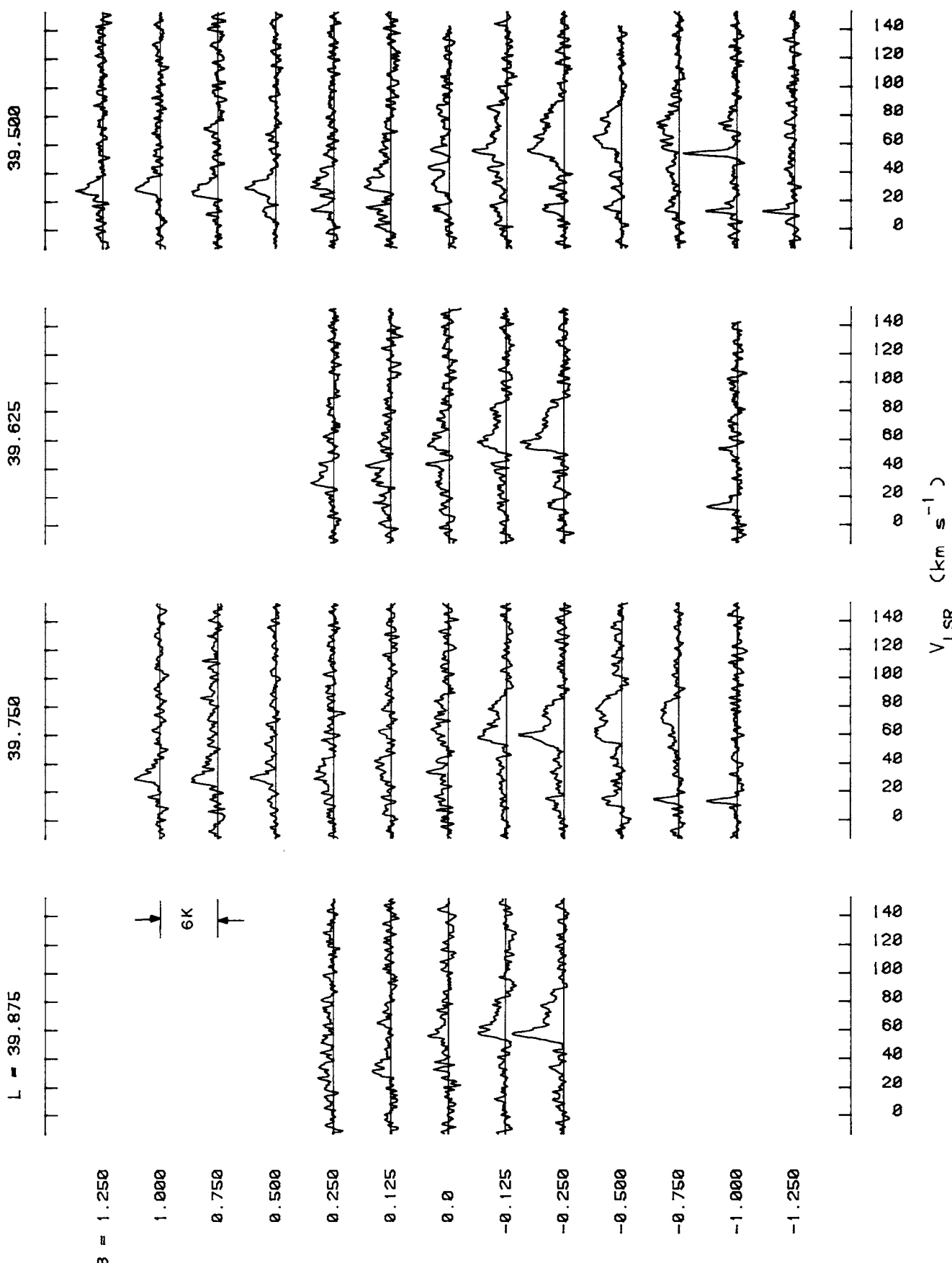


FIG. 11—Continued

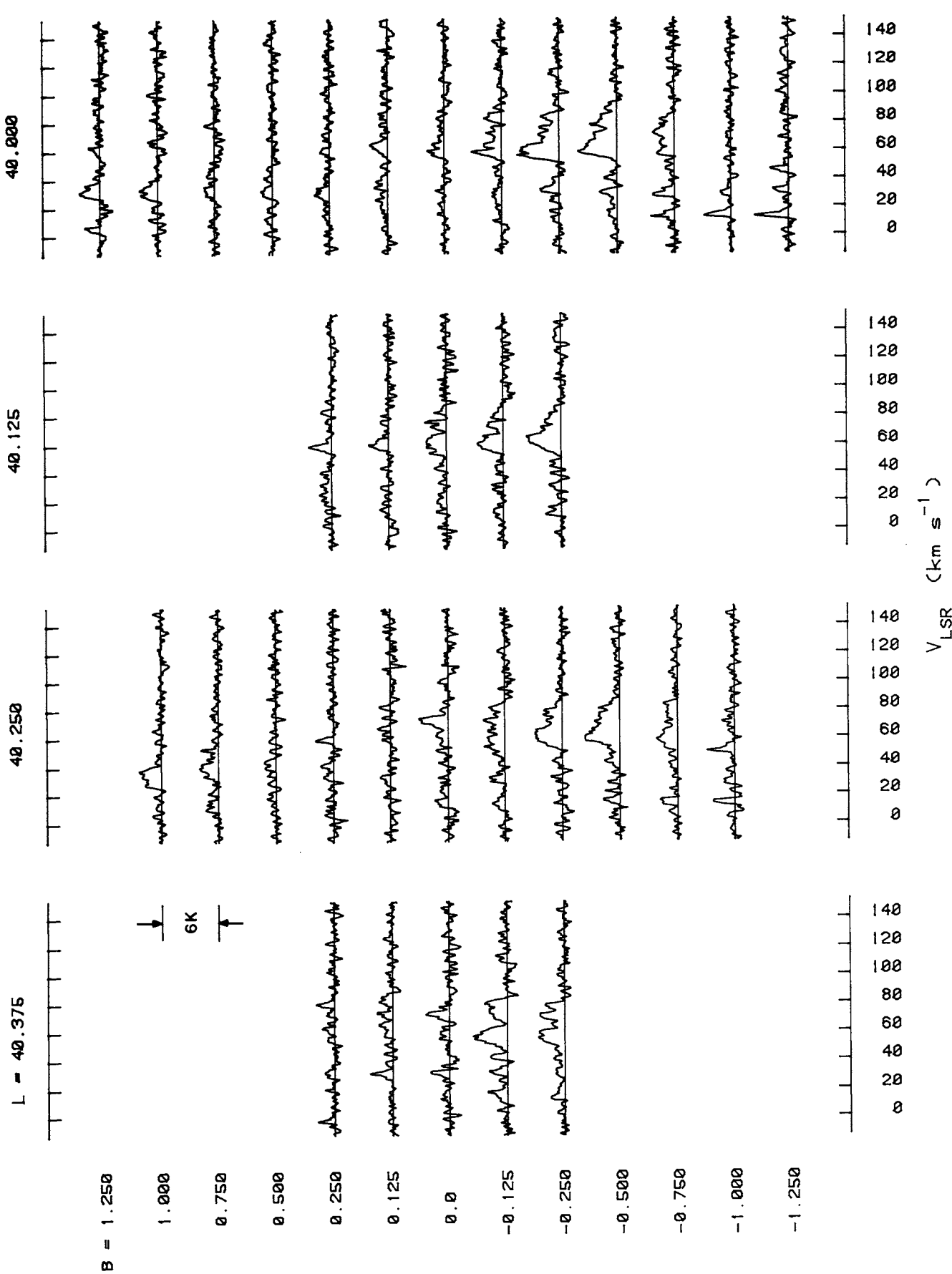


FIG. 11—Continued

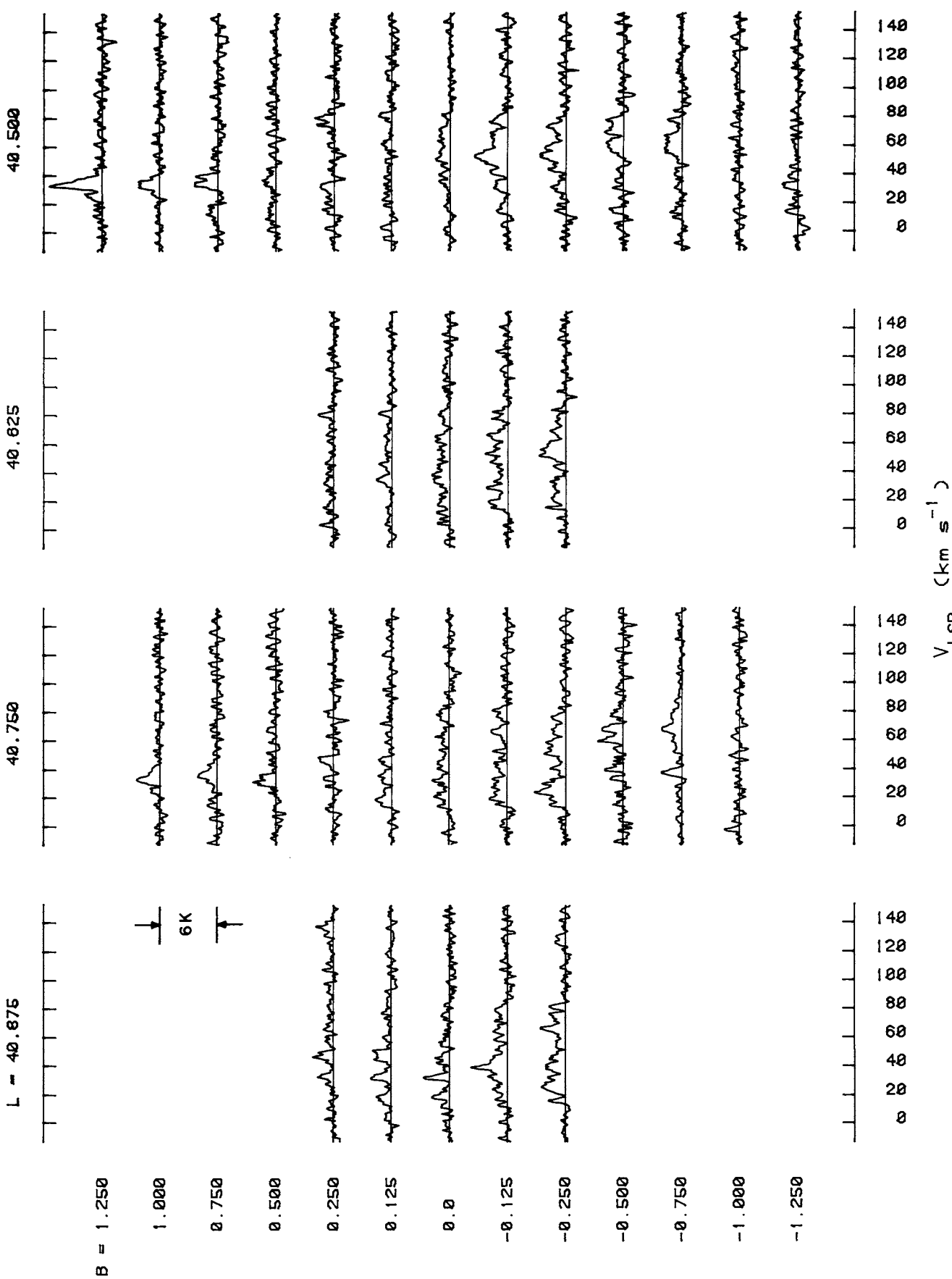


FIG. 11—Continued

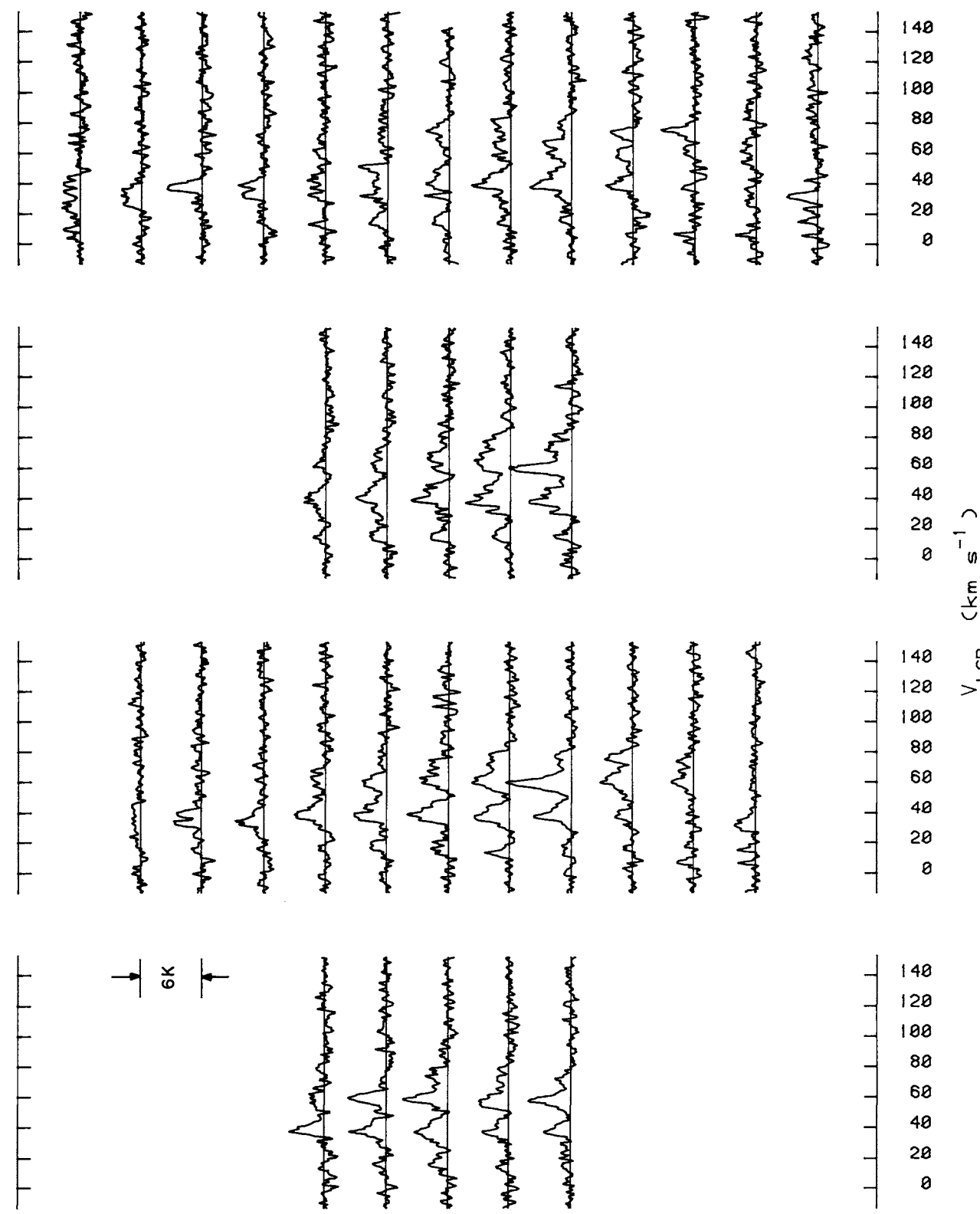
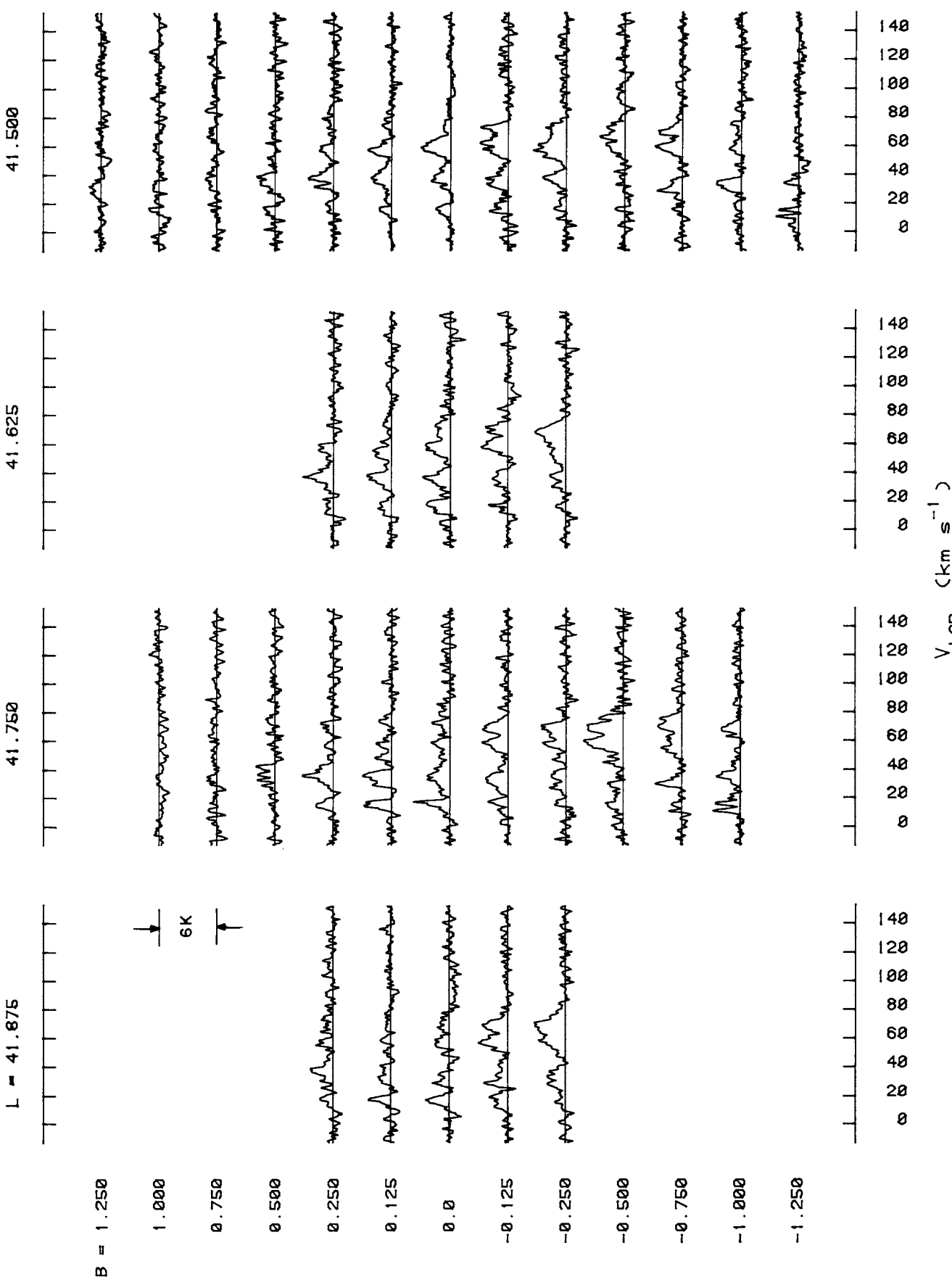
$41.250$  $41.250$  $41.250$  $41.200$  $B = 1.250$  $1.000$  $\rightarrow$  $0.750$  $\rightarrow$  $0.500$  $\rightarrow$  $0.250$  $\rightarrow$  $0.125$  $\rightarrow$  $0.0$  $\rightarrow$  $-0.125$  $\rightarrow$  $-0.250$  $\rightarrow$  $-0.500$  $\rightarrow$  $-0.750$  $\rightarrow$  $-1.000$  $\rightarrow$  $-1.250$  $\rightarrow$  $\rightarrow$  $\rightarrow$  $\rightarrow$  $V_{\text{LSR}}$  ( $\text{km s}^{-1}$ )

FIG. 11—Continued



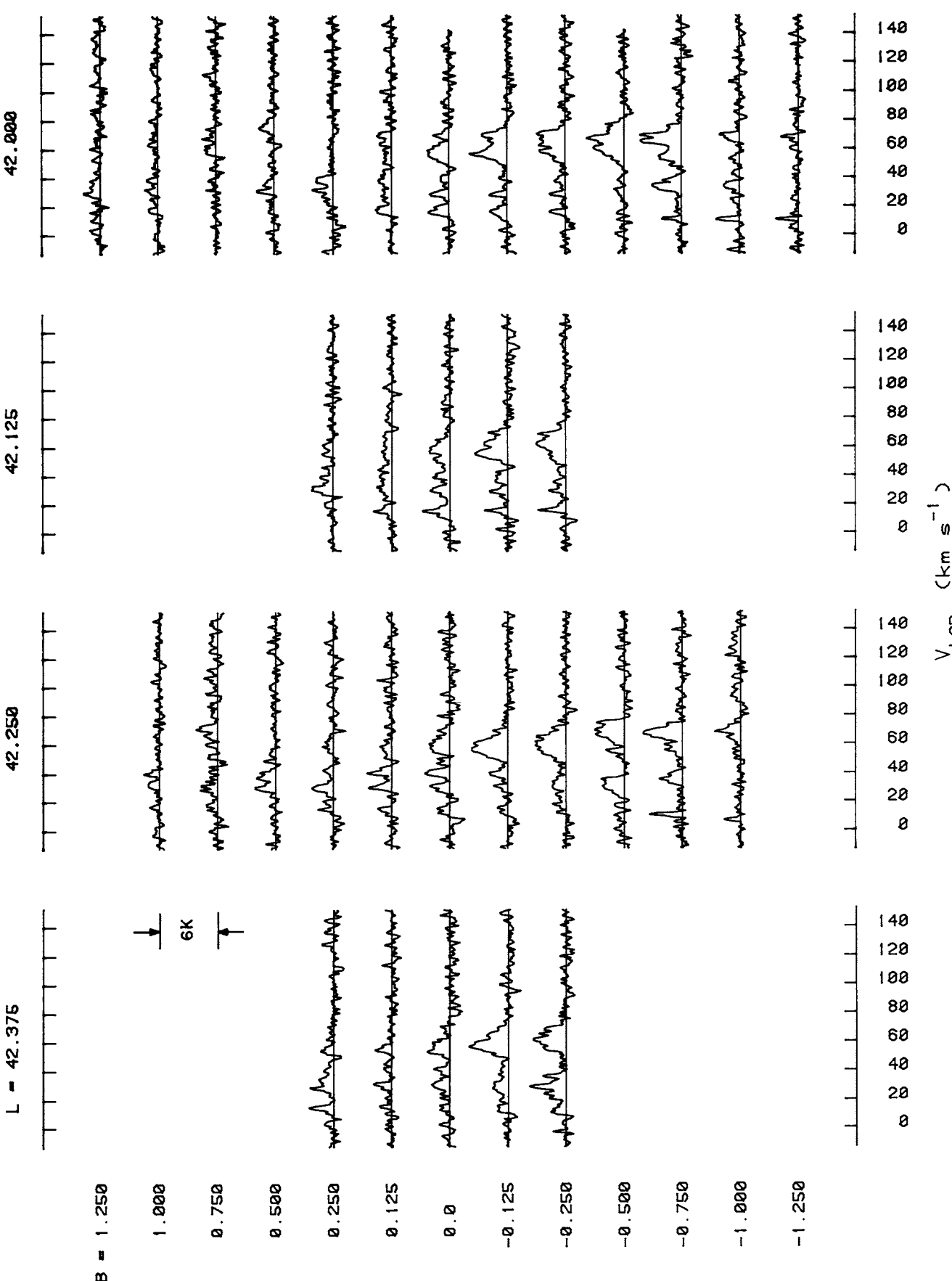


FIG. 11—Continued

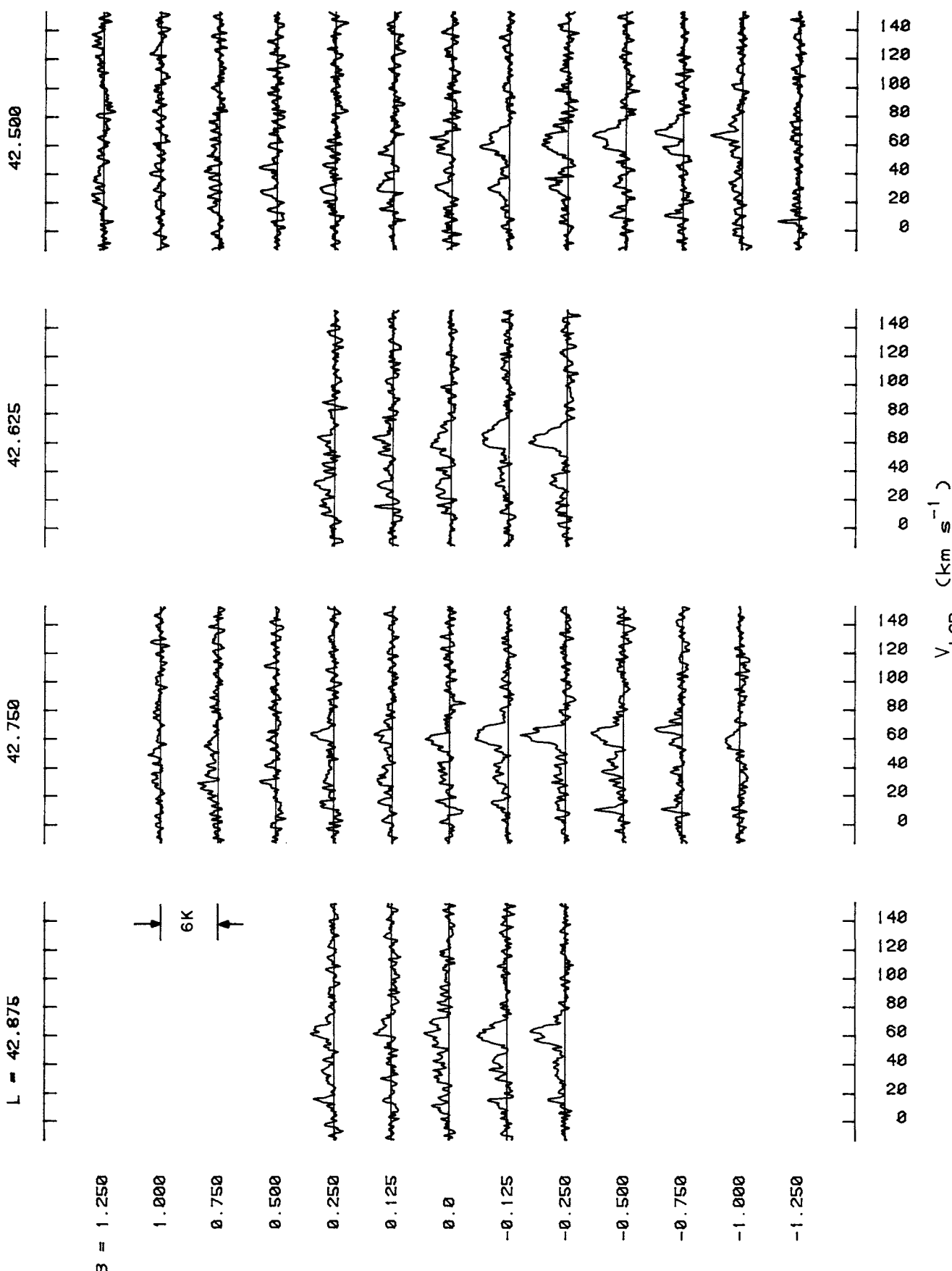


FIG. 11—Continued

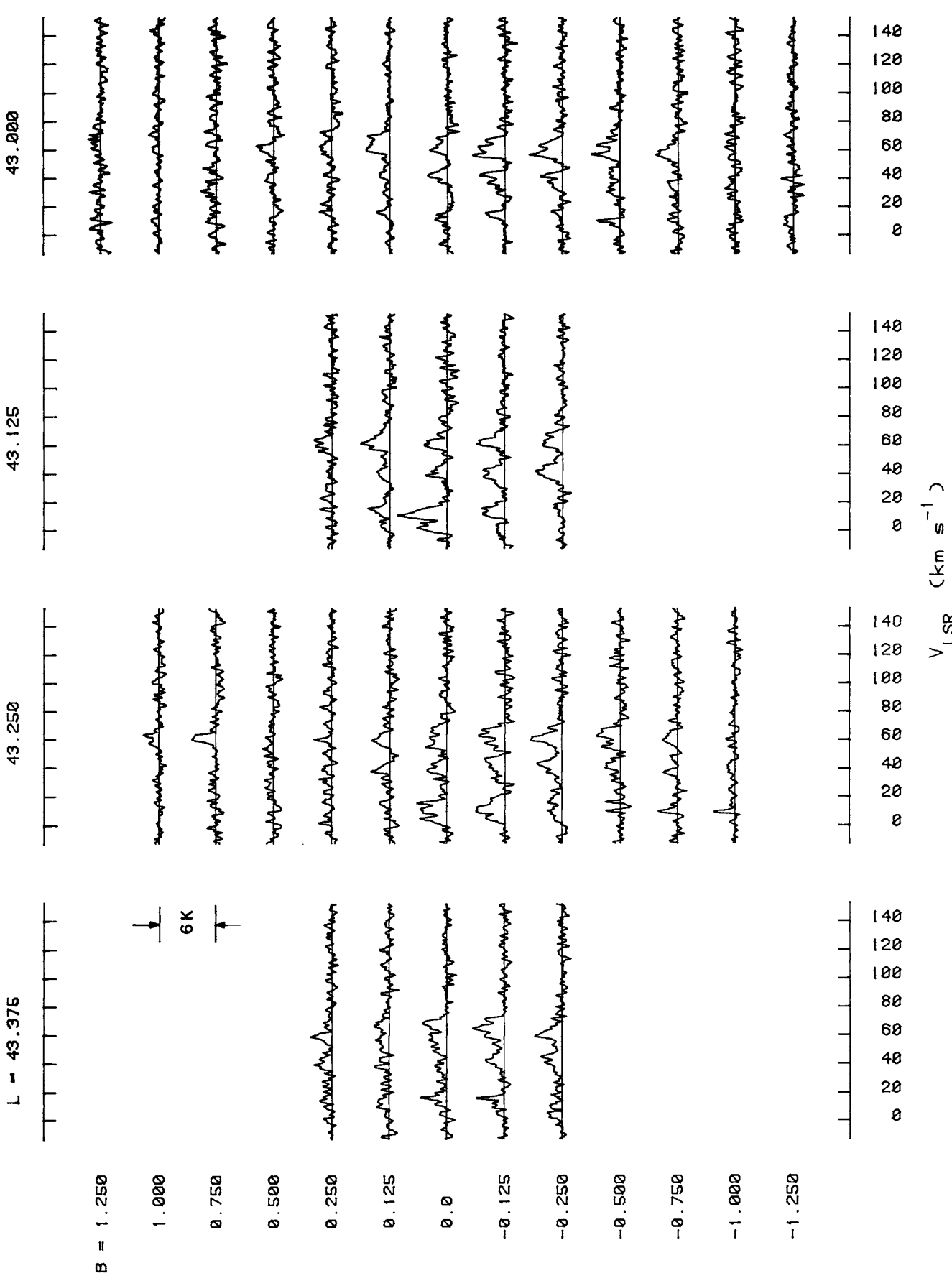


FIG. 11—Continued

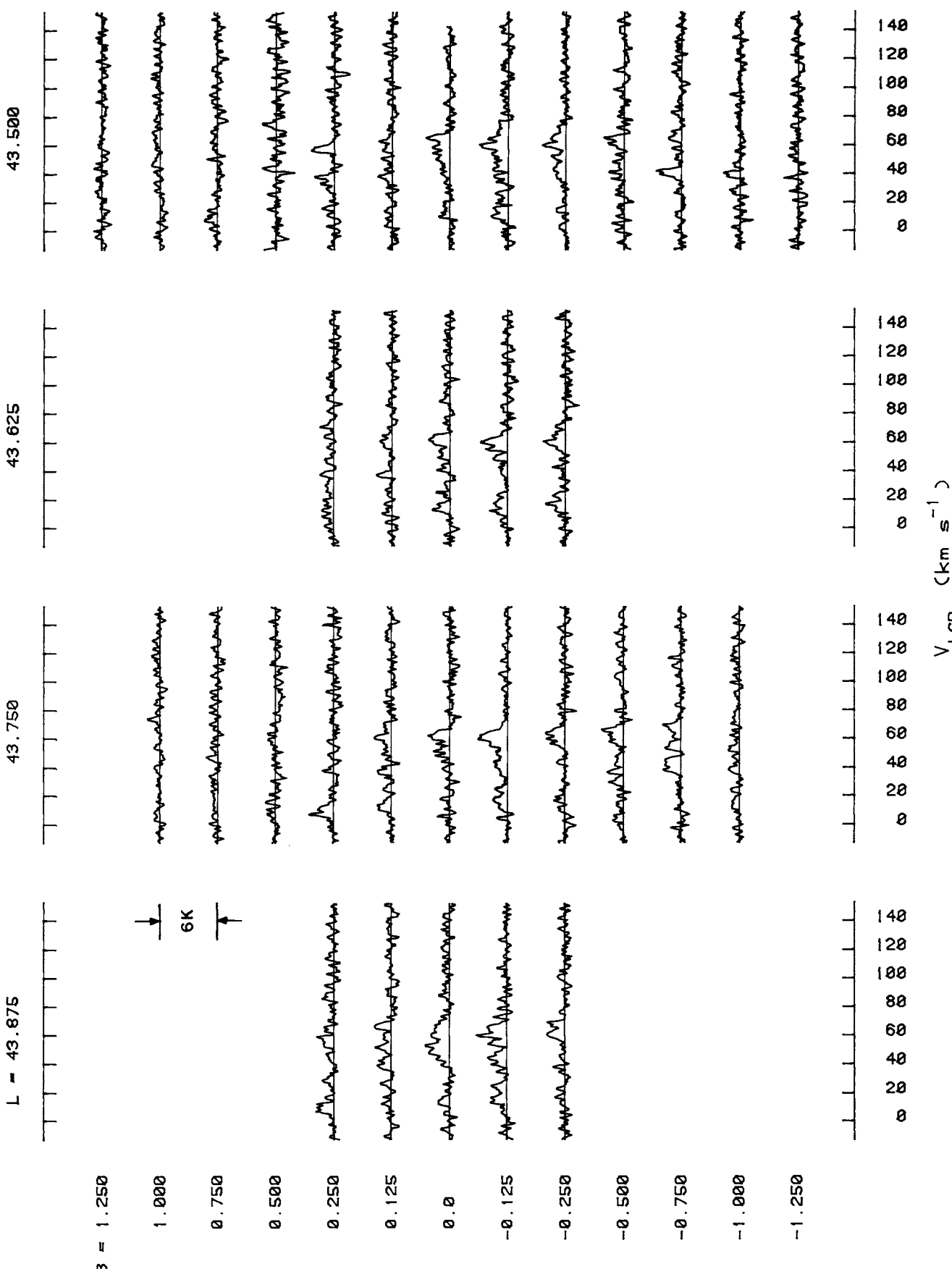
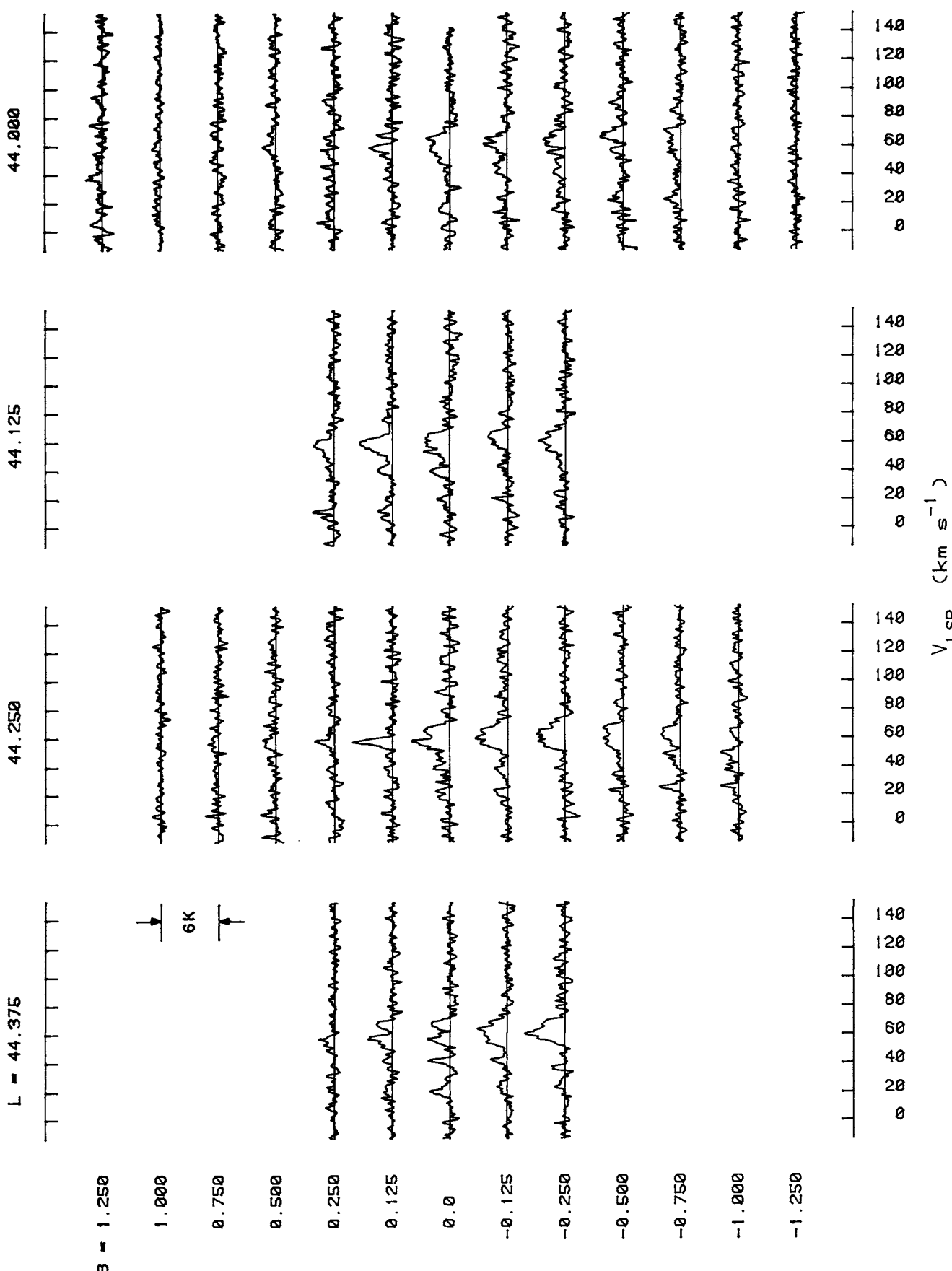


FIG. 11—Continued



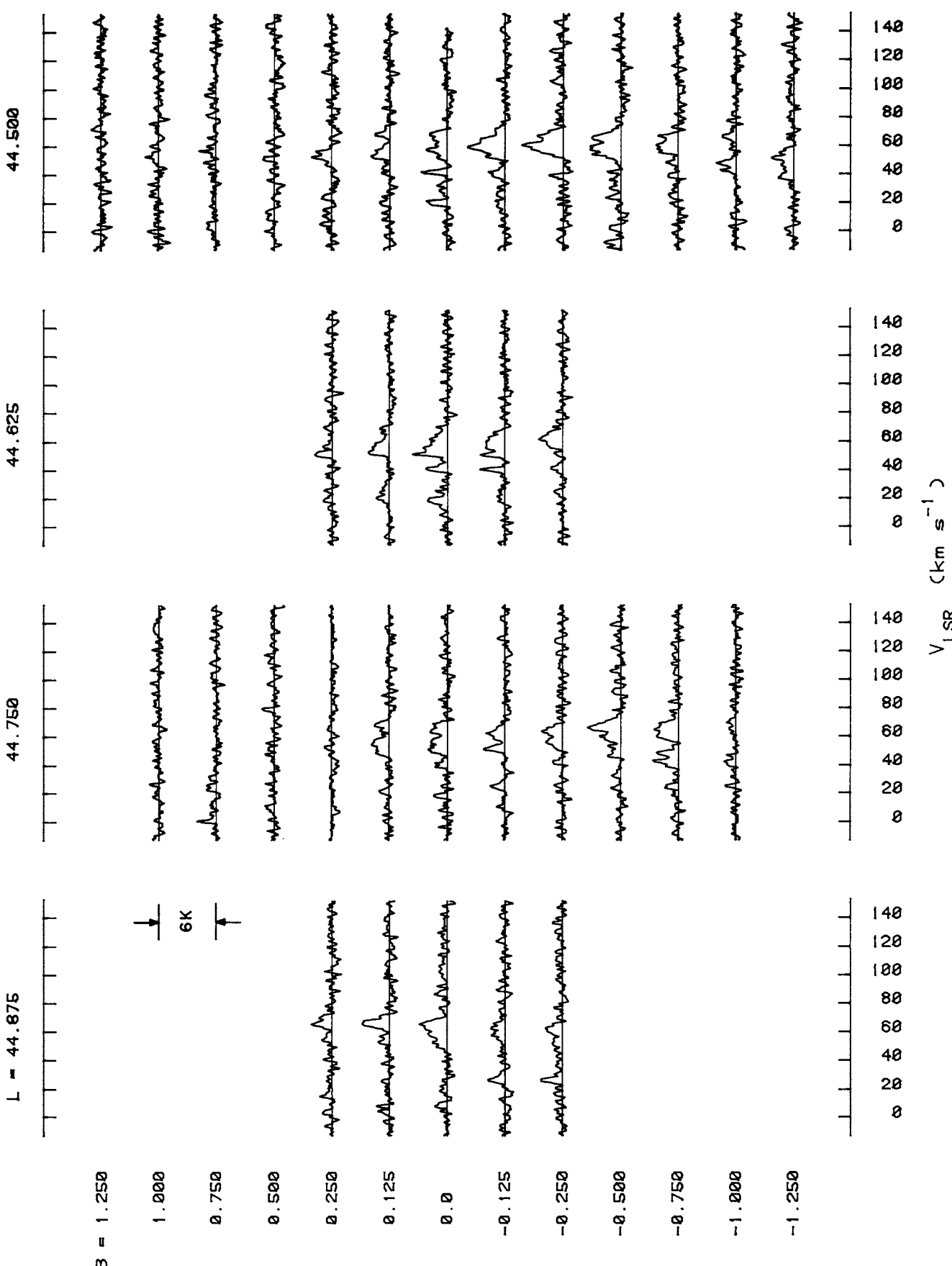


FIG. 11—Continued

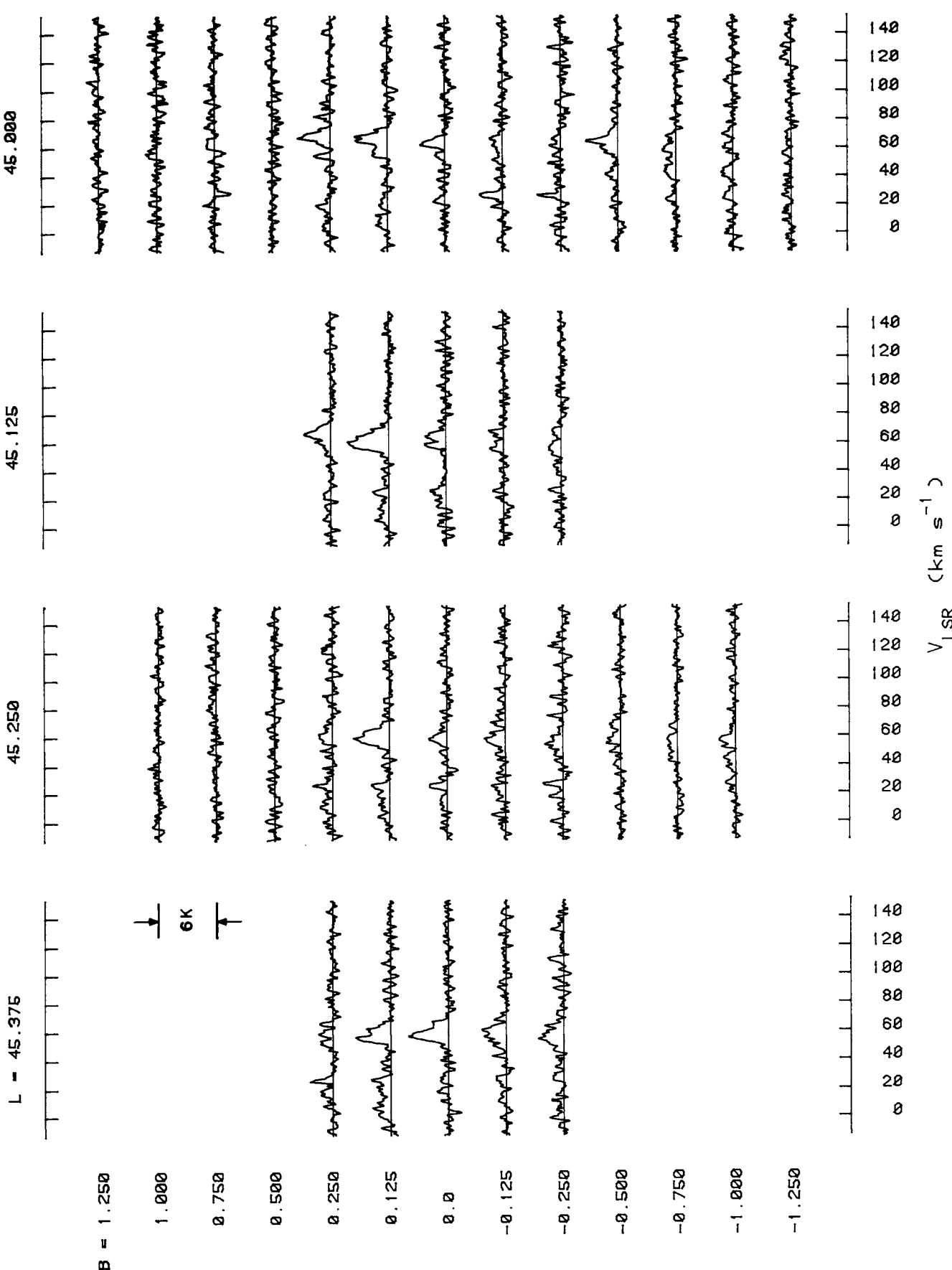


FIG. 11—Continued

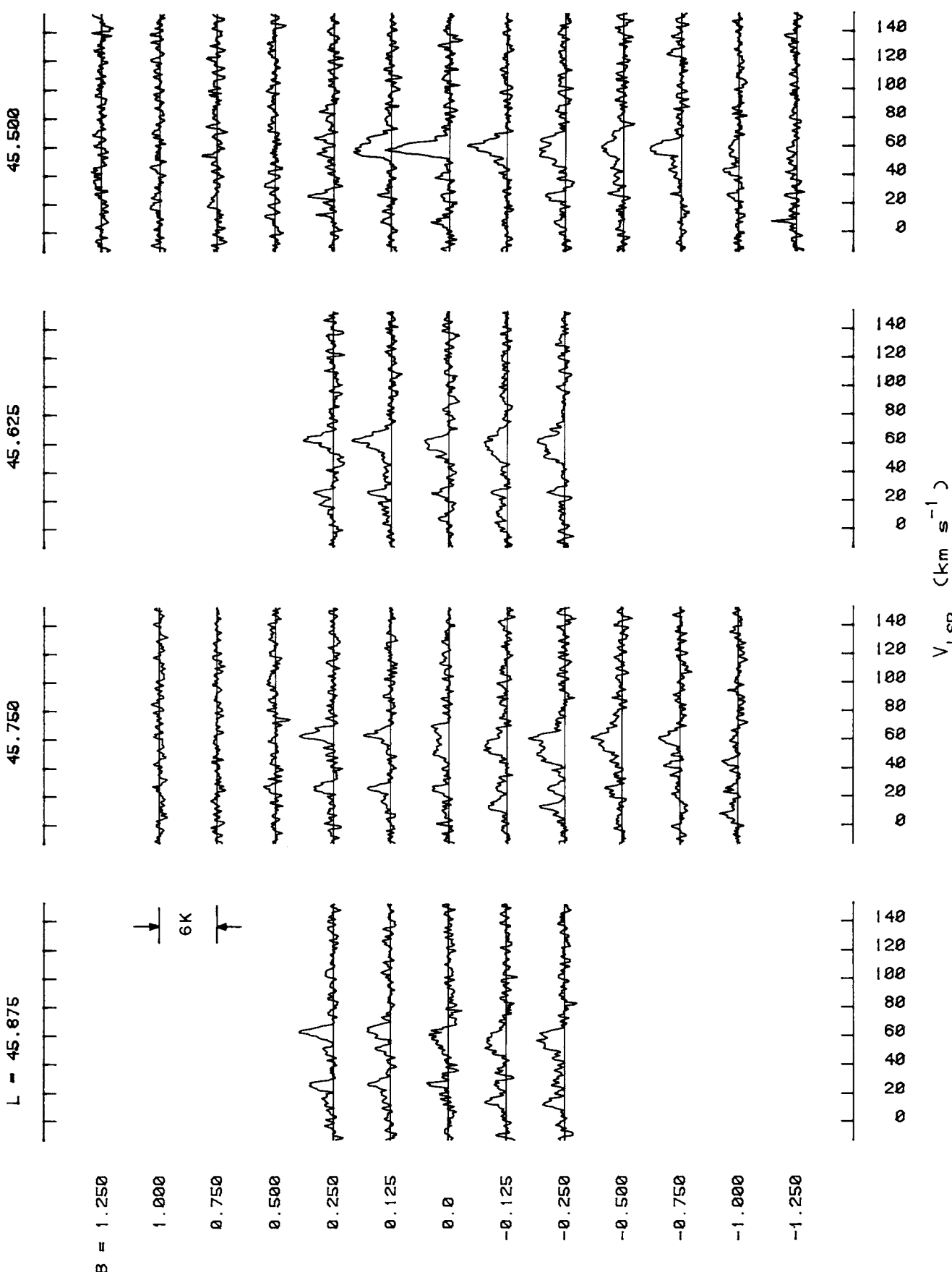


FIG. 11.—Continued

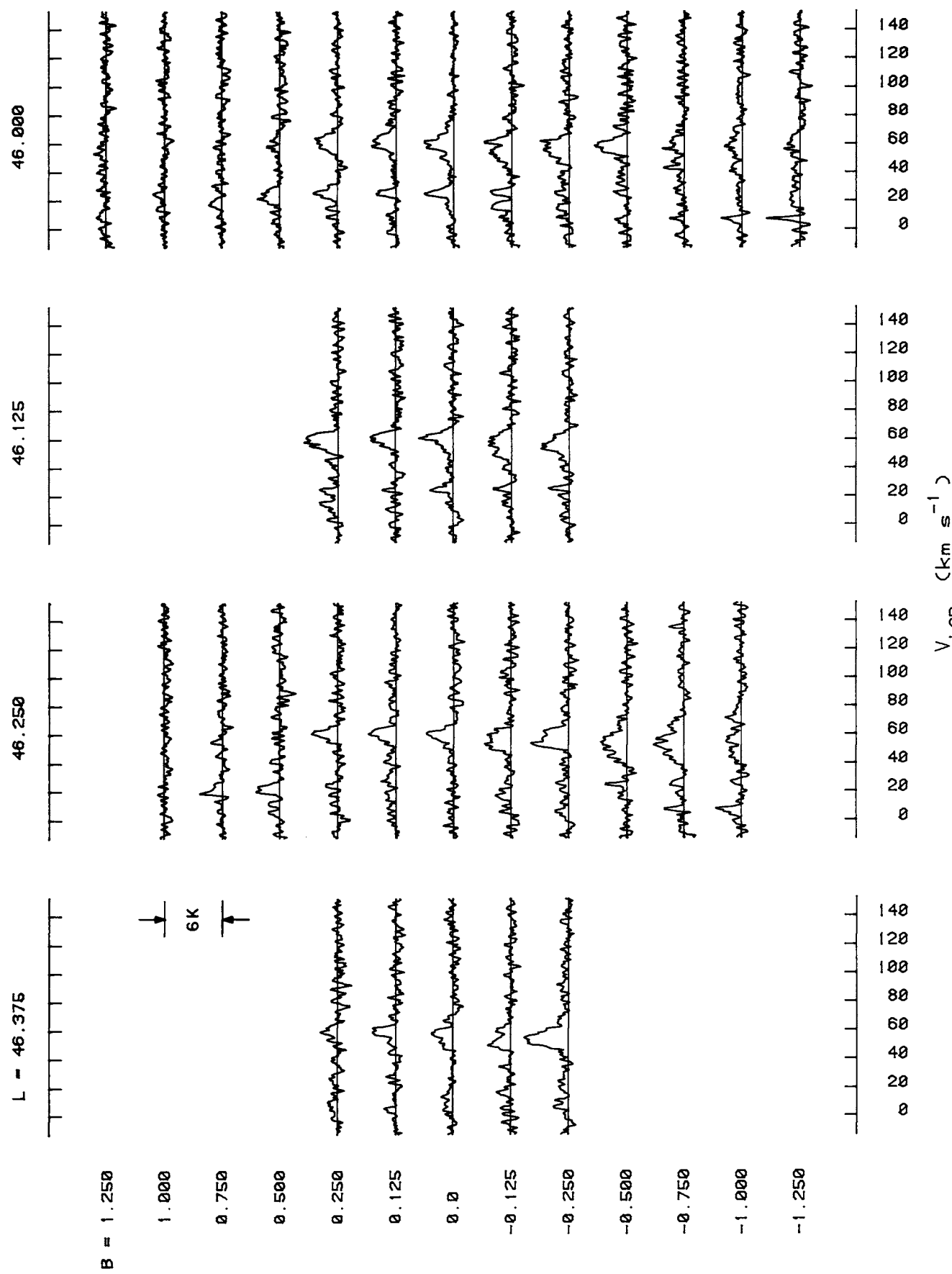


FIG. 11—Continued

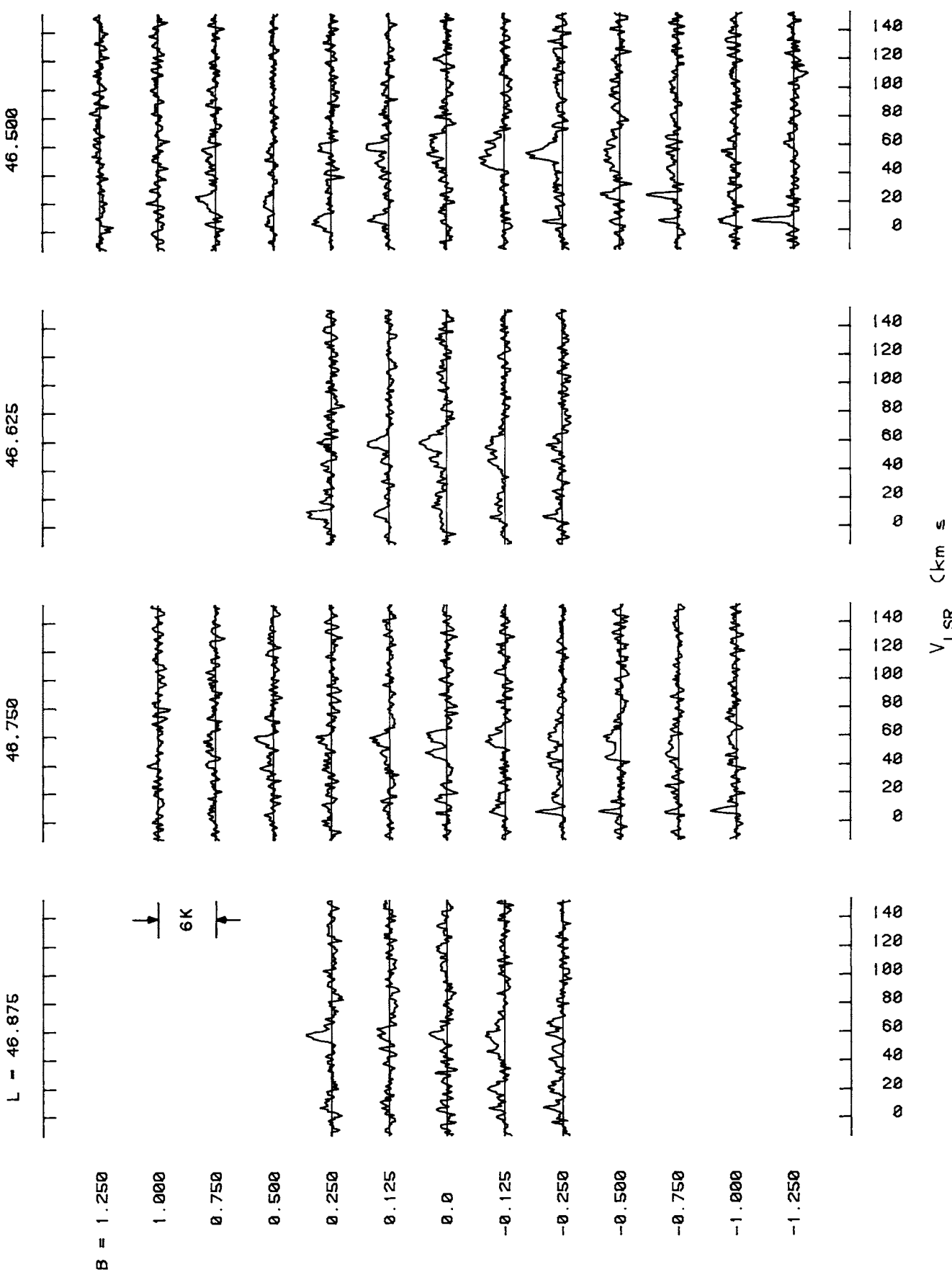


FIG. 11—Continued

47.250

47.375

L = 47.375

47.125

47.000

 $B = 1.250$ 

1.000

6K

0.750

0.500

0.250

0.125

0.0

-0.125

-0.250

-0.500

-0.750

-1.000

-1.250

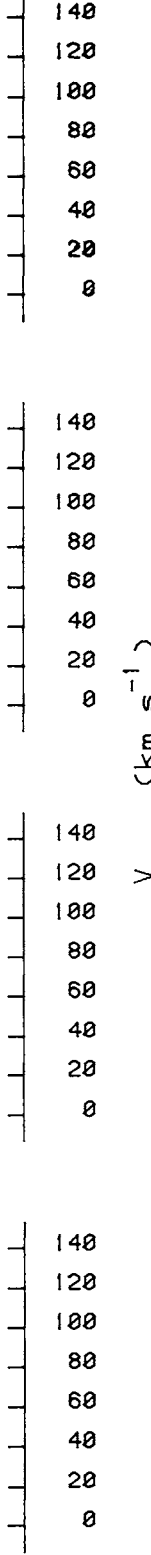
 $V_{\text{LSR}}$  ( $\text{km s}^{-1}$ )

FIG. 11—Continued

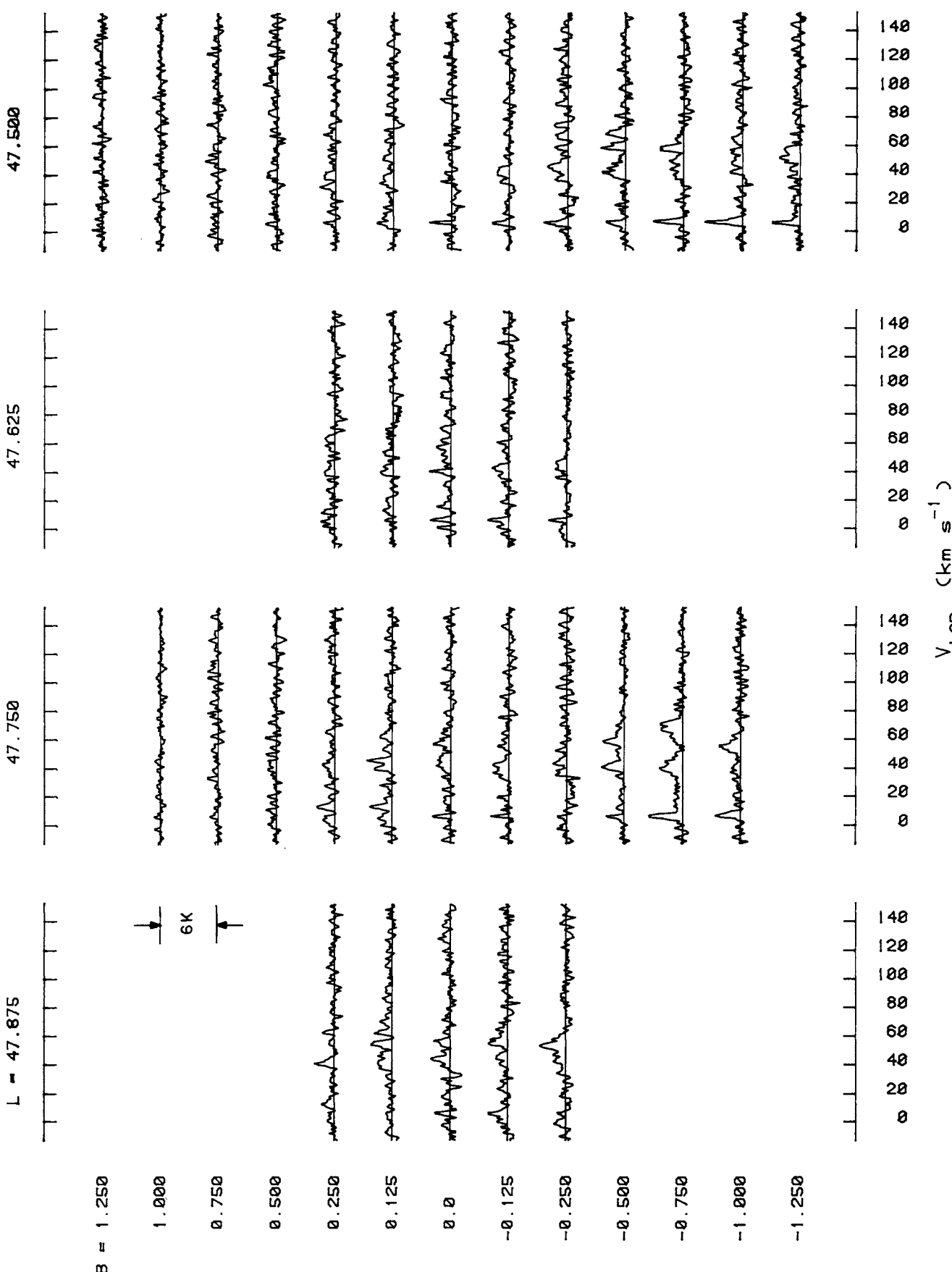


FIG. 11—Continued

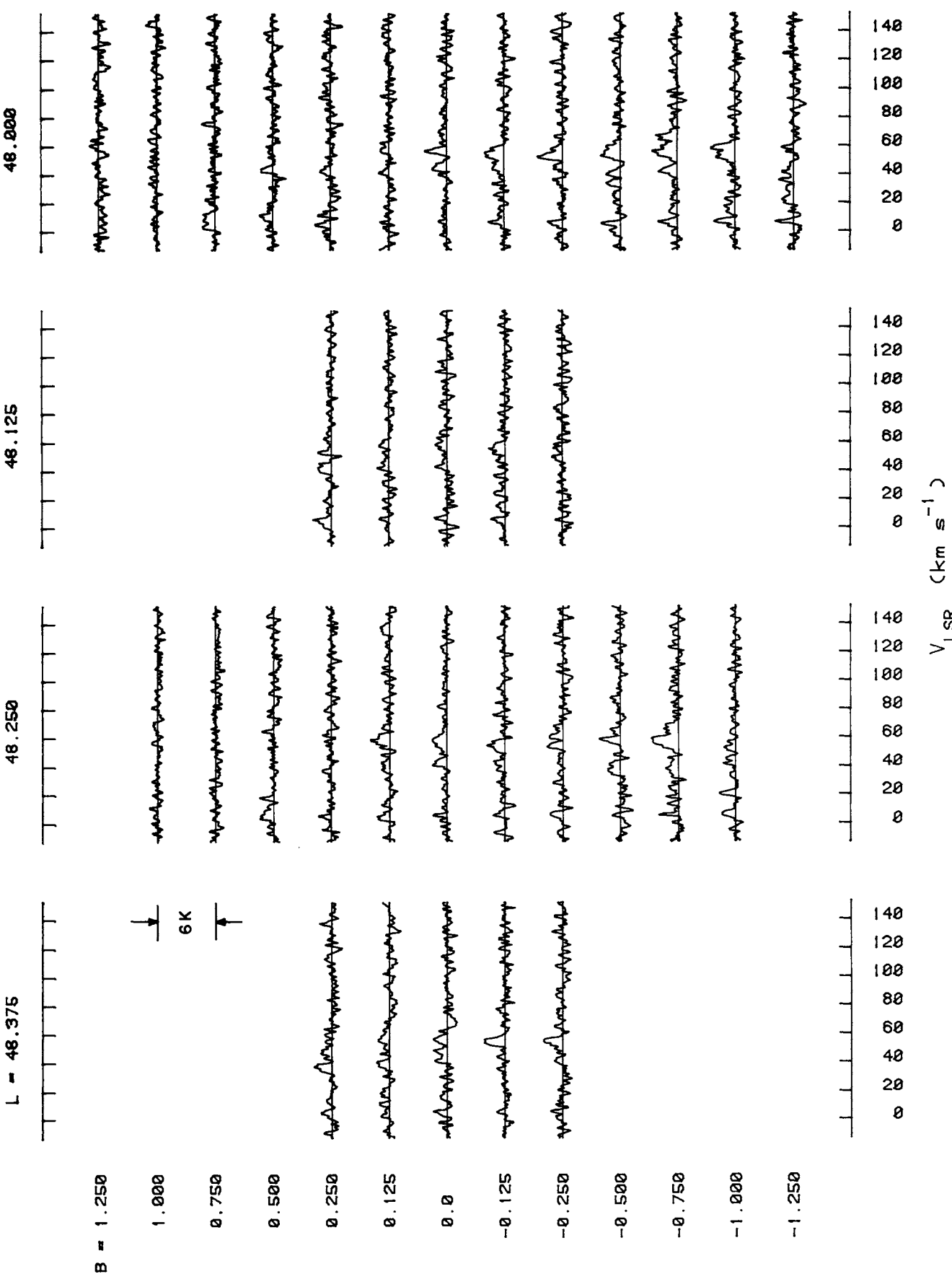
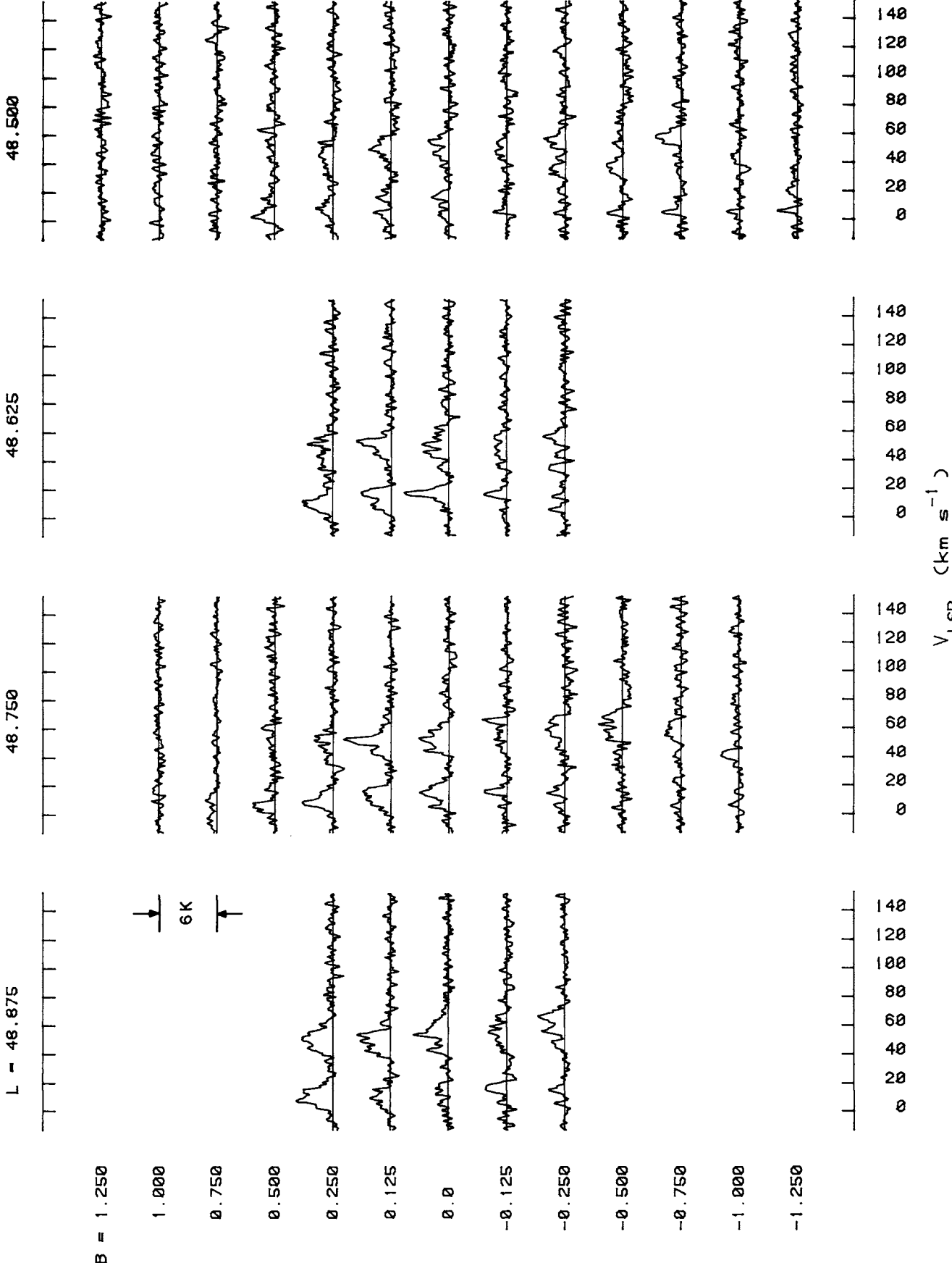


FIG. 11—Continued

$48.875$  $48.750$  $L = 48.875$ 

795

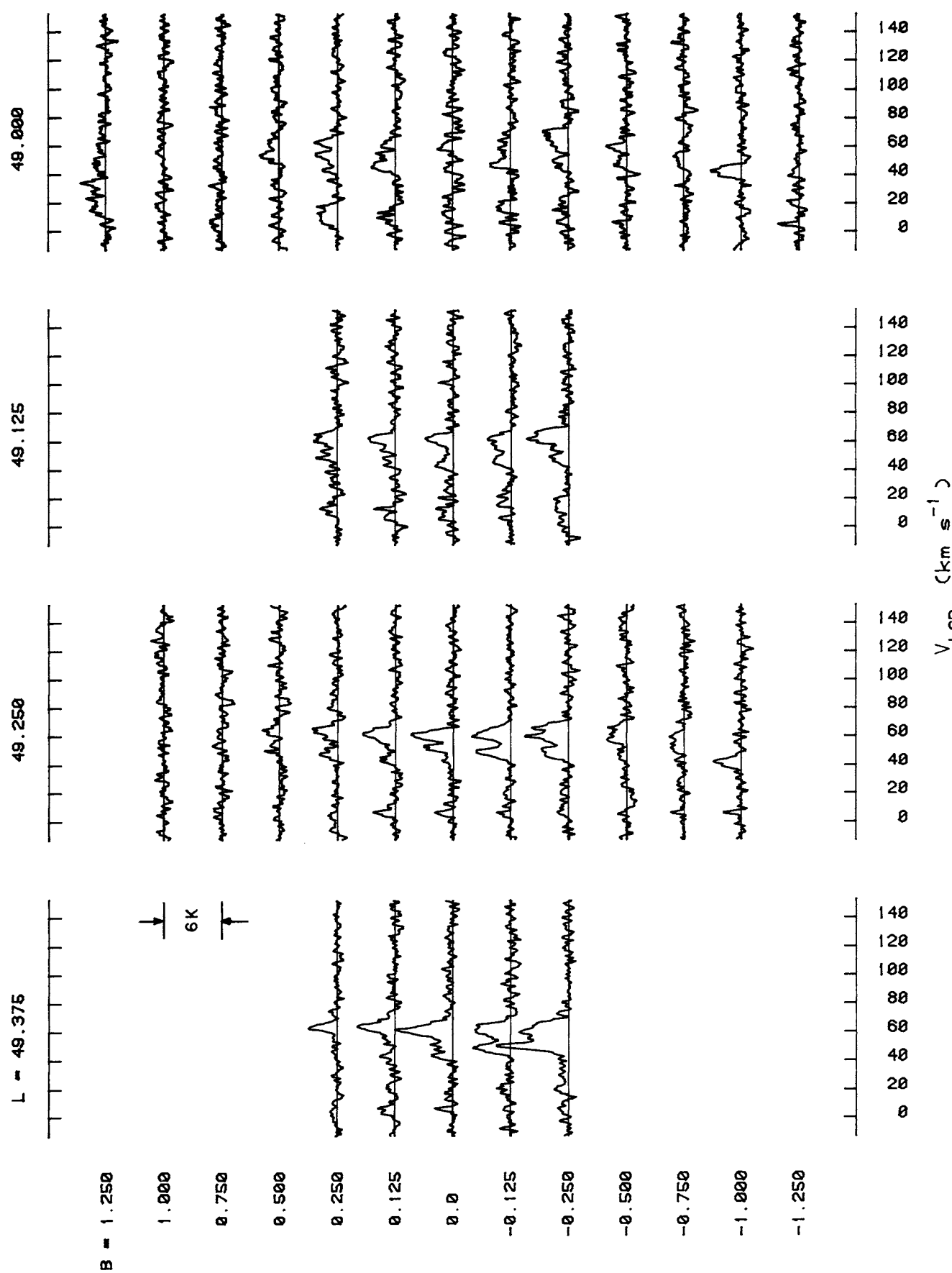


FIG. 11—Continued

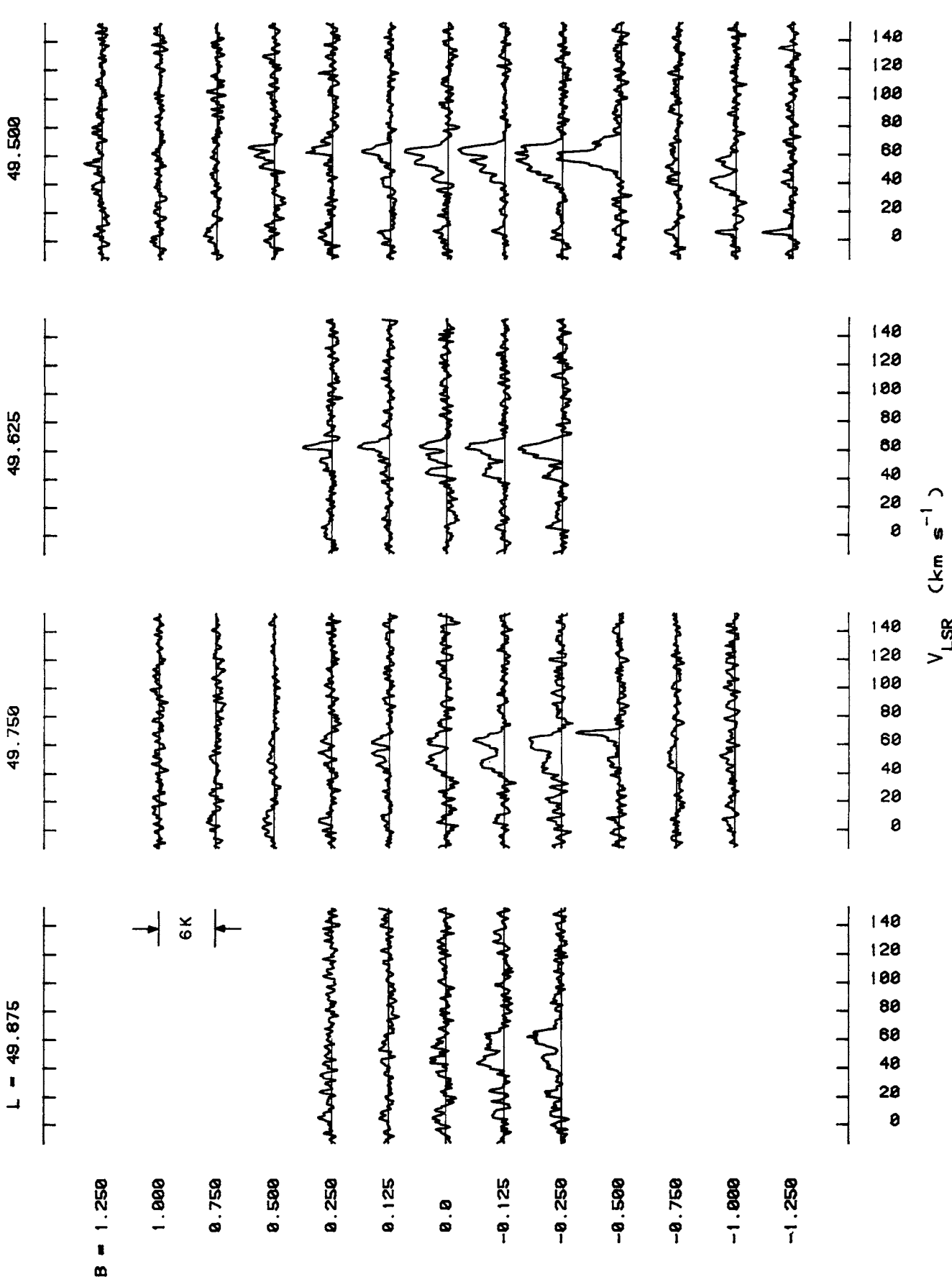


FIG. 11—Continued

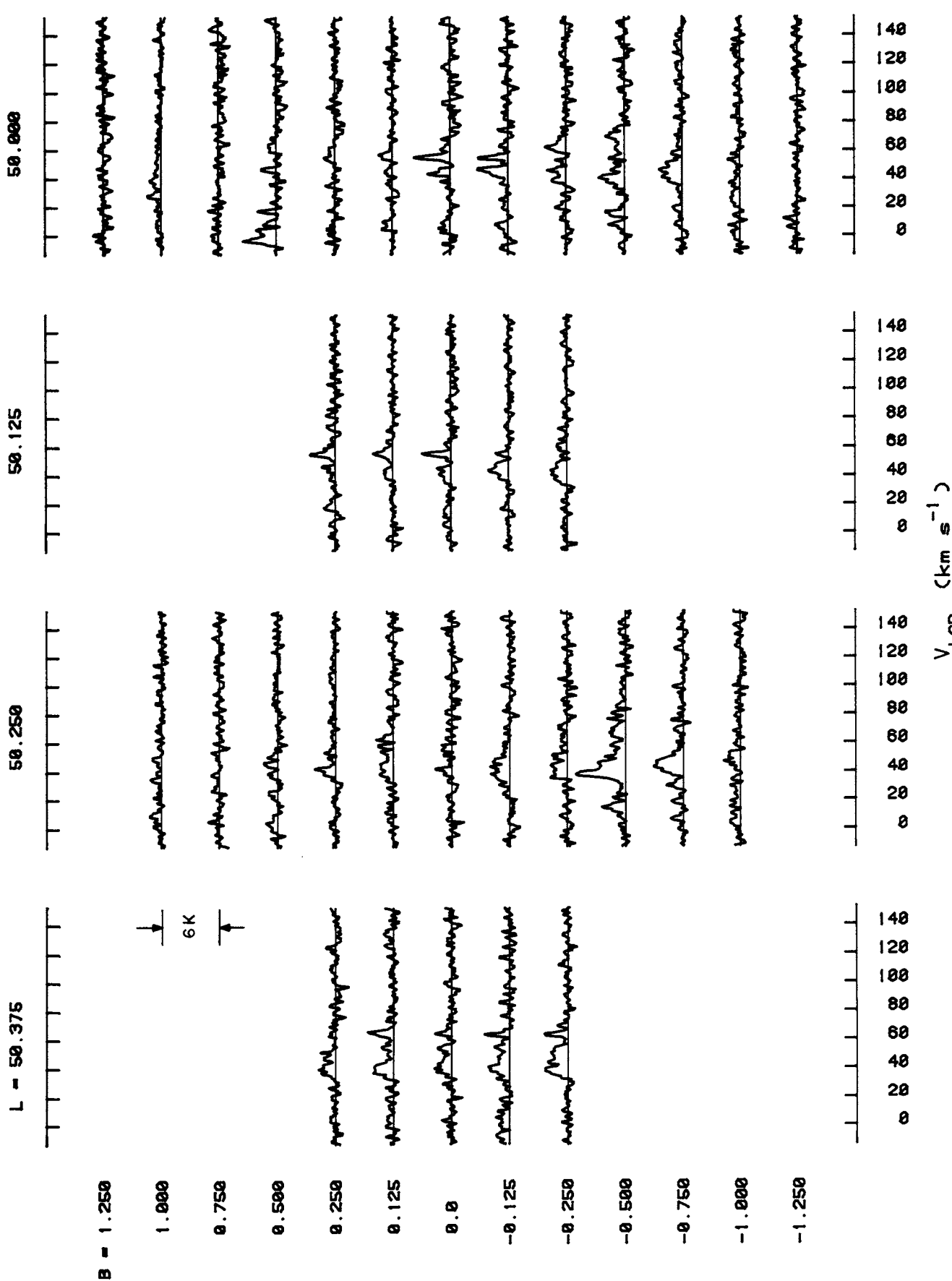
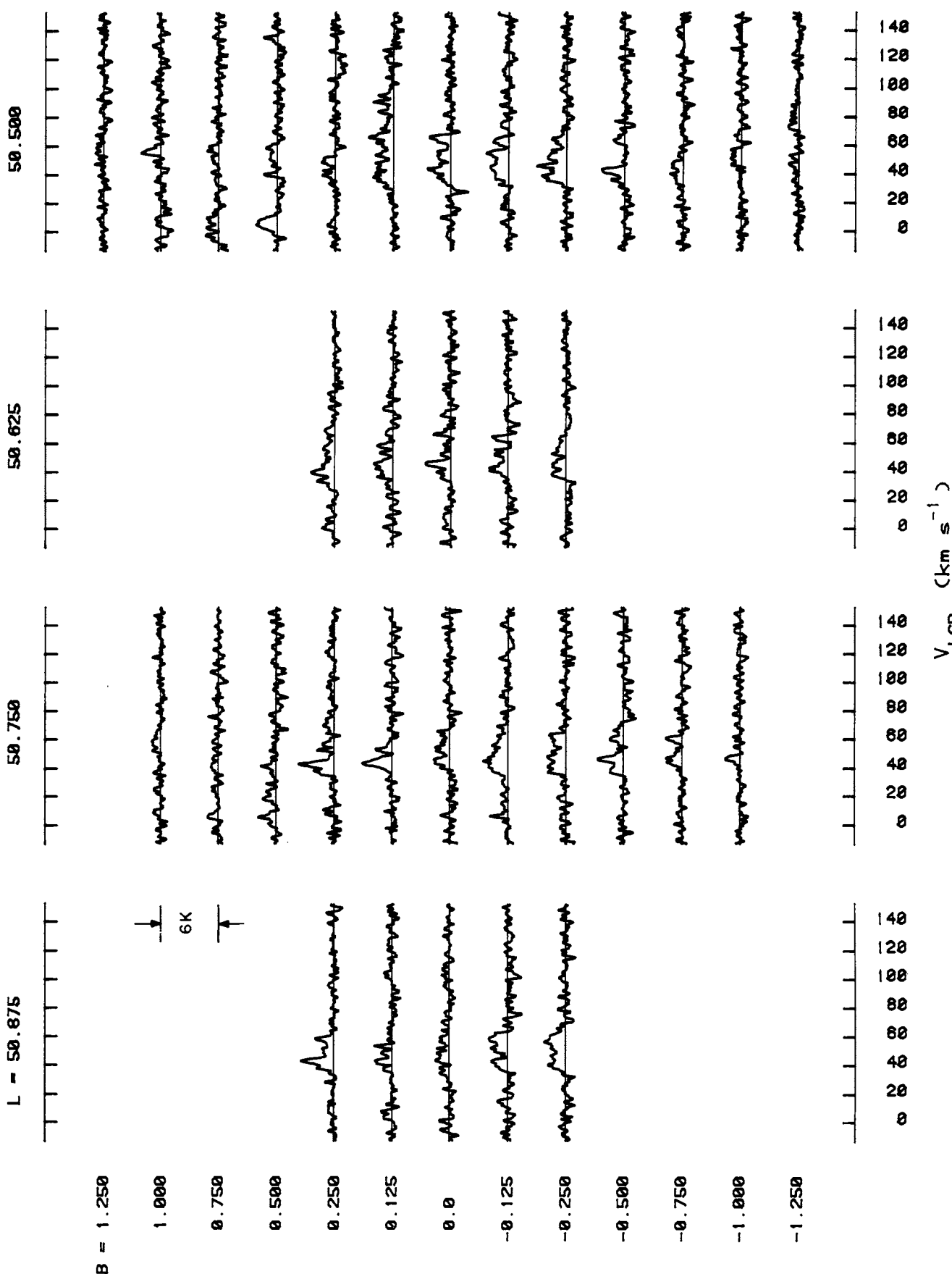


FIG. 11—Continued



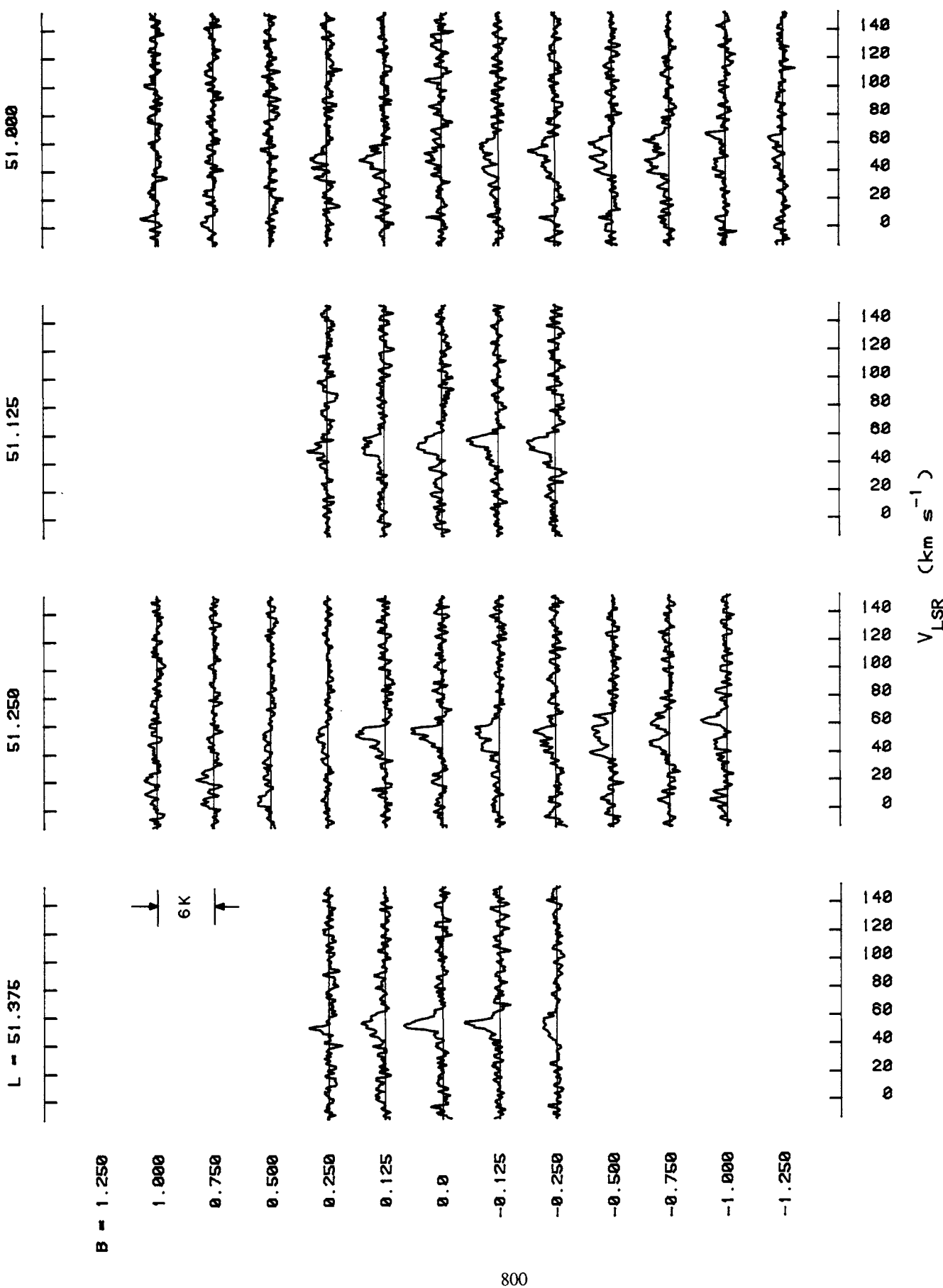
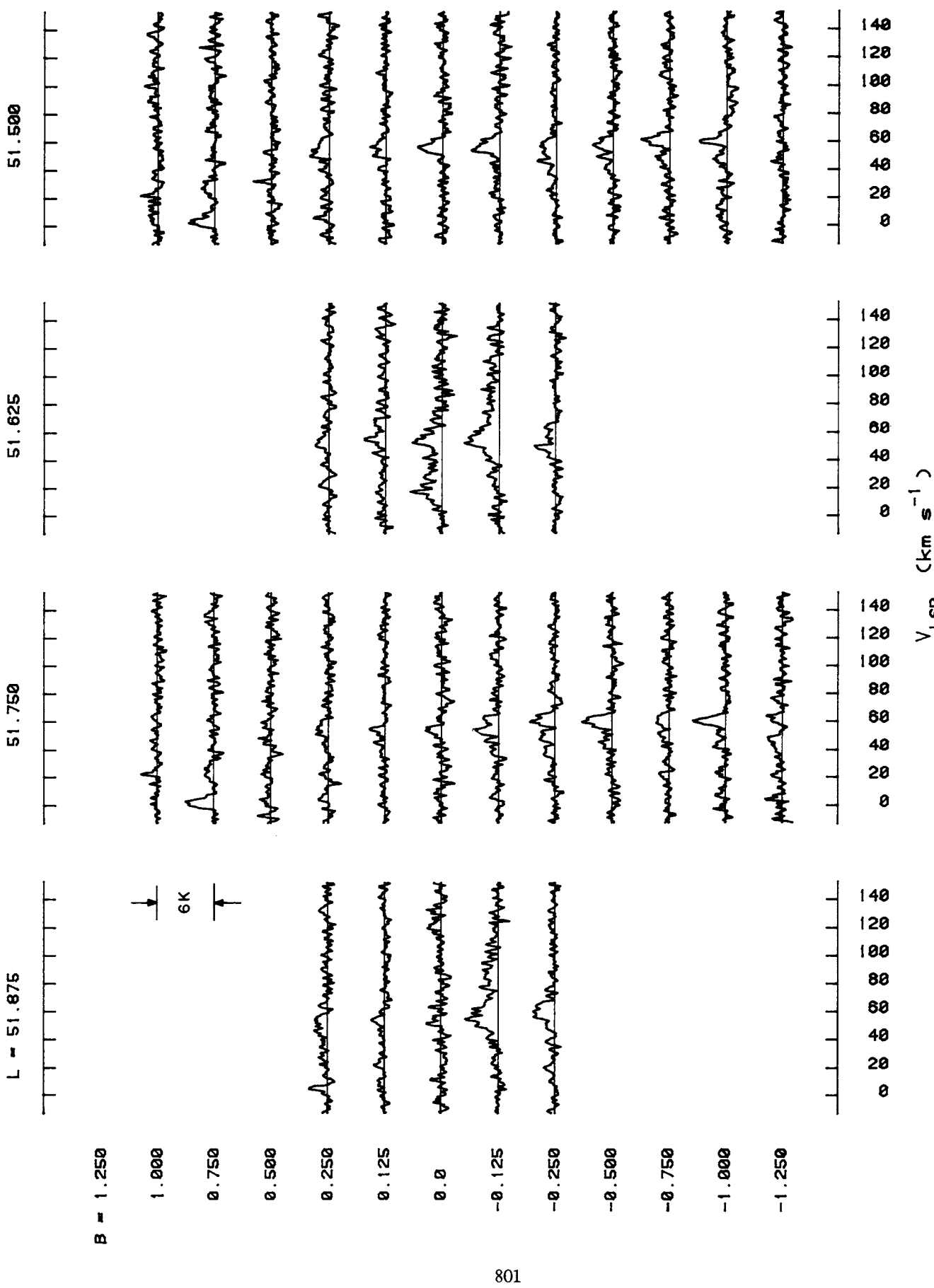


FIG. 11—Continued.



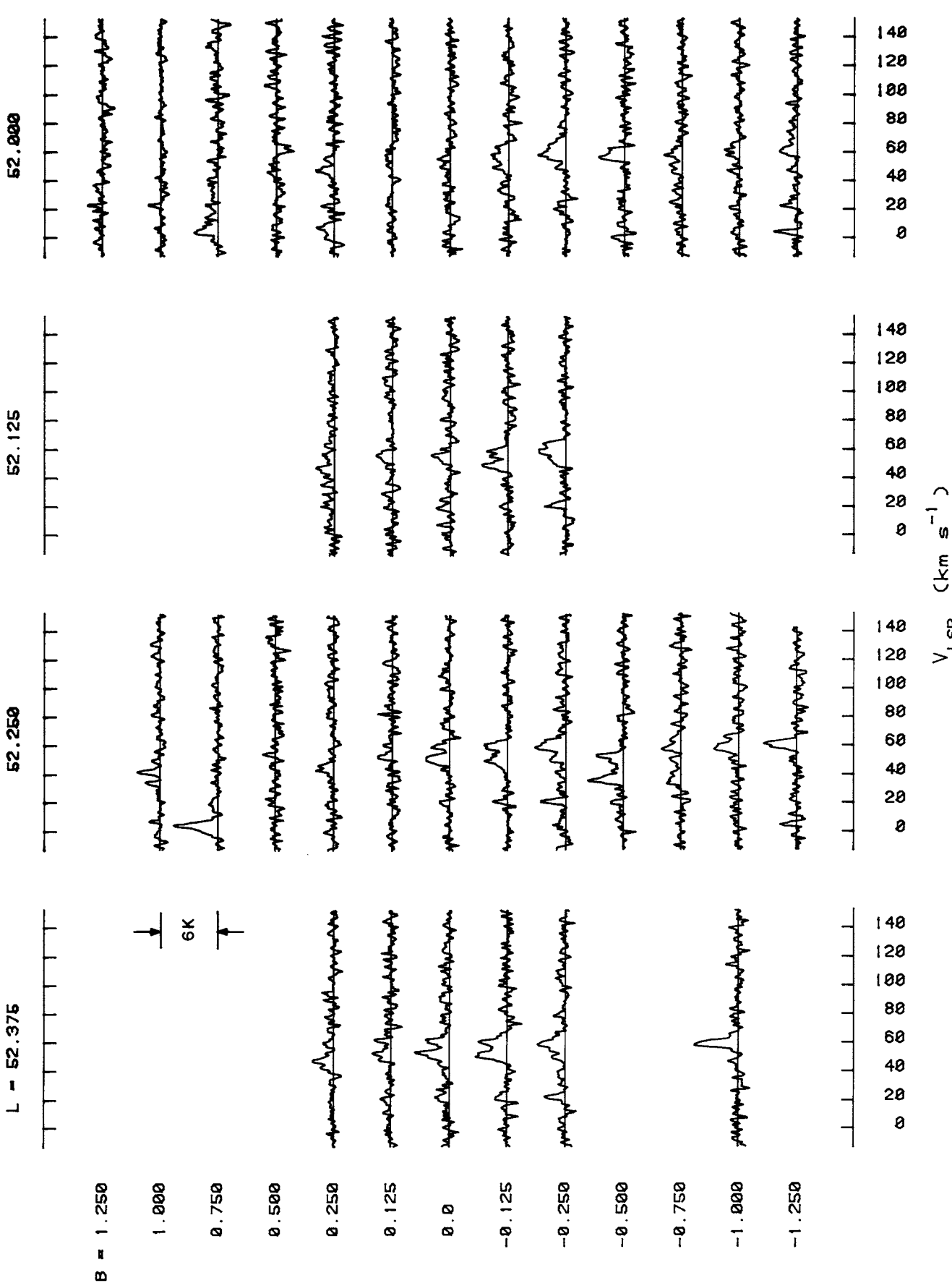


FIG. 11—Continued

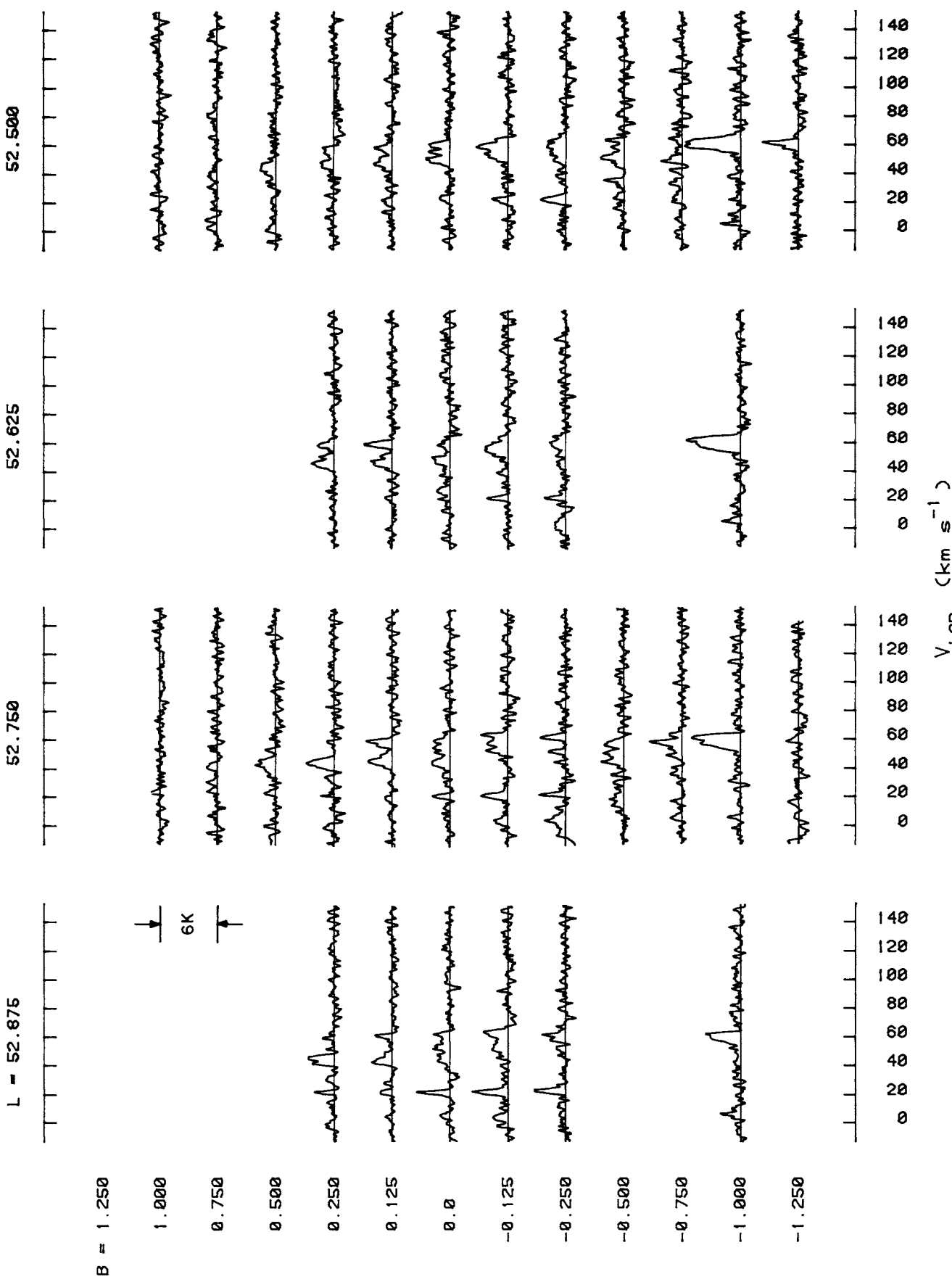


FIG. 11—Continued

53.000

53.125

53.250

L = 53.375

 $B = 1.250$ 

1.000

0.750

0.500

0.250

0.125

0.0

-0.125

-0.250

-0.500

-0.750

-1.000

-1.250

6K  
60006K  
60006K  
60006K  
60006K  
60006K  
60006K  
6000

53.000

53.125

53.250

53.375

53.400

53.425

53.450

53.475

 $V_{\text{LSR}}$  (km s<sup>-1</sup>)

804

FIG. 11—Continued

53.500

53.625

53.750

L = 53.875

 $B = 1.250$ 

1.000

0.750

0.500

0.250

0.0

-0.125

-0.250

-0.500

-0.750

-1.000

-1.250

805

6K

 $V_{\text{LSR}}$  (km s<sup>-1</sup>)

FIG. 11—Continued

54.000

54.125

54.250

L = 54.375

B = 1.250

1.000

6K

0.750

0.500

0.250

0.125

0.0

-0.125

-0.250

-0.500

-0.750

-1.000

-1.250

806

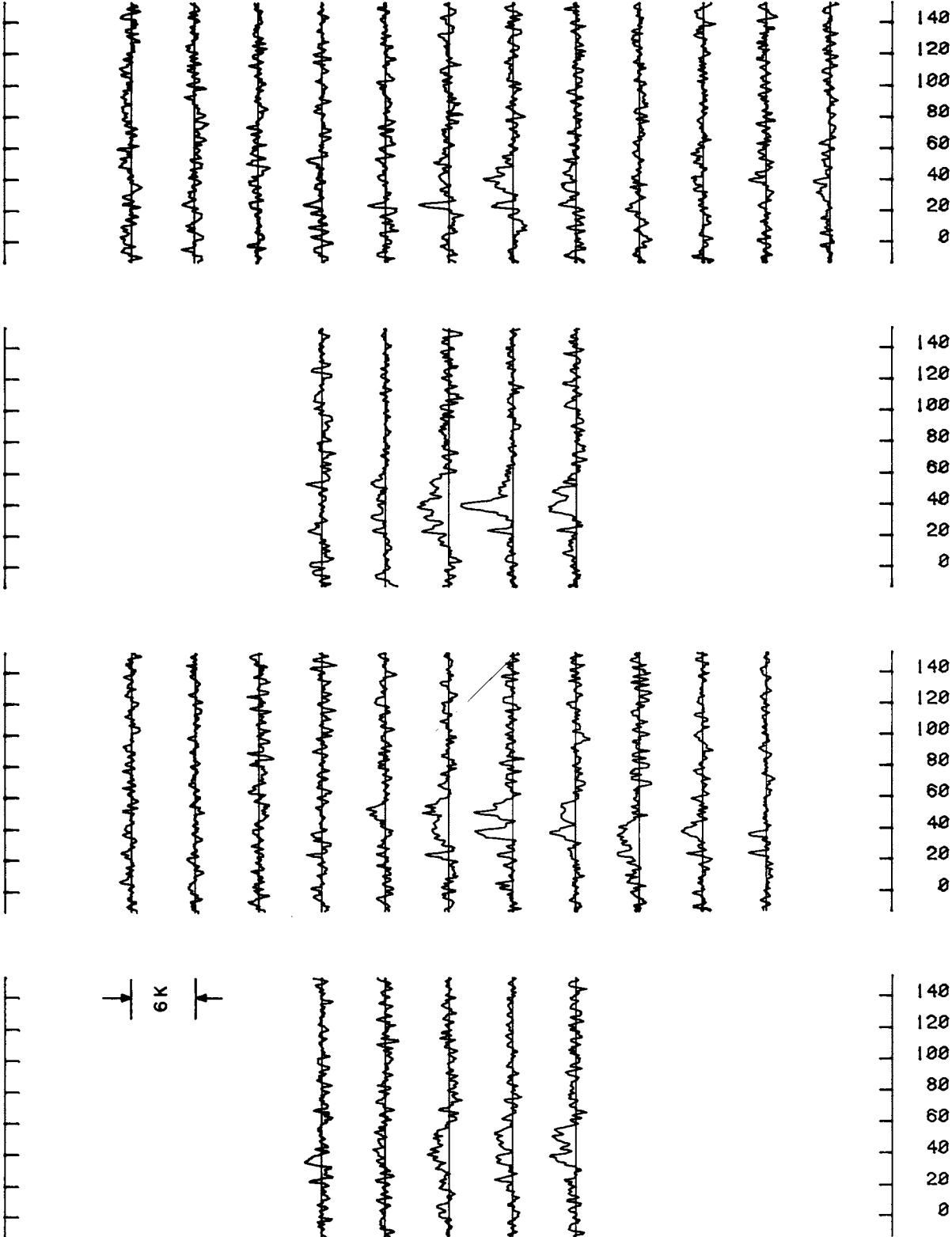
 $V_{\text{LSR}}$  (km s $^{-1}$ )

FIG. 11.—Continued

54.500

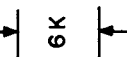
54.625

54.750

L = 54.875

B = 1.250

1.000



0.750

0.500

0.250

0.125

0.0

-0.125

-0.250

-0.500

-0.750

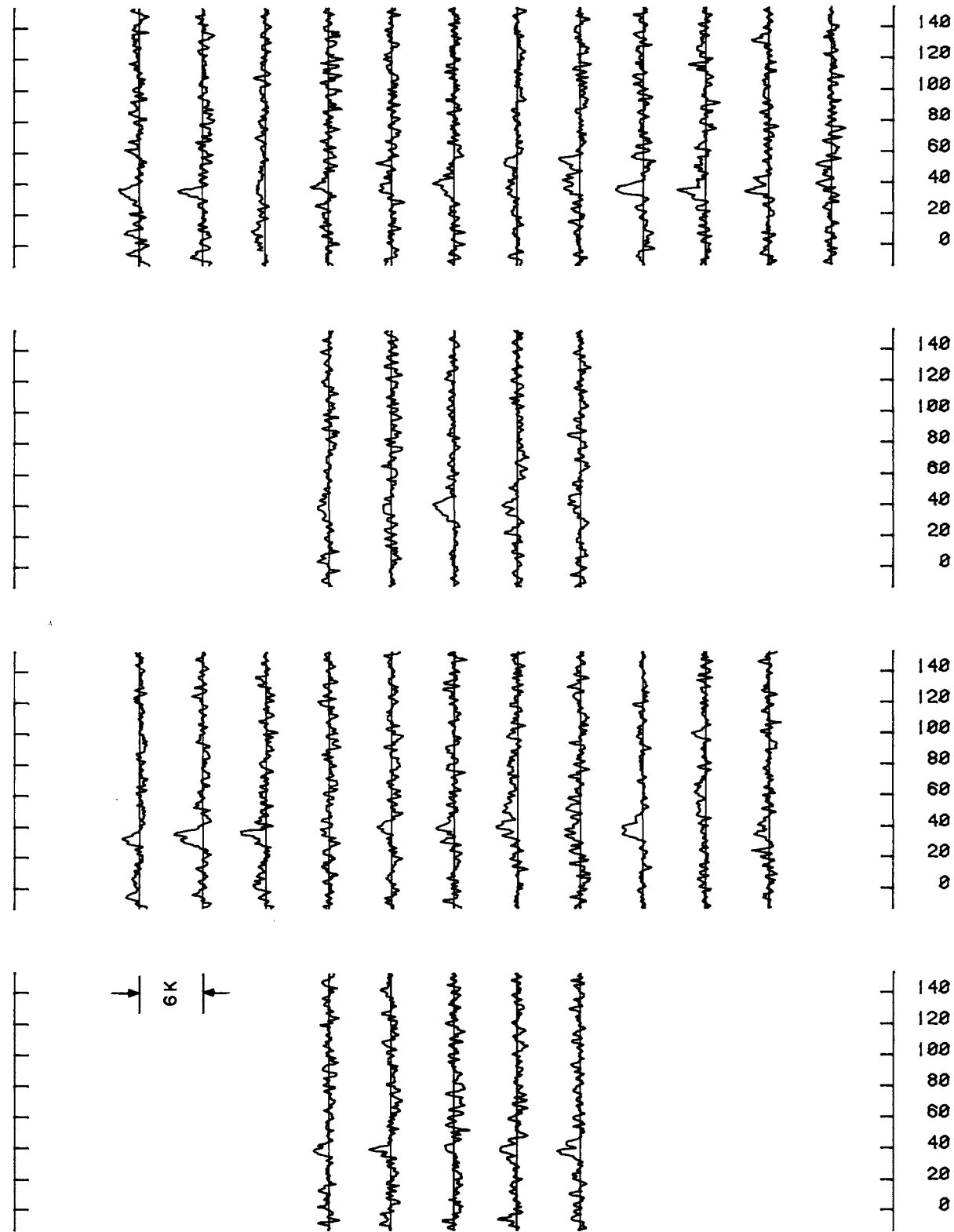
-1.000

-1.250

807

 $V_{\text{LSR}}$  (km s<sup>-1</sup>)

FIG. 11.—Continued



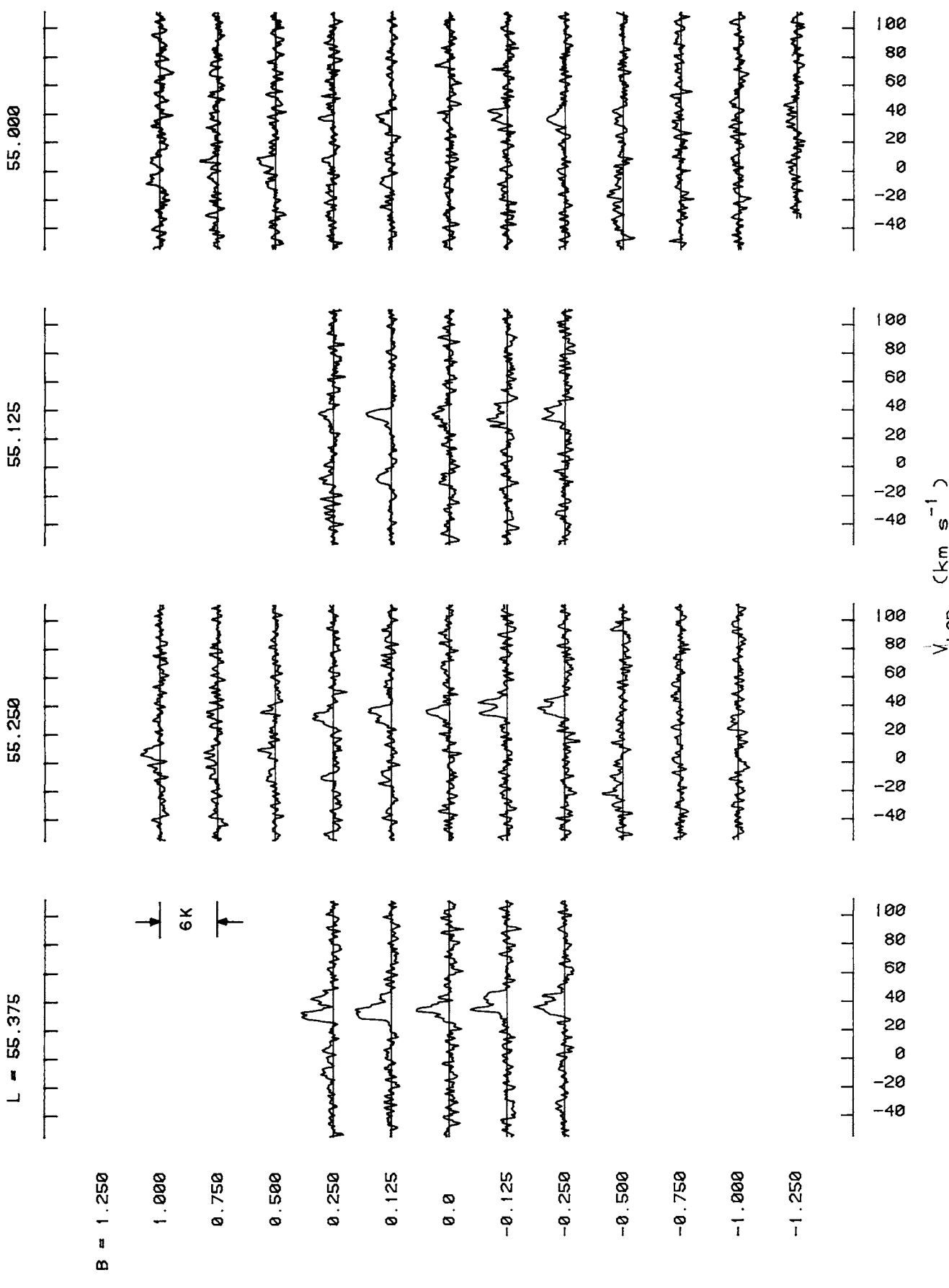


FIG. 11—Continued

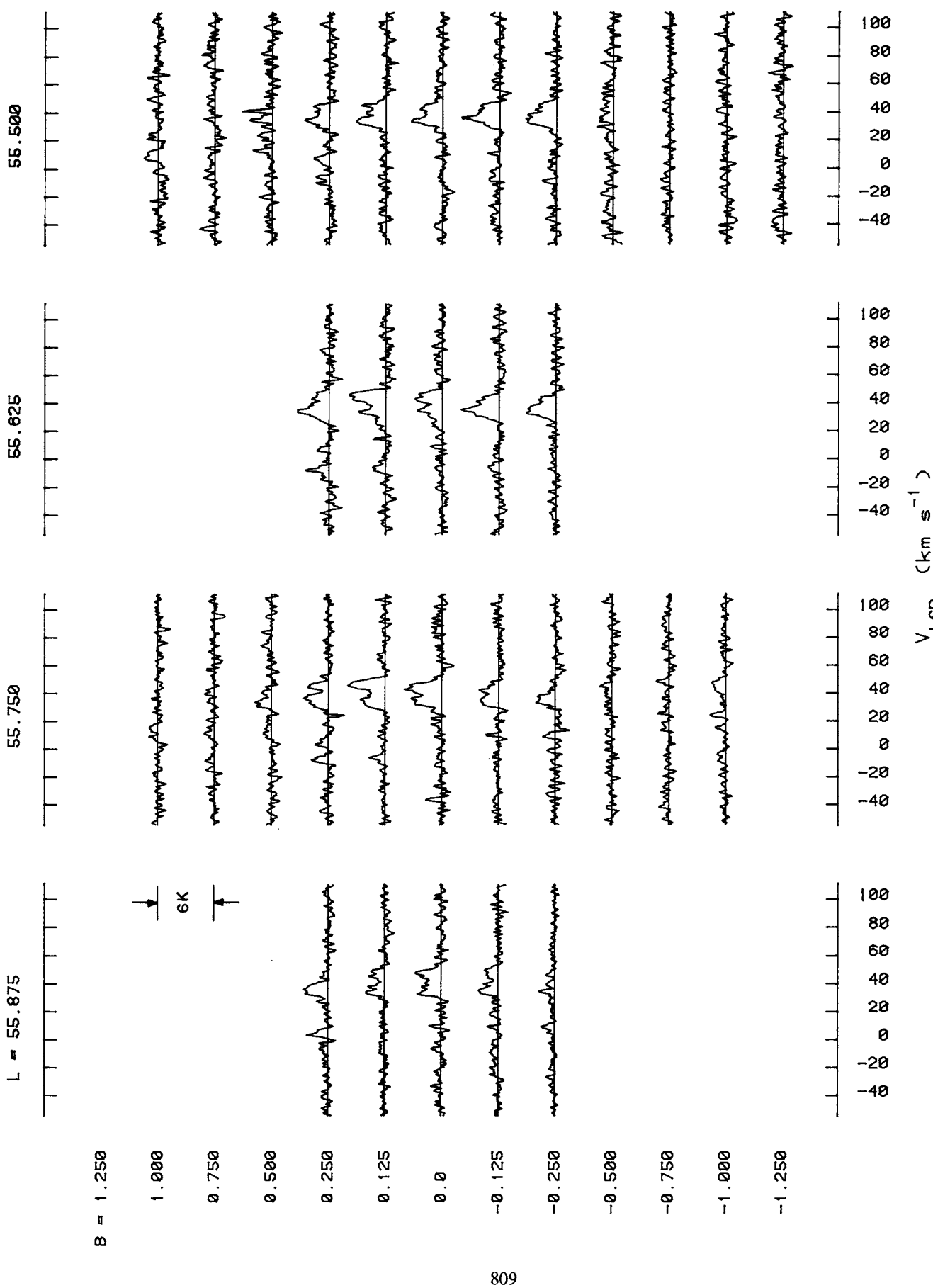


FIG. 11—Continued

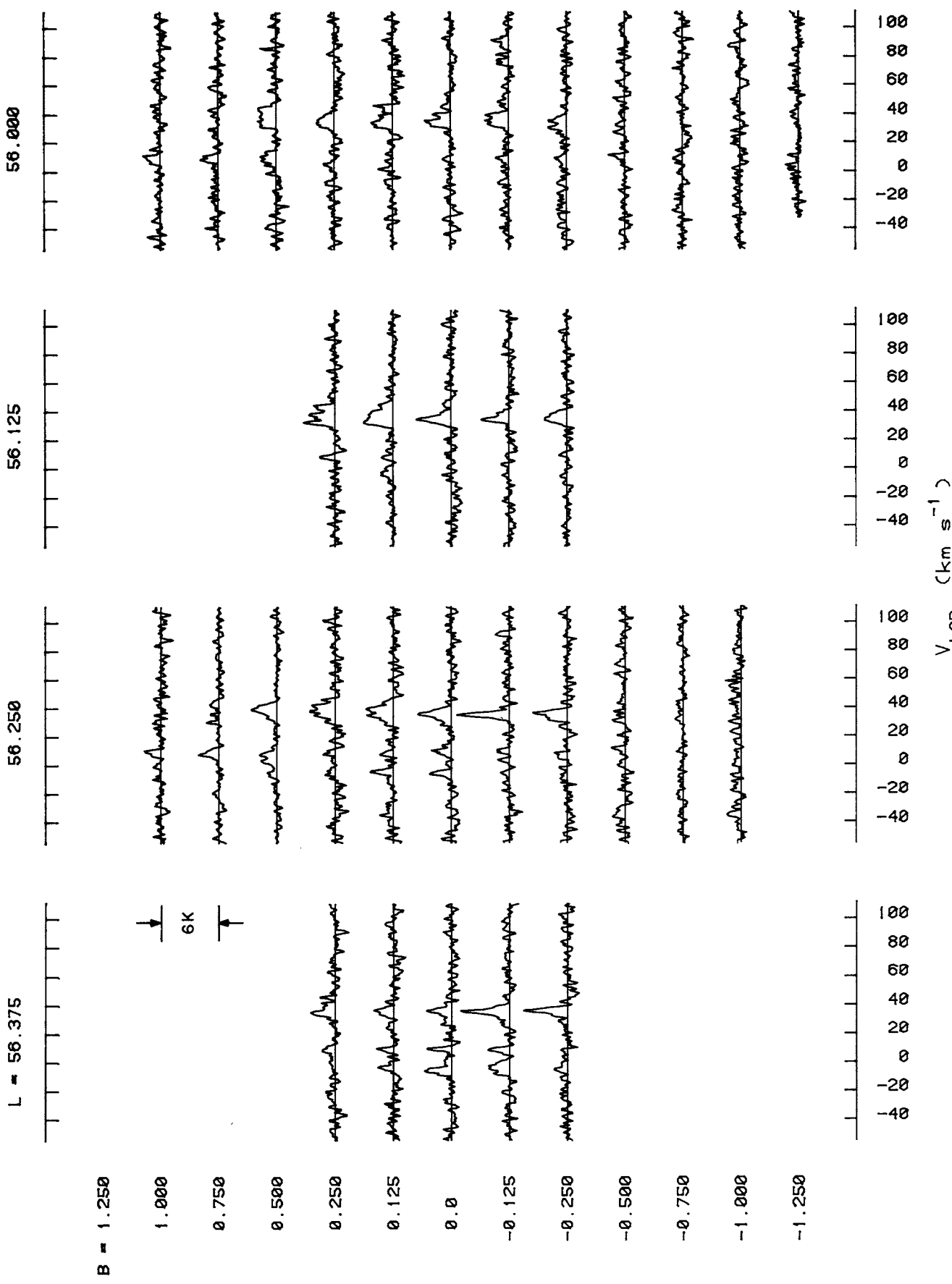


FIG. 11—Continued

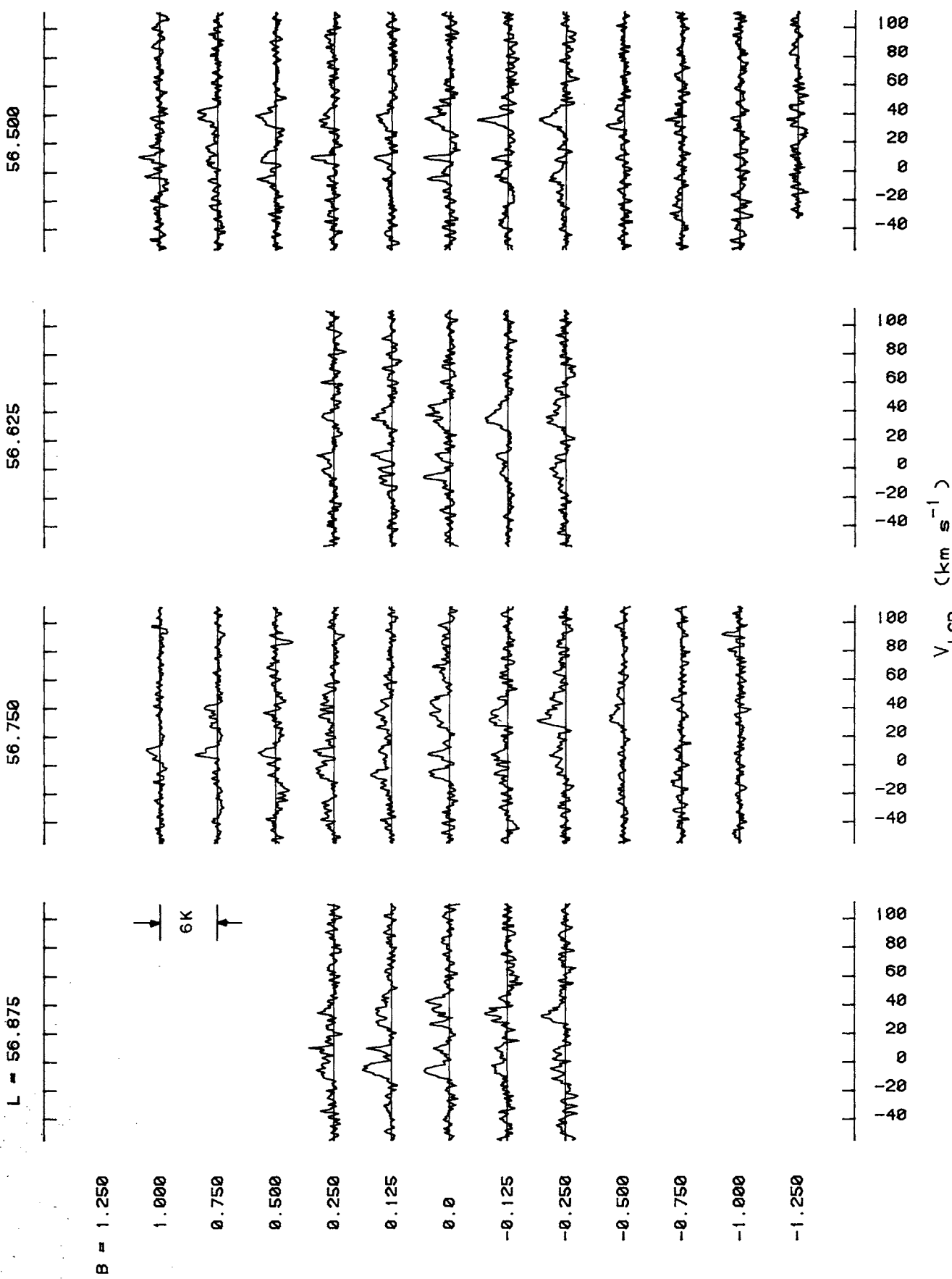


FIG. 11—Continued

57.000

57.125

57.250

L = 57.375

B = 1.250

1.000

6K

0.750

0.500

0.250

0.125

0.0

-0.125

-0.250

-0.500

-0.750

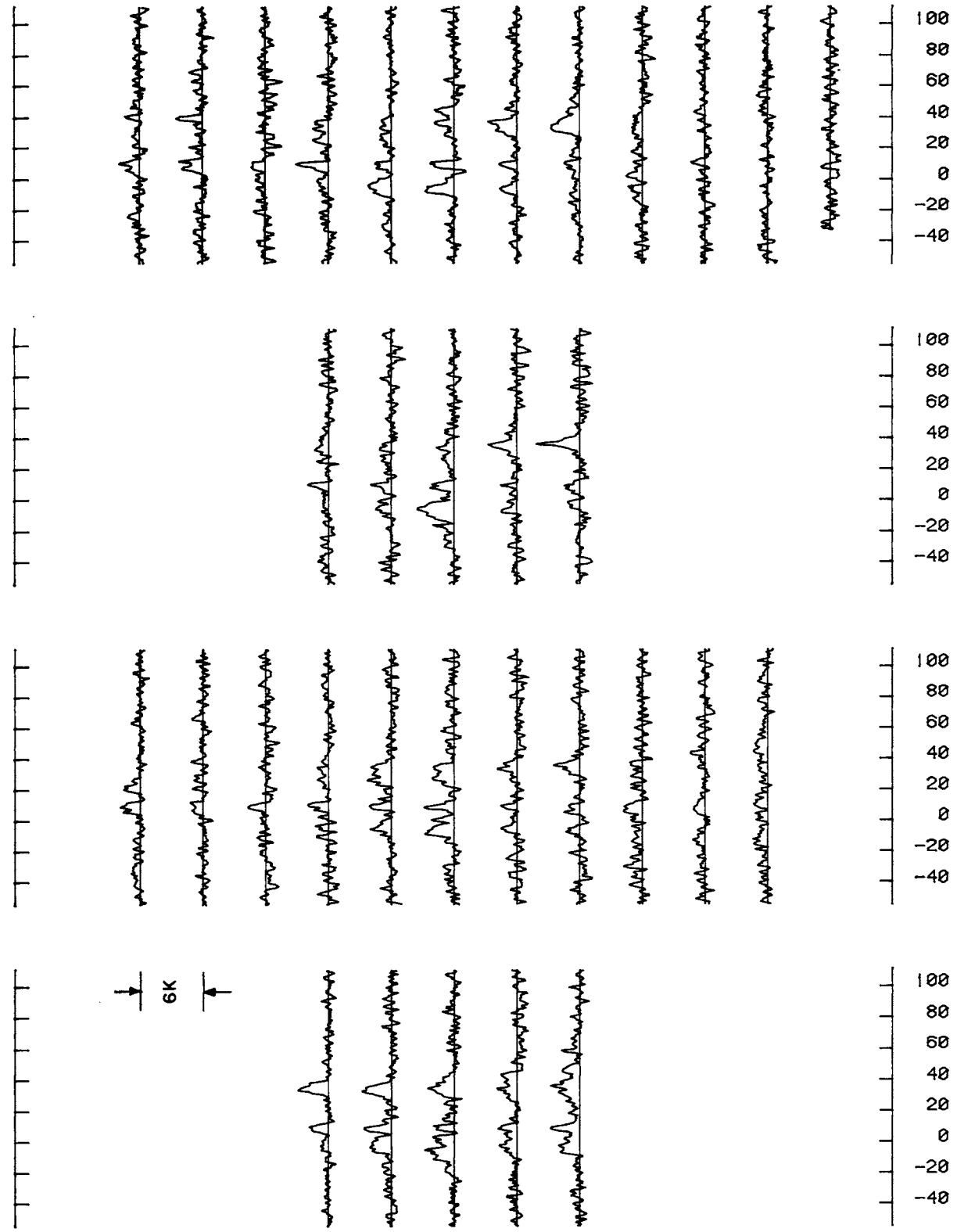
-1.000

-1.250

812

 $V_{\text{LSR}}$  ( $\text{km s}^{-1}$ )

FIG. 11—Continued



57.500

57.625

57.750

L = 57.875

 $B = 1.250$ 

1.000

6K

0.750

0.500

0.250

0.125

0.0

-0.125

-0.250

-0.500

-0.750

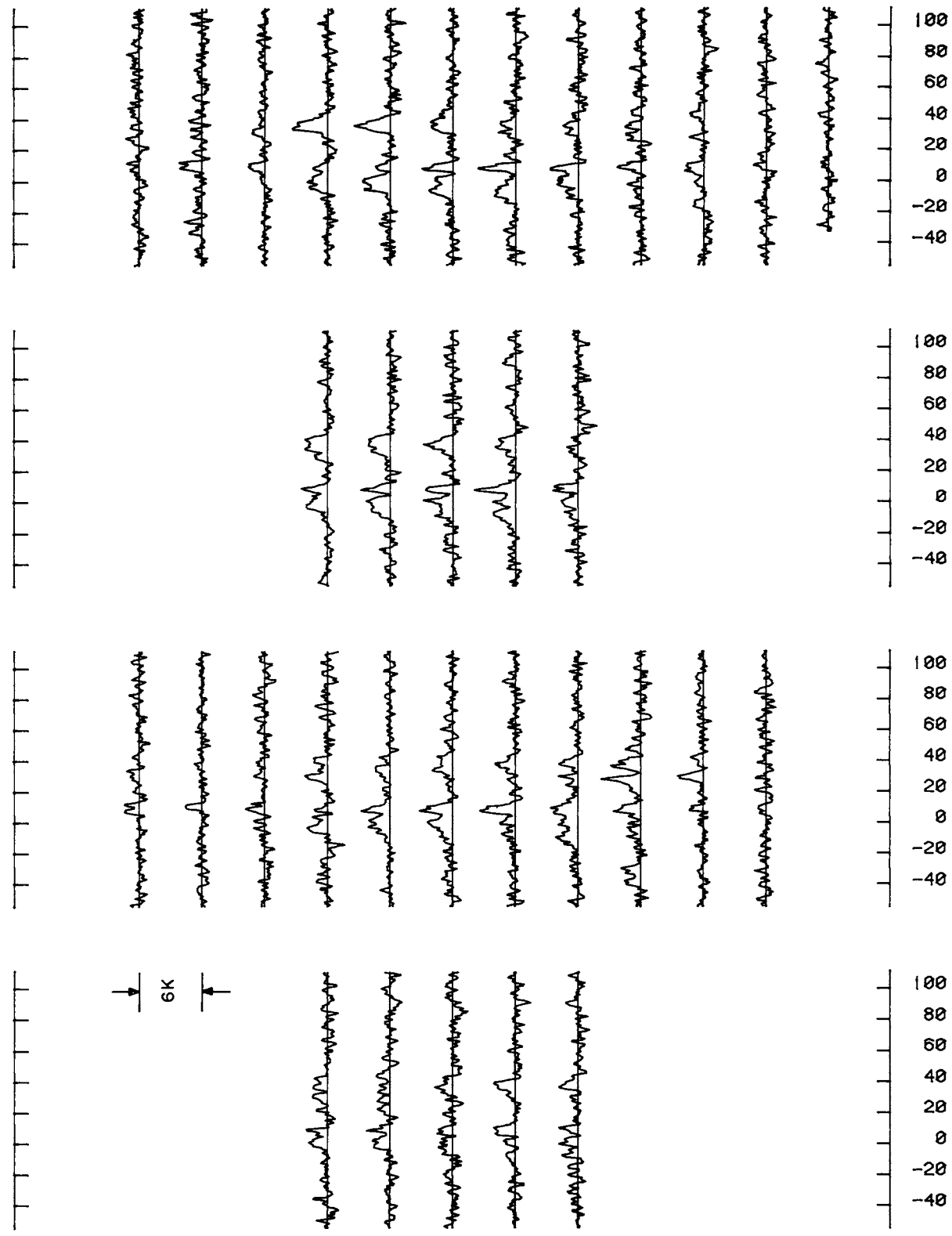
-1.000

-1.250

813

 $V_{\text{LSR}}$  ( $\text{km s}^{-1}$ )

FIG. 11—Continued



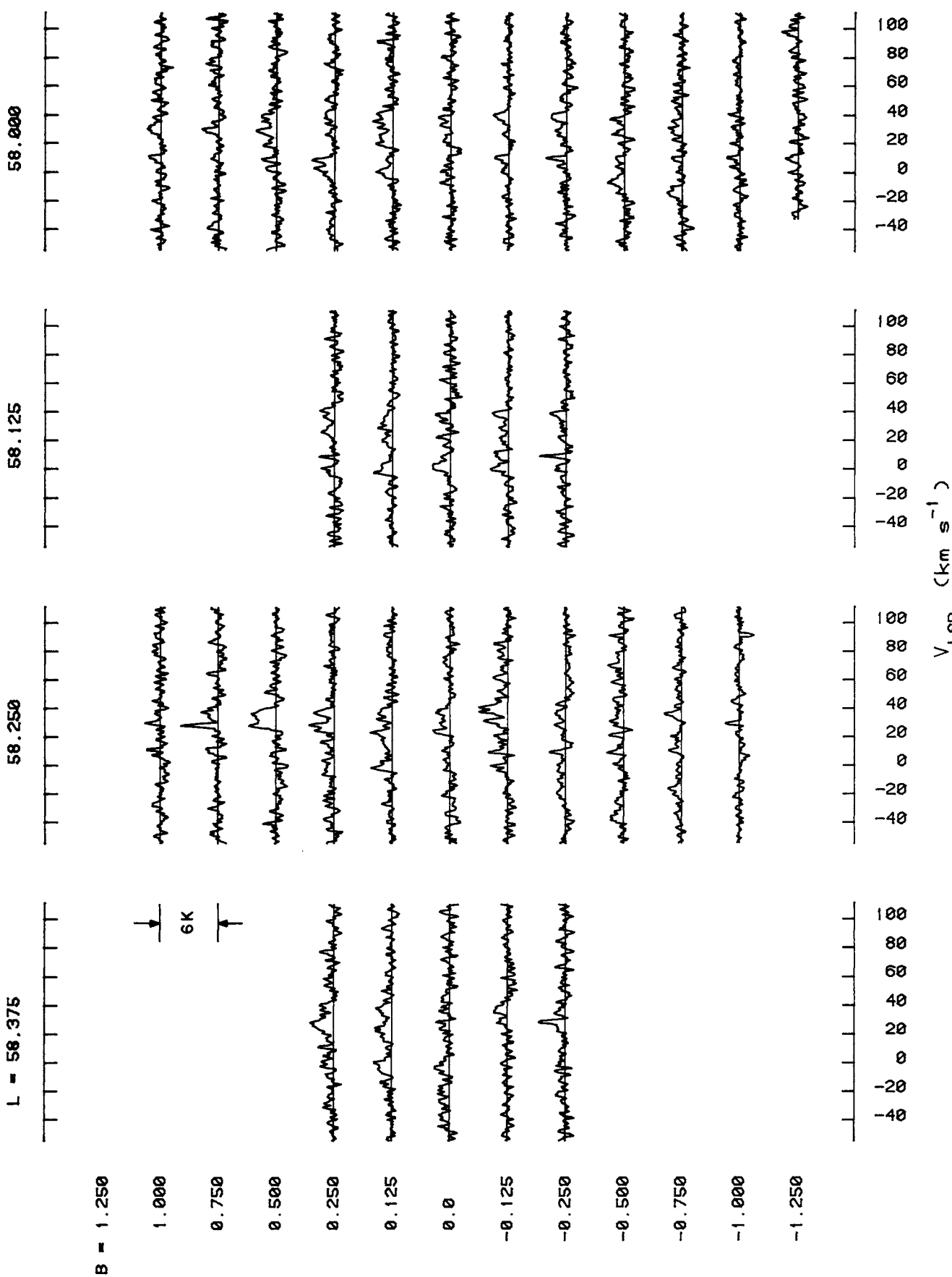


FIG. 11—Continued

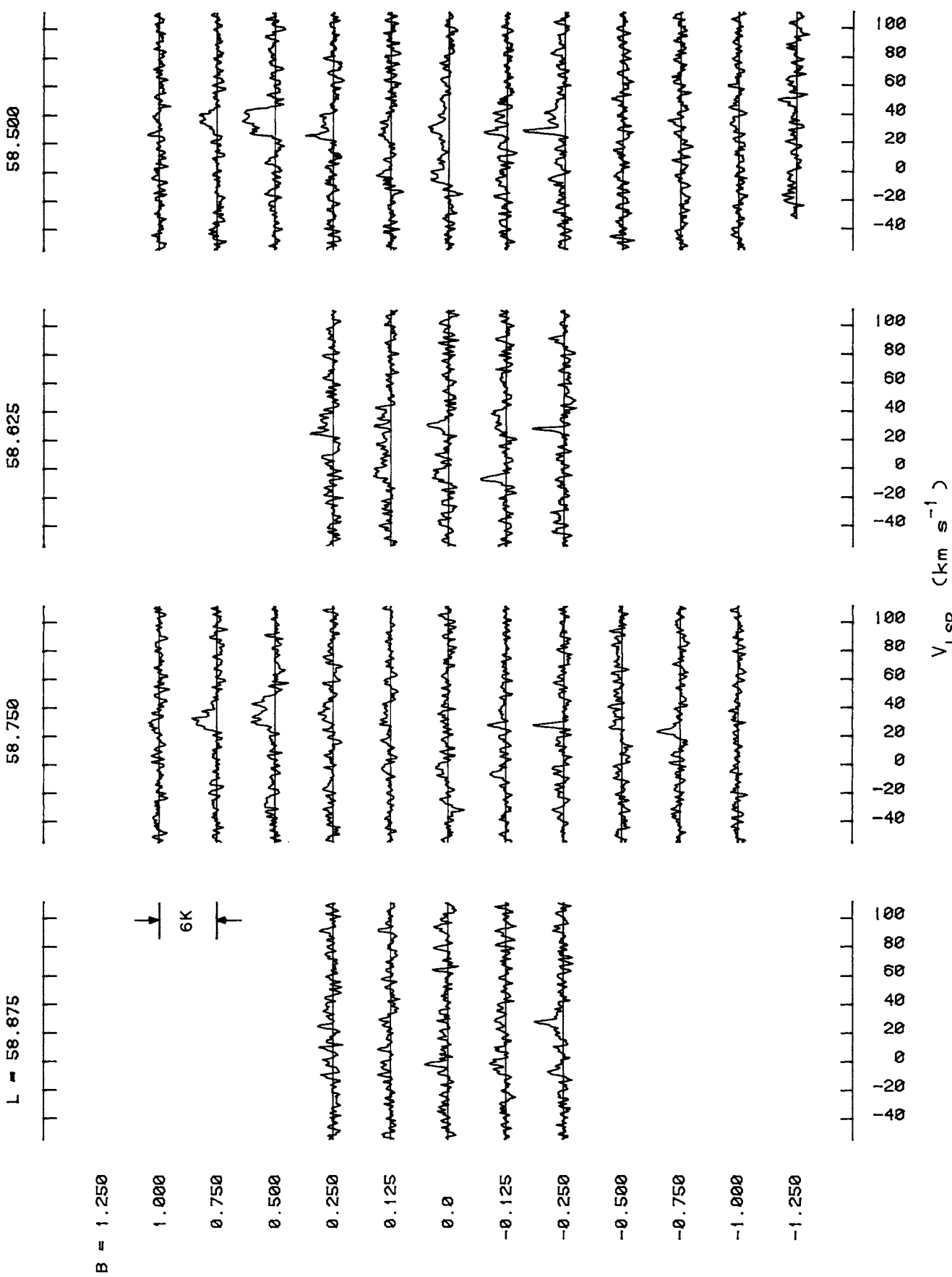


FIG. 11—Continued

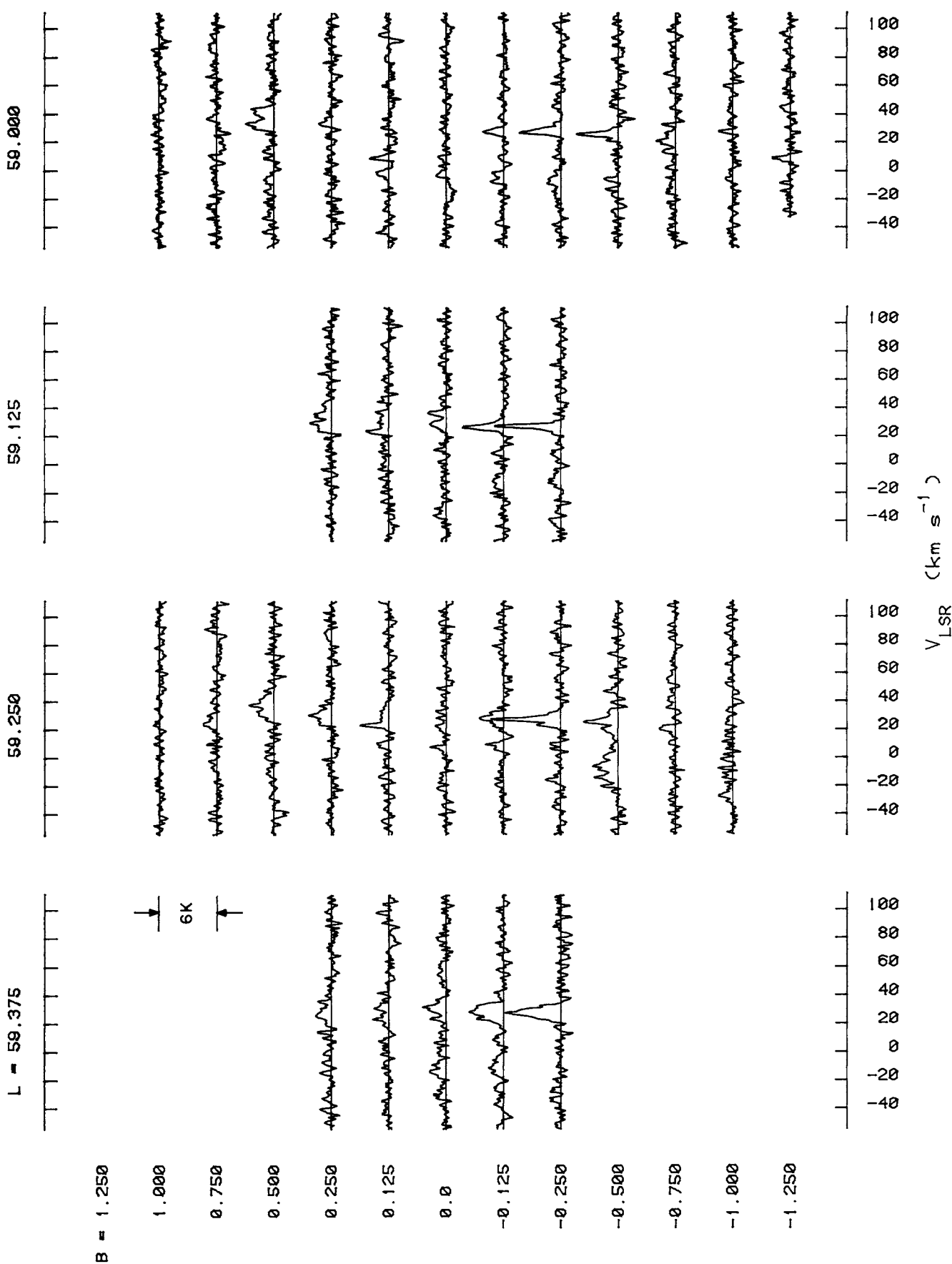


FIG. 11—Continued

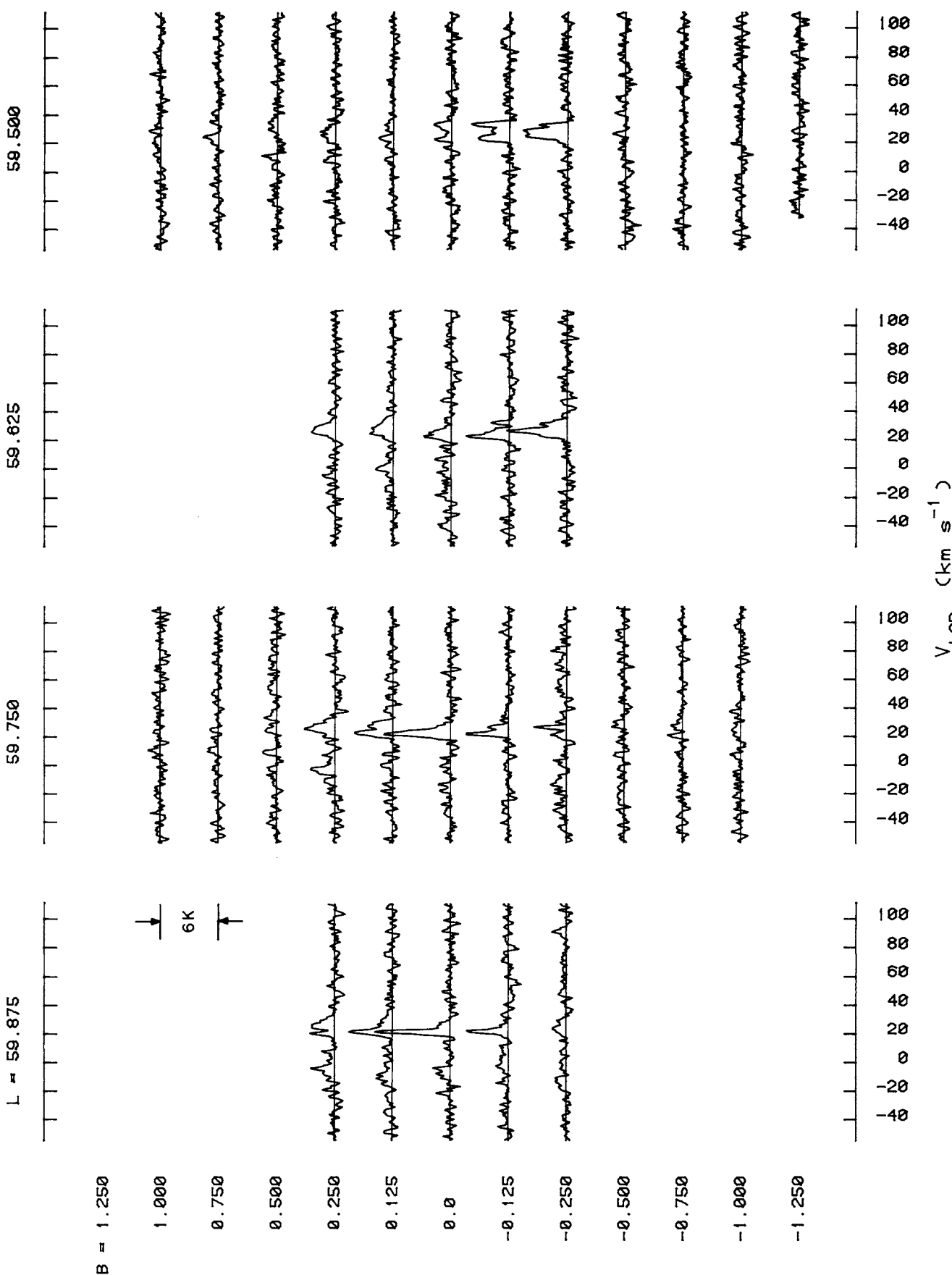


FIG. 11—Continued

60.000

L -

$$B = 1.250$$

$$1.000$$

$$0.750$$

$$0.500$$

$$0.250$$

$$0.125$$

$$0.0$$

$$-0.125$$

$$-0.250$$

$$-0.500$$

$$-0.750$$

$$-1.000$$

$$-1.250$$

$$V_{\text{LSR}} \text{ (km s}^{-1}\text{)}$$

FIG. 11—Continued